Study on Characteristic Stimuli-Responsive Polymer Thin Films

Takayuki Uekusa

Department of Molecular Design and Engineering
Nagoya University

2007

Contents

Chapter I

General Introduction

1. 1. Outline

There are large numbers of polymer materials in our immediate circle. Polymer materials have an advantage in terms of the lightweight, high-strength, and fabrication convenience. Large parts of them have been used in bulk states, such as resins, fibers, and crystals. On the other hand, polymer thin films, which have some designed molecular order, can exhibit different material properties in a restricted geometry.[1] Many scientific and engineering investigations have been made to elucidate physical or chemical properties at interfaces of polymer materials, and have been attracted great attention for many technological applications.[2] Traditionally, polymer film coatings are made by physical attachment to the surface; *i. e.* cast, spin-casting, dip-coating and adsorption. The most widely applied method for polymer film coating is spin-casting because of its simple performance. Nonetheless, other methods are also important in light of fabrications of precisely controlled and organized structures (architectures).

For the syntheses of novel polymer materials, on the other hand, it is necessary to design primary structures and secondary structures. The primary structures include monomer design, polymerization control and copolymerization etc. The secondary structures include chain orientation or molecular alignment retaining polymer primary structures. In this case, light irradiation and thermal treatment largely influence the organization structures (Figure 1-1). This thesis proposes unique characteristics in polymer thin films and the stimuli-responsive property based on the organized structures. This work focuses on polymer brushes and block copolymers for fabrication of polymer thin films that exhibit unique photo- and thermo-responsive properties.

This introductory chapter summarizes the background and characters of thin films composed by polymers. First, the essential and common backgrounds including

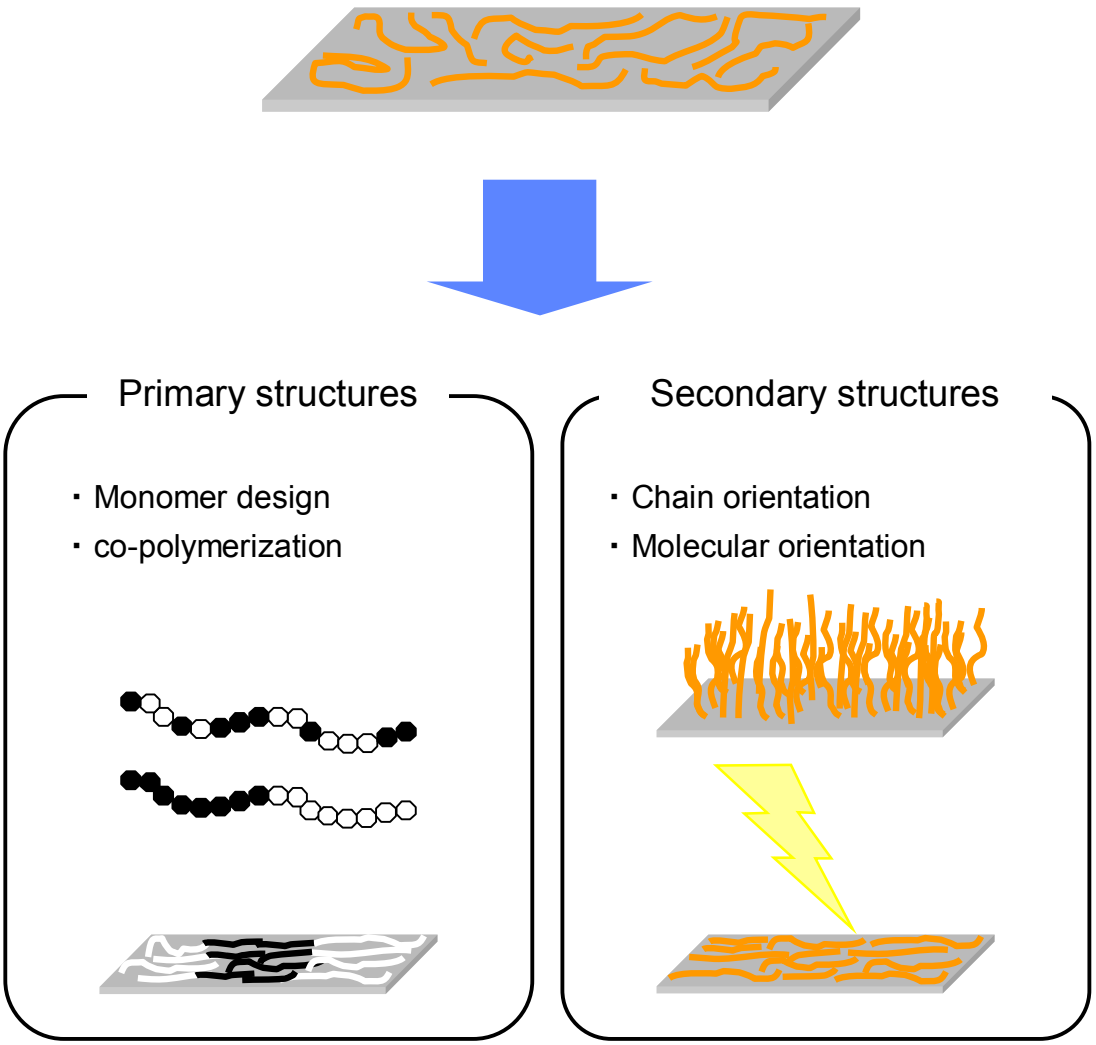

Figure 1-1. Schematic illustration of fabrication of polymer architectures by altering primary structures or secondary structures.

the basic behavior of polymer thin films are introduced. Next, two characteristic types of polymer layers, polymer brushes and monolayers of block copolymers, are separately described. The motivation of this thesis and chapter constitutions are finally described at the end of this chapter.

1.2. Characteristics of Polymer Thin Films

Polymer materials are unique in terms of interfacial behaviors. The organization and state of coils or segments of polymers adjacent to the interface are known to be deviated from those of the bulk. Their thermophysical properties and chemical properties of polymer thin films at interface influence the overall material performance.

1.2.1. Thermophysical Properties

The understandings of physical properties at surfaces and interfaces of polymeric materials are important in many technological applications. So, many experimental results have been reported on the glass transition temperature (T_g) in polymer thin films by means of spectroscopic methods and microscopic observations.[3-9]

The first report of a direct observation of T_g and its film thickness dependence of polystyrene (PS) films emphasized the influence of "liquid-like" surface layer by using ellipsometry.[3] Wu et al. reported that PS films on silicon native-oxide surfaces exhibit reductions of T_g as decreasing the film thickness by using X-ray reflectivity.[4] Their work also presented the importance of the interactions between the polymer and the substrate. The PS films' T_g on hydrophilic silicon substrates with thickness less than 40 nm is raised to a substantially higher temperature than that in bulk.[5] Kajiyama et al. examined the surface molecular motion of monodisperse polystyrene thin films by scanning viscoelasticity microscopy (SVM) in conjunction with lateral force microscopy (LFM). They found that T_g of the polymer in the vicinity of the surface is lowered than that of the bulk, and the discrepancy of T_g between surface and bulk becomes larger with the decreasing M_n (Figure 1-2).[6]

Prucker et al. studied influence of preparative ways to T_g of poly(methyl

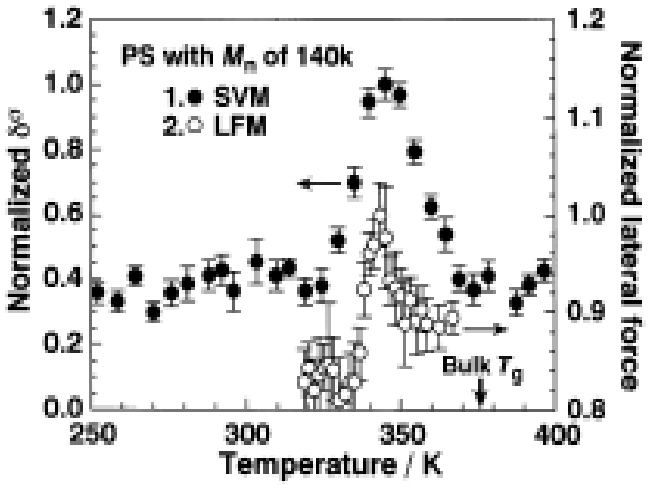

Figure 1-2. Temperature depencence of the surface phase lag, δ (by SVM) and lateral force (by LFM) for the PS films. T_g in the bulk state is of 103 °C was evaluated by DSC (taken from reference 6).

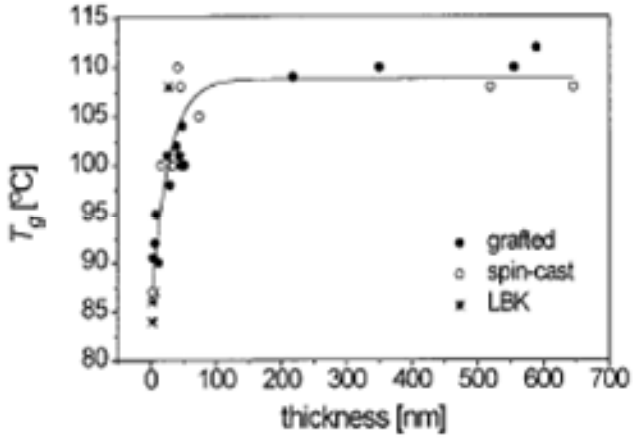

Figure 1-3. Summary of T_g values for PMMA films of varied thickness *d* prepared by different preparation methods, spin-cast films, grafted films, LB multilayers. (taken from reference 8).

methacrylate) (PMMA) thin films. They also observed depression of T_g for PMMA thin films prepared by different techniques, Langmuir-Blodgett multilayers, spincast films, and polymer grafted films. However, this effect appears to be independent of the internal architecture because all procedures used here exhibit essentially the identical results (Figure 1-3).[7,8] Tsujii and co-workers investigated T_g of high density PMMA grafted films. T_g observed in this state, in contrast, is about 8 °C higher than that in cast films.[9] They explained this phenomenon as an effect of end-grafted and an anisotropic structure of chain conformation.

Consequently, thermophysical properties of polymer thin films can be drastically influenced by film thickness, the nature of the substrate, and orientation of polymer chains.

1.2.2. Chain Orientations

Chain orientations of polymer are also affected by film thickness and preparation methods. It is known that the polymer chains in the thin films are preferentially oriented in the plane of the film.

Prest et al. found that the polymer chains such as polystyrene and polycarbonate is aligned in parallel to the substrate surface.[10,11] The orientation of polymer chain has been evaluated as a function of the coating conditions (film thickness, molecular weight, plasticizer content, casting solvent, and substrate temperature). Cohen et al. also studied the orientation of polystyrene in thin film in relation to the molecular weight.[12] Film of monodisperse low molecular weight (M_w = 800) polystyrene exhibit a high parallel orientation in a region very close to the substrate, but this orientation becomes disordered within 1 μm from the glass substrate. On the other hand, films of monodisperse high molecular weight material ($M_w = 1 \times 10^5$) exhibit much poorer orders, but it is also found that the long range order still exists to a thickness of 10 μm.

On the other hand, polymer thin films spread onto water surface are influenced by spreading solvents and their chain conformations are different even though same polymer is used. Kajiyama et al. investigated the conformation and packing of PS chains in two-dimensional ultrathin film of which the thickness is less than the polymer

dimension.[13,14] The two-dimensional PS ultrathin films were prepared by water casting method spread from cyclohexanone, and evaluated the radius of gyration of polymer chain by X-ray scattering and neutron scattering measurements. They found the morphology of thin film strongly depends on the spreadibility of the solution[13] and the packing of PS was looser than that in bulk state.[14] Kumaki reported that the formation monomolecular particle of PS with a diameter of ca. 50 nm is performed by spreading from a very dilute benzene solution (about 2×10^{-6} g / mL) onto a water surface.[15,16]

Nagano et al. reported a method to prepare ideally spread monolayers of fully hydrophobic polysilanes on water with the assistance of a polar liquid crystal molecule.[17,18] This procedure allows for precise evaluations of the conformational state of polymer chains near a solid surface by the stepwise LB depositions.[19]

1.2.3. Orientation of Organization Structures

In thinner region, not only physical properties of polymer chains but also meso-structures configured by themo are deviated. The orientation of liquid crystalline (LC) mesogen in polymer chains,[20,21,22] microphase separation of block copolymers[23, 24] in ultrathin film states have been reported.

The molecular orientation of LC polymers abruptly changed in the ultrathin films by X-ray scattering technique. Stamm et al. reported that the influence of solid interface and their ultrathin restriction affected the smectic layer and the orientation of LC polymers (Figure 1-4).[20,21]

Knoll et al. demonstrated that the morphology features produced by microphase separation of block copolymers are highly sensitive to the film thickness in the range below 100 nm. They also indicated that the film thickness is an important control parameter (Figure 1-5).[23] Seki et al. reported that out-of-plane and in-plane alignment of cylinder structures composed of microphase separation of photoresponsive liquid crystalline block copolymer are attained by patterned irradiation. Modulations in film thickness and polarization nature of the light control the out-of-plane and in-plane alignment of cylinders, respectively.[24]

As described above, the behavior of polymers at the interfaces are influenced

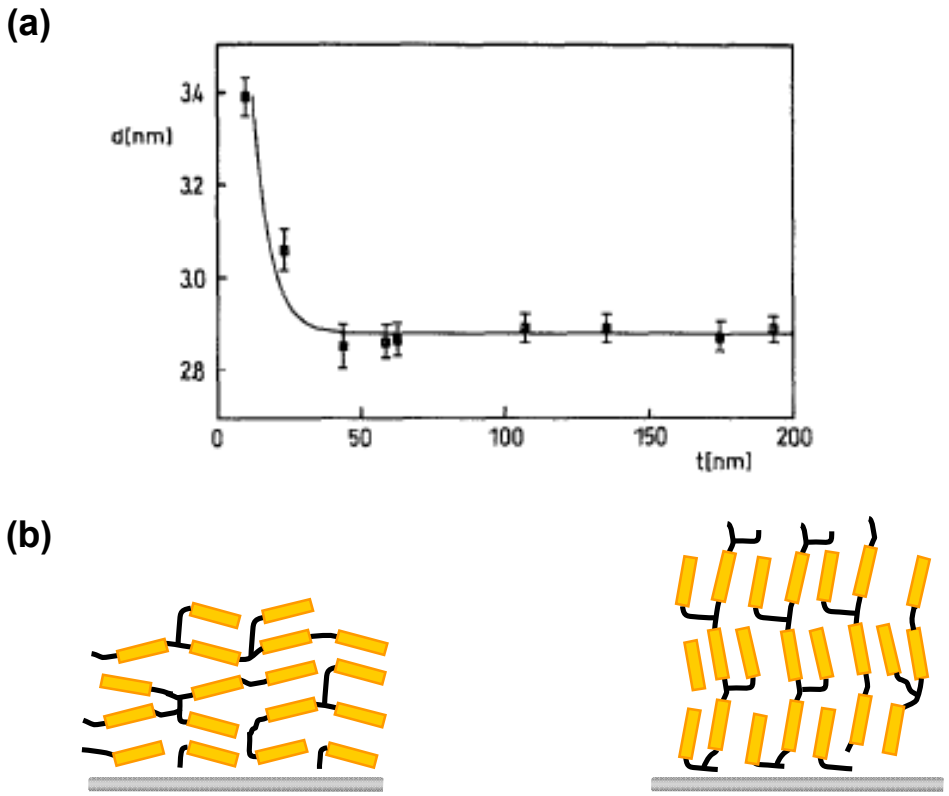

Figure 1-4. Layer spacing *d* of a smectic liquid crystalline polymers as a function of film thickness *t* (a), and schematic models of chain orientation depending on film thickness (b) (taken from reference 20).

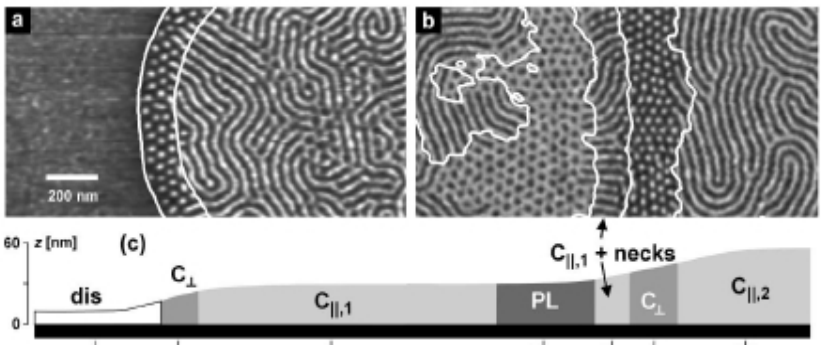

Figure 1-5. Thickness dependence of microphese separation composed of block copolymer thin films (taken from reference 23).

greatly by the presence of substrate surface. Thus, it is strongly expected that characteristic structures and properties in ultrathin films are attained when the chain state in the film is properly designed and altered. To tune the state of polymer chains, this work focuses on polymer brushes and block copolymers.

1.3. Polymer Brushes

Polymers brushes are one of the recently developed surface modification techniques, and now play important roles in many areas of science and technology, such as colloidal stabilization, adhesion, lubrication, tribology and rhology.[25] They refer to an assembly of polymer chains which are tethered by one end to a surface or an interface.[26,27] Tethering is sufficiently dense that the polymer chains are crowded and forced to stretch away from the surface or interface to avoid overlapping, sometimes much farther than the typical unstretched size of a chain. A series of discoveries show that the deformation of densely tethered chains affects many aspects of their behavior and results in many novel properties of polymer brushes. Moreover, their properties are affected by graft density of polymer brushes and polymer main chain's orientations. This section describes fabrication methods of the brushes and some characteristic properties of in comparisons with those of spincoated films.

1.3.1 Fabrication of Polymer Brushes

The polymer brushes can be synthesized by physisorption from solution or chemical vapor deposition ("graft-to" method) or surface-initiated polymerization ("graft-from" method) (Figure 1-6). Their main difference is the procedure by which polymers are attached to the surface.[25]

In "graft-to" method, preformed polymer chains are simply attached to a surface via chemical reaction or physical adsorption between the functional groups present on the surface and those along polymer chains. The advantage of such polymer assembly is that a molecular weight of grafted polymer chains is characterized. However, the disadvantage of this method is difficult to form a high density grafted polymer layers due to steric constraint caused by a previously grafted polymer chains. On the other hand,

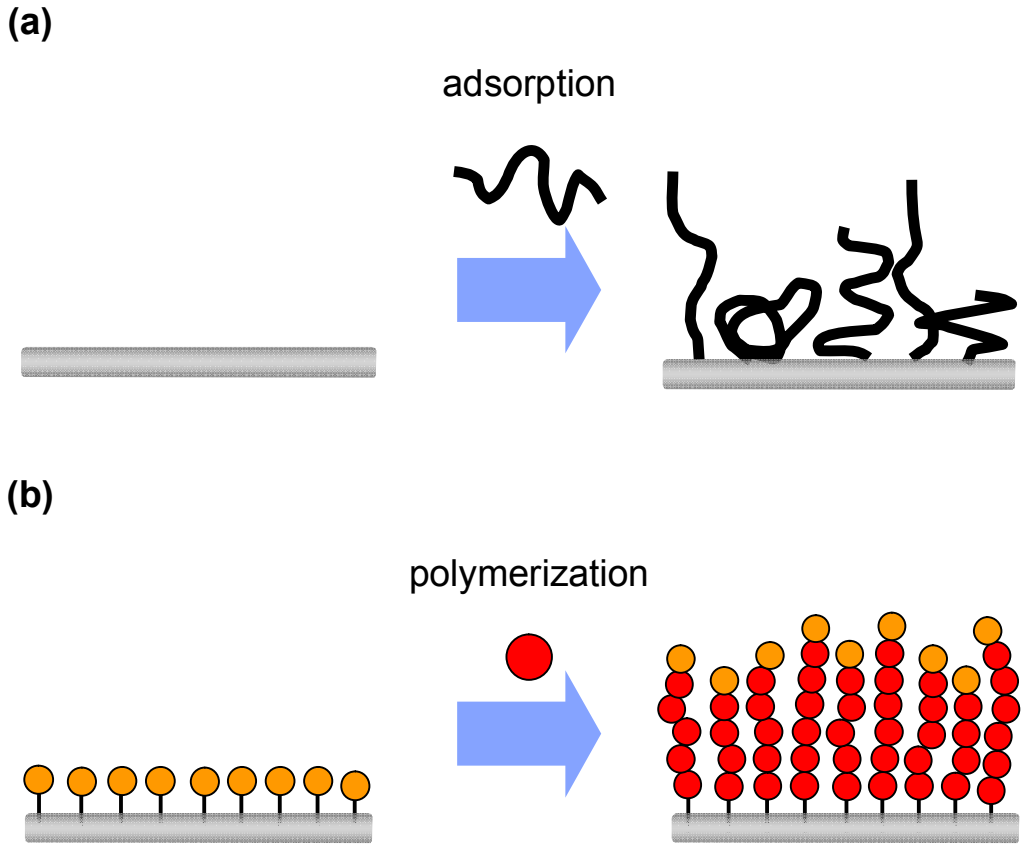

Figure 1-6. Schematic illustration of preparation method of polymer brushes; adsorption of polymers ("graft-to" method) (a), and surface-initiated polymerization ("graft-from" method) (b).

"graft-from" method indicates that polymer brushes are prepared by using surface-initiated polymerization from surface-bound polymerization initiators. The advantages of "graft-from" method over the "graft-to" method include, i) a high surface density of grafted polymer is achieved, and ii) variety monomers can be employed. Early works which prepared by "graft-from" method have focused on radical polymerization utilized by glow-discharge[28], corona-discharge,[29] and the self-assembled monolayer (SAM) techniques to immobilize initiator.[30] However, it is difficult to control the initiator amount when plasma and glow-discharge polymerization are used. Thus, many researchers in recent years reported polymer brushes synthesized from initiator-modified SAMs.[37-62]

All of the major polymerization systems have been applied to the surface-initiated synthesis of polymer brushes. Recently, living polymerization including anionic,[31] cationic,[32,33] ring-opening metathesis,[34,35] photo-iniferter[36] and living radical[37,38] polymerizations have been successfully applied to surface-initiated graft polymerization to prepare a polymer brushes controlled. In particular, living radical polymerization technique such as atom transfer radical polymerization (ATRP), nitroxide-mediated polymerization (NMP) and reversible addition-fragmentation chain transfer (RAFT) polymerization has been most widely used.[39,40,41,42] The advantage of living polymerization is that all polymer chains grow slowly and nearly simultaneously. However, the characterizations of the formed polymers are not easy tasks because of low concentration of dormant species immobilized on substrates. Therefore, the graft polymerization is monitored by added the free initiator[39] or the appropriate amount of the capping agent like $CuCl_2$ or $CuBr_2$.[41] With additional free initiator, number-average molecular weight (M_n) of grafted polymer and free polymer produced from free initiator are almost same, and the amount of graft polymer is proportional to the M_n of free polymers (Figure 1-7). The surface density of the polymer chains obtained in this way is so high that the polymer chains are forced to stretch along the direction normal to the graft surface.

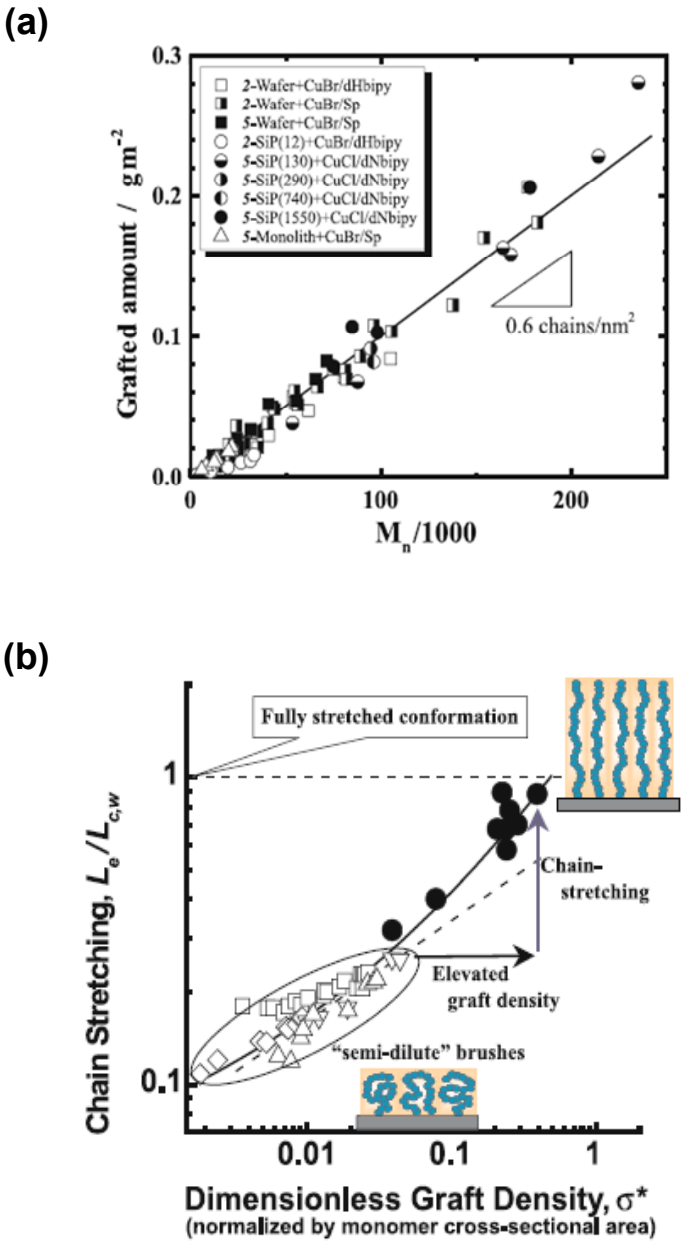

Figure 1-7. Relationship between the amount of graft polymers and M_n of free polymers. The graft polymerization was carried out under various conditions (taken from reference 37).

1.3.2. Graft Densities and Their Properties

The conformation of polymers can be drastically changed by the graft density (Figure 1-8). At low graft densities, polymer conformation is shrunk and their coil dimension resembles that of ungrafted (free) polymer chains. This structure assumes a "mushroom" or "pancake" conformation. With increasing graft density, polymer chains will be obliged to stretch away from the surface, forming the so-called "semi-dilute polymer brush", in which polymer chains overlap with each other. Structure and properties of semi-dilute polymer brushes are relatively well understood experimental and theoretical aspects. Furthermore with increasing graft density, "concentrated brush" or "high density brush", for which graft chains are expected to exhibit different properties from those in the semi-dilute brushes due to higher-order interactions between graft chains.

The high density polymer brushes have characteristic properties quite different and unpredictable from those of the moderately or low dense polymer brushes, such as glass transition temperature (T_g),[7,8,9] tribological property,[43,44,45] wettability, adhesion properties,[46] and so on. Takahara et al. reported that the friction coefficient of high density PMMA brushes was lower than that of spincast films (Figure 1-9).[43] On the other hand, the adsorption behavior of proteins on poly(2-hydroxyethyl methacrylate) brushes as a function of graft density was investigated. The high density brush leads to no protein adsorption and the low density one adsorbed proteins.[46]

1.3.3. Functionalized Polymer Brushes and Their Stimuli-Responsiveness

Since living radical polymerizations are tolerable to various types of monomers, many researchers have been investigated the fabrication and their surface properties of various functional polymer brushes, such as glycopolymers,[47] polyelectrolytes,[48,49] hydrophilic,[50,51,52] cross-linkable,[53] thermo-responsive,[54,55,56] bioconjugated,[57,58] photo-functional,[59,60] electro chemically active,[61] and liquid crystalline polymers.[62] The functionalized monomers reported previous literatures were summarized in Figure 1-10.

There is also an increasing interest of polymer brushes for 'smart' or responsive

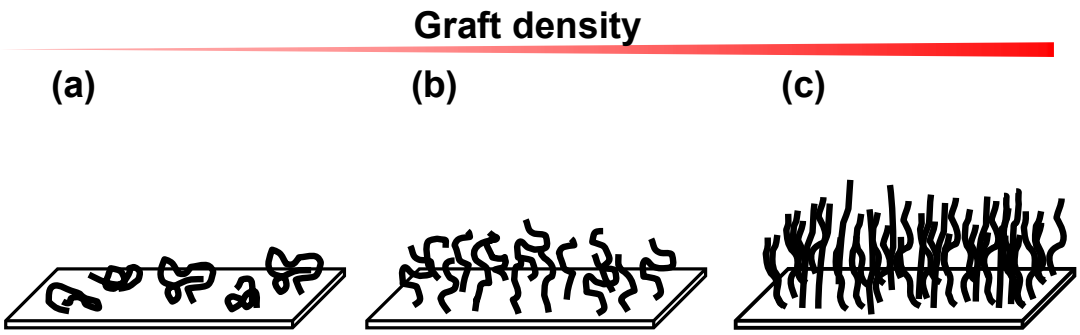

Figure 1-8. Schematic illustrations of the conformations of grafted polymer chains; 'mushroom' (a), semi-dilute brush (b) and concentrated brush (c).

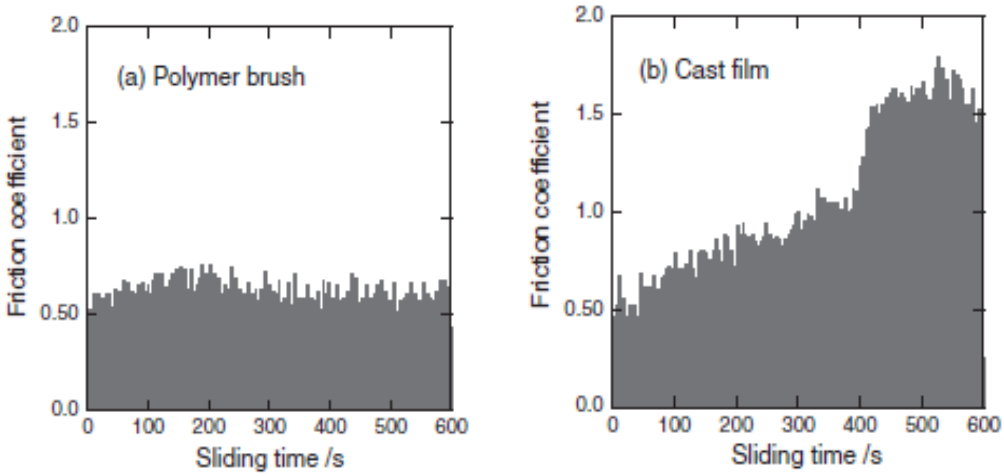

Figure 1-9. Time dependence of friction coefficient of PMMA brush (a) and cast films (b) under a load of 0.49 N at a sliding velocity of 90mm / min (taken from reference 43).

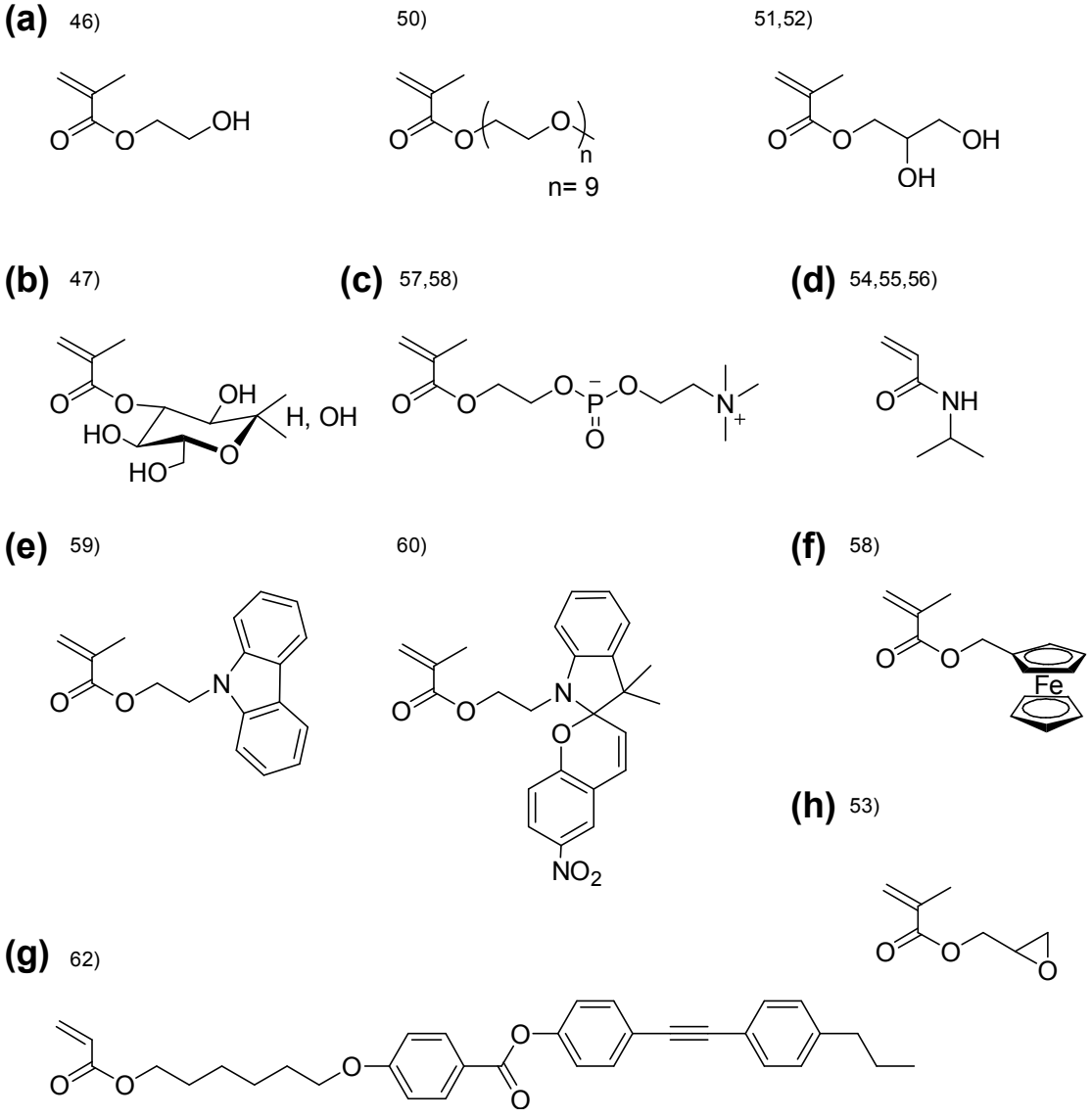

Figure 1-10. Chemical structures of typical functionalized monomers; hydrophilic (a), glycopolymer (b), bio-conjugated (c), thermal-responsive (d) photo-functional (e) electro-functional (f), liquid crystalline (g) and cross-linkable (h) monomers.

surfaces, which can change a physical property upon an external stimuli such as light, electron, temperature, pH and so on. In particular, thermo-responsive polymer brushes have been reported extensively for application to biointerface. Balamurugan et al. investigated the thermally induced hydration of poly(*N*-isopropylacrylamide) (PNIPA) brush by surface plasmon resonance spectroscopy and water contact angle measurement.[54] The water contact angle indicated a sharp wettability transition around 32 °C consistent with the low critical solution temperature. In contrast, several reports have been dealt with photo-responsive and liquid crystalline brushes.[59,60,62]

1.4. Langmuir-Blodgett Technique

The fundamental procedure of the Langmuir-Blodgett technique was reported by Pockels as early as in 1891.[63] She performed monolayer formation of amphiphiles spread at the air-water interface and monitored their compression by moving a barrier. In 1917, Langmuir reported the study of two-dimensional organization of molecular thin films at the air-water interface as the genesis Pochel's experiment.[64] Moreover, spread monolayers can be transferred onto solid substrates.[65,66] The studies about LB film are expanded to a functional molecules such as dye, liquid crystal and photochromic molecules.[67]

So far, LB technique is applicable not just for low molecules but for polymeric materials. Polymer monolayers are alluring research target because precise structural and conformational control of chains can be achieved at molecular levels. In the next section, polymer LB films and their applications are described.

1.4.1. Polymer Monolayers

The monolayers of synthetic polymer were first described by Katz and Samwel in 1928.[68] Since then, the numerous numbers of knowledge have been reported to the Langmuir monolayer of polymers and their spreading behavior,[69] In general, polymer chains adopt different conformations in solutions and at the air-water interface. In solutions, polymers generally exist as random three-dimensional coils whose bounding dimensions are a few tens of nanometers.[69,70] When the polymer solution is cast onto

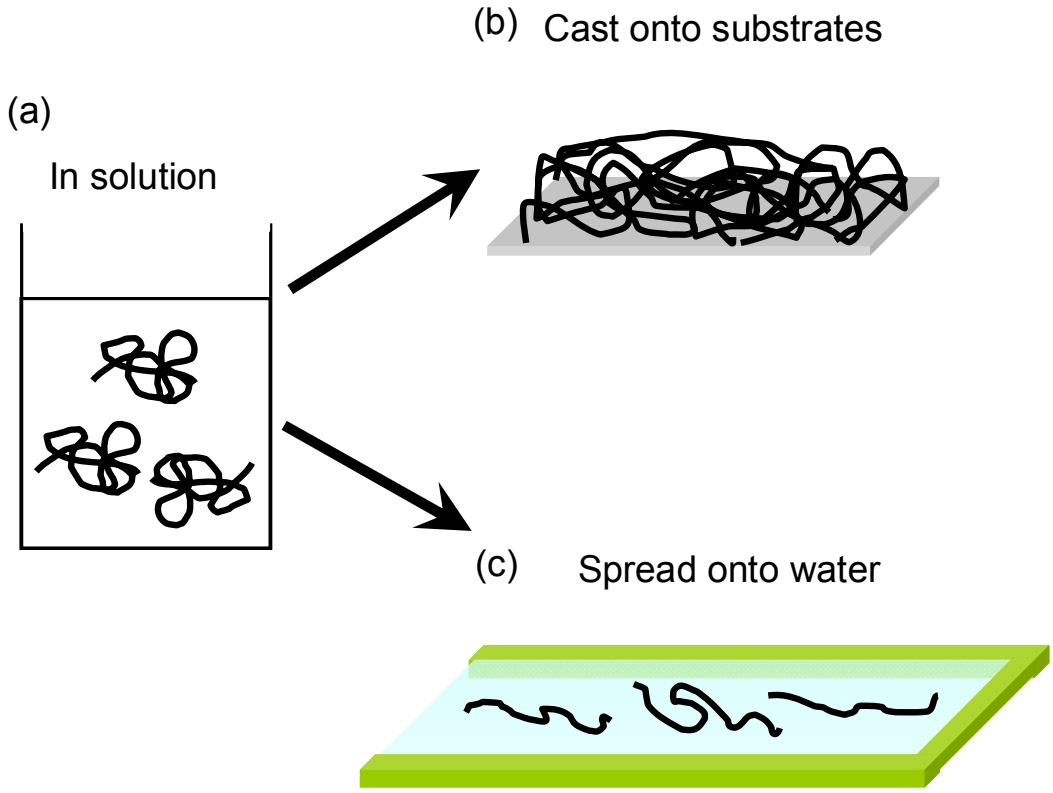

Figure 1-11. Schematic illustration of polymer conformations; from three-dimensional coil in solution (a) to cast onto substrates (b) and spread polymers at the air-water interface (c)

substrates, the polymer chains are usually in random orientations. In contrast, they are stretched upon spreading on water, and the polymer chains are assumed to be extended with the repeating units being adsorbed on the air-water interface (Figure 1-11). Thus, LB technique may provide polymer thin films showing characteristic features derived from the extended conformations.

The study of polymer monolayers has been expanded from homopolymer[68,69,71] in earlier to various copolymers such as random,[72,73] block,[74,75] telechelic[76,77] copolymers nowadays. Especially, explorations using block copolymers have been rapidly extending because they form self-assembled regular periodic microstructures as well as the persistence lengths of the each block that will be of particular use for nanotechnologies for next generation. In the next section, surface patterns formed by block copolymers at the air-water interface are briefly described.

1.4.2. Surface Patterns of Block Copolymers and Their Morphological Changes

Block copolymers are useful materials that form nanometer-scale ordered microphase separated patterns in bulk films,[78,79,80] thin films, micelles in solution,[81] and at air-water interface.[75,82] Particularly, monolayers are attracting research target because of the feasibility of precise structure control. When block copolymers are spread on water, characteristic two-dimensional morphologies are formed based on microphase separation.

In a series of publications Eisenberg and Lennox et al. demonstrated the preparation of two-dimensional surface micelles on the air-water interface.[83,84,85,86] When various amphiphilic block copolymers containing a hydrophobic PS segment are spread onto water surface, two-dimensional surface micelle aggregates are formed. The resulting aggregate structures are altered by many experimental conditions such as the nature of the block copolymer, the relative block size and the amount of material spread on water and experimental parameters such as solubility or concentration of solution, subphase temperature and compression speed (Figure 1-12).[87,88,89] Baker et al. observed the morphologies of a predominantly hydrophobic polystyrene-*block*-poly(ethylene oxide) (PS-PEO) monolayers by using atomic force microscopy, and found significant

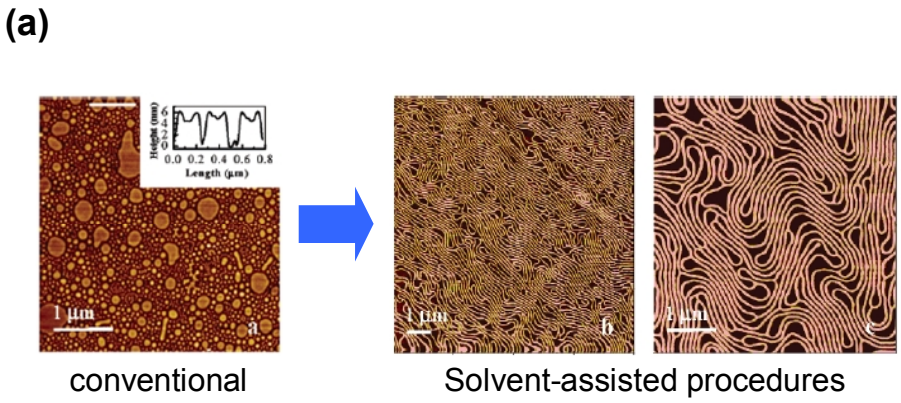

Figure 1-12. Examples of process-dependent morphological changes of block copolymer monolayers; "solvent-assisted procedures" (a) (taken from reference 87), and solvent concentration dependence of surfacemorphologies (b) (taken from reference 89).

effects of the concentration of the spreading solution on the resulting 2D morphologies.[89,90]

The factors affecting the spread behavior and resulting morphologies are dissipative, and thus have not been well understood.

1.5. Motivation of This Thesis

This thesis is focused on polymer thin films, in particular, interplays between the surface and polymer materials. As mentioned in Section 1.2., polymer thin films are dramatically influenced by the substrate surface. For creation of characteristic structures and properties, the development of new methods to tune-up the polymer chain conformations is important. Thus, this thesis summarizes my new findings in the systems of polymer brushes (surface-initiated polymerization) and Langmuir-Blodgett films in the above respects.

Photo-Responsive Polymer Brushes

This topics in the former part of this thesis focus on molecular orientation of LC mesogens in polymer brushes and the control of molecular alignment by irradiation with light. Many studies on thermo- and pH-responsive polymer brushes have been reported at various research fields, such as bio-interface,[59] cell culture substrates[91] and chromatography.[92,93] In contrast, polymer brushes for application to photonic or electronic device have outnumbered so far.[59,60,62] Thus, it should be of great value to extend the study of liquid crystalline polymer materials and photo-functionalized materials.

In this study azobenzene (Az) is employed as the photochromic molecules. The Az derivatives have been studied widely because of their simple chemical structures, wide possibility of chemical modification, and acceptable photofatigue resistance. Numerous efforts have been made to understand photoisomerization behavior of Az in polymer matrices. In particular, optical anisotropy at molecular levels has been established.[94,95,96] The previous works on the liquid crystalline Az-polymer thin films have been limited to spincast films,[97,98] monolayers and LB multilayers.[99] No research

has been undertaken for the photoorientation in grafted films. This is the first attempt to fabricate photoresponsive grafted chains on a solid substrate.

Temperature Dependency of Spreading Behaviors in Block Copolymers

To tune or modify the nanopatterns by external stimuli such as light or temperature is a challenging attempt. In our laboratory, a novel triblock copolymer composed of Az containing-polymethacrylate and poly(ethylene oxide) (PEO) exhibits light-tunable phase separation behavior on water and substrate surfaces.[100,101] For tuning by light, however, photo-responsive unit are required in block copolymer. The same tendency is true for thermo-response.

The latter part of work in this thesis has started with my serendipitous finding. A very sharp temperature dependent area changes at the air-water interface are observed, when a conventional block copolymer such as polystyrene-*block*-poly(4-vinyl pyridine) without particular thermo-responsive segment is spread onto water surface. Unexpectedly, this phenomenon is only observed when a theta solvent for polystyrene with low evaporation rate is employed. The new knowledge obtained here should be of help in fundamental understandings in polymer chain conformations and in polymer thin film technology. Thus, great efforts are made here for understanding of this particular phenomenon.

1.6. Scope of This Thesis

Based on the above mentioned backgrounds, this work has been conducted to pave ways in such untrampled areas of polymer thin films. Unique organization structures are prepared by using graft polymerization or LB method. For possible applications, their structures are altered by external stimuli such as light or temperature. This thesis describes two regions of research areas, a photo-responsive liquid crystalline polymer brushes (Chapter II, III and IV) and a thermal-dependency of block copolymer thin films (Chapter V and VI).

In Chapter II, synthesis of novel LC polymer brushes containing Az moiety by surface-initiated living radical polymerization and their molecular orientation of mesogen

are investigated. The molecular orientations are also evaluated in comparisons with those of spincast films.

Chapter III describes the photoalignment of LC mesogen on the graft films. The in-plane photoalignment of Az mesogens in polymer chains grafted to the substrate is achieved by irradiation of linearly polarized visible light. Their particular mesogenic orientation may lead to different photo-responsive nature from that in spincast films.

In Chapter IV, the effect of graft density is investigated. Low density Az-polymer grafted substrates are synthesized from sparsely introduced surface-initiator on the substrates. This approach should be of great significance in that the parameter of graft density is particularly important parameter to define various properties.

Chapter V and Chapter VI describes the sharp temperature dependence of amphiphilic block copolymer thin films observed at the air-water interface by LB technique. In Chapter V, novel characteristic spread behaviors of conventional amphiphilic block copolymer are observed. The mechanism of this finding is discussed.

Chapter VI emphasizes the siginificant role of polystyrene block for the expression of the strong temperature dependency. To justify this assumption, amphiphilic block copolymers having other hydrophilic blocks and those with various polystyrene composition copolymers are used.

Finally, the significance of this thesis and referred to the outlook for future evolutions are summarized in Chapter VII.

Reference

[1] Swalen, J. D. *Organic Thin Films Structure and Applications*, Frank, C. W. (Ed.), ACS, **1998** Chapter 1 pp2.

[2] Garbassi, F.; Morra, M.; Occhiello, E. *Polymer Surfaces, from Physics to Technology*, Wiley, **1994**.

[3] Kaddie, J. L.; Jones, P. A. L.; Cory, R. A. *Europhys. Lett.* **1994**, 27, 59.

[4] Orts, W. J.; Zanten, J. H.; Wu, W.; L.; Satija, S. K. *Phys. Rev. Lett.* **1993**, 71, 867.

[5] Wallace, W. E.; van Zanten, J. H.; Wu, W. L. *Phys. Rev.* **1995**, E 52, 3329.

[6] Kajiyama, T.; Tanaka, K.; Satomi, N.; Takahara, A. *Sci. and Tech. of Adv. Mater.* **2000**, 1, 31.

[7] Prucker, O.; Christian, S.; Bock, Harald, Rühe, J.; Frank, C. W.; Knoll, W. *Organic Thin Films Structure and Applications*, Frank, C. W. (Ed.), ACS, **1998** Chapter 17 pp233.

[8] Prucher, O.; Christian, S.; Bock, H.; Rühe, J.; Frank, C. W.; Knoll, W. *Macromol. Chem. Phys.* **1998**, 199, 1435.

[9] Yamamoto, S.; Tsujii, Y.; Fukuda, T. *Macromolecules* **2002**, 35, 6077.

[10] Prest, W. M.; Luca, D. J. *J. Appl. Phys.* **1980**, 51, 5170.

[11] Prest, W. M.; Luca, D. J. *J. Appl. Phys.* **1979**, 50, 6067.

[12] Cohen, Y.; Reich, S. *J. Polym. Sci.: Polym. Phys.* **1981**, 19, 599.

[13] Shuto, K.; Oishi, Y.; Kajiyama, T.; Han, C. C. *Polymer Journal* **1993**, 25, 291.

[14] Shuto, K.; Oishi, Y.; Kajiyama, T.; Han, C. C. *Macromolecules* **1993**, 26, 2589.

[15] Kumaki, J. *Macromolecules* **1986**, 19, 2258.

[16] Kumaki, J. *Macromolecules* **1988**, 21, 749.

[17] Nagano, S.; Seki, T.; Ichimura, K. *Chem. Lett.* **2000**, 613.

[18] Nagano, S.; Seki, T.; Ichimura, K. *Langmuir* **2001**, *17*, 2199.

[19] Nagano, S.; Seki, T. *J. Am. Chem. Soc.* **2002**, *124*, 2074.

[20] Mensinger, H.; Stamm, M.; Boeffel, C. *J. Chem. Phys.* **1992**, 96, 3183.

[21] Henn, G.; Stamm, M.; Poths, H.; Rücher, M.; Rabe, J. P. *Physica B*, **1996**, 221, 174.

[22] Elben, H.; Strobl, G. *Macromolecules* **1993**, 26, 1013.

[23] Knoll, A.; Horvat, A.; Lyakhova, K. S.; Kraush, G.; Sevink, G. J. A.; Zvelindovsky, A. V.; Magerle, R. *Phys. Rev. Lett.* **2002**, 89, 035501

[24] Morikawa, Y.; Nagano, S.; Watanabe, K.; Kamata, K.; Iyoda, T.; Seki, T. *Adv. Mater.* **2005**,

[25] Advincula, R. C.; Brittain, W. J.; Caster, K. C.; Rühe, J. (Ed.) *Polymer Brushes*, WILEY-VCH, **2004**.

[26] Milner, S. T. *Science* **1991**, 251, 905.

[27] Zhao, B.; Brittain, W. J. *Prog. Polym, Sci.* **2000**, 25, 677.

[28] Ito, Y.; Ochiai, Y.; Park, Y. S., Imanishi, Y. *J. Am. Chem. Soc.* **1997**, 119, 1619.

[29] Iwasaki, Y.; Sawada, S.; Nakabayashi, N.; Khang, G.; Lee, H. B.; Ishihara, K. *Biomaterials* **1999**, 20, 2185.

[30] Hamann, R.; Laible, R. *Angew. Makromol. Chem.* **1975**, 48, 97.

[31] Jordan, R.; Ulman, A.; Kang, J. F.; Rafailovich, M. H.; Sokolov, J. *J. Am. Chem. Soc.* **1999**, 121, 1016.

[32] Zhao, B.; Brittain, W. J. *J. Am. Chem. Soc.* **1999**, 121, 3557.

[33] Advincula, R. *Adv. Polym. Sci.* **2006**, 197, 107.

[34] Jordan, R.; Ulman, A. *J. Am. Chem. Soc.* **1998**, 120, 243.

[35] Buchmeiser, M. R. *Adv. Polym. Sci.* **2006**, 197, 137.

[36] Matsuda, T. *Adv. Polym. Sci.* **2006**, 197, 67.

[37] Tsujii, Y.; Ohno, K.; Yamamoto, S.; Goto, A.; Fukuda, T. *Adv. Polym. Sci.*, **2006**, 197, 1.

[38] Edmondoson, S.; Osborne, V. L.; Huck, W. T. S. *Chem. Soc. Rev.*, **2004**, 33, 14.

[39] Ejaz, M.; Yamamoto, S.; Ohno, K.; Tsujii, Y.; Fukuda, T. *Macromolecules*, **1998**, 31, 5934.

[40] Zhao, B.; Brittain W. J. *J. Am. Chem. Soc.*, **1999**, 121, 3557.

[41] Matyjaszewski, K.; Miller, P. J.; Shukla, N.; Immarapom, B.; Gelman, A.; Luokala, B. B.; Siclovan, T. M.; Kickelbick, G.; Vallant, T.; Hoffmann, H.; Pakula, T. *Macromolecules*, **1999**, 32, 8716.

[42] Husseman, M.; Malmström, E.; McNamara, M.; Mate, M.; Mecerreyes, D.; Benoit, D. G.; Hedrick, J. L.; Mansky, P.; Huang, E.; Russell, T. P.; Hawker, C. J. *Macromolecules*, **1999**, 32. 1424.

[43] Sakata, H.; Kobayashi, M.; Otsuka, H.; Takahara, A. *Polym. J.* **2005**, 37, 767.

[44] Yamamoto, S.; Ejaz, M.; Tsujii, Y.; Fukuda, T. *Macromolecules* **2000**, 33, 5602.

[45] Yamamoto, S.; Ejaz, M.; Tsujii, Y.; Fukuda, T. *Macromolecules* **2000**, 33, 5608.

[46] Yoshikawa, C.; Goto, A.; Tsujii, Y.; Fukuda, T.; Kimura, T.; Yamamotto, K.; Kishida, A. *Macromolecules* **2006**, 39, 2284.

[47] Ejaz, M.; Ohno, K.; Tsujii, Y.; Fukuda, T. *Macromolecules* **2000**, 33, 2870.

[48] Rühe, J.; Ballauff, M.; Biesalski, M.; Dziezok, P.; Grohn, F.; Johannsmann, D.; Houbenov, N.; Hugenberg, N.; Konradi, R.; Minko, S.; Motornov, M.; Netz, R. R.; Schmidt, M.; Seidel, C.; Stamm, M.; Stephan, T.; Usov, D.; Zhang, H. N. *Adv. Polym. Sci.* **2004**, 165, 79.

[49] Ohsedo, Y.; Takashina, R.; Gong, J. P.; Osada, Y. *Langmuir* **2004**, 20, 6549.

[50] Ma, H.; Hyun, J.; Stiller, P.; Chilkoti, A. *Adv. Mater.* **2004**, 16, 338.

[51] Kobayashi, M.; Takahara, A. *Chem. Lett.* **2005**, 34, 1582.

[52] Kobayashi, M.; Takahara, A. *Tran. Mater. Res. Soc. Jpn.* **2005**, 30, 647.

[53] Edmondson, S.; Huck, W. T. S. *J. Mater. Chem.* **2004**, 14, 730.

[54] Balamurugan, S.; Mendez, S.; Balamurugan, S. S. O'Brien, M. J.; López, G. P. *Langmuir* **2003**, 19, 2545.

[55] Jones, D. M.; Smith, J. R.; Huck, W. T. S. *Adv. Mater.* **2002**, 14, 1130.

[56] Kaholek, M.; Lee, W.-K.; Ahn, S.-J.; Ma, H.; Caster, K. C.; LaMattina, B.; Zauscher, S. *Chem. Mater.* **2004**, 16, 3688.

[57] Iwata, R.; Suk-In, P.; Hoven, V. P.; Takahara, A.; Akiyoshi, K.; Iwasaki, Y. *Biomacromolecules*, **2004**, 5, 2308.

[58] Feng, W.; Brash, J.; Zhu, S. *J. Polym. Sci. A Phys. Chem.*, **2004**, 42, 2931.

[59] Ito, S.; Kuno, J.; Yamashita, K.; Ohoka, M.; Ohkita, H.; Tsujii, Y.; Fukuda, T. *Trans. Mater. Res. Soc. Jpn.*, **2005**, 30, 687.

[60] Piech, M.; Bell, N. S. *Macromolecules* **2006**, 39, 915.

[61] Sakakiyama, T.; Ohkita, H.; Ohoka, M.; Ito, S.; Tsujii, Y.; Fukuda, T. *Chem. Lett.*, **2005**, 34, 1366.

[62] Hamelinck P. J.; Huck, W. T. S. *J. Mater., Chem.*, **2005**, 15, 381.

[63] Pockels, A. *Nature* **1891**, 43, 437.

[64] Langmuir, I. *J. Am. Chem. Soc.* **1917**, 39, 1848.

[65] Blodgett, K. B. *J. Am. Chem. Soc.* **1935**, 57, 1007.

[66] Blodgett, K. B.; Langmuir, I. *Phys. Rev.* **1937**, 51, 964.

[67] Ulman, A. *An Introduction to Ultrathin Organic Films from Langmuir-Blodgett to Self-Assembly* Academic press, **1991**.

[68] Katz, J. R.; Samwell, P. J. P. *Naturewissenschaften* **1928**, 16, 592.

[69] Gaines, G. L. *Langmuir* **1991**, 7, 834.

[70] Strobl, G. R. *The Physics of Polymers*, Berlin, **1996**.

[71] Mumby, S. J.; Swalen, J. D.; Rabolt, J. F. *Macromolecules* **1986**, 19, 1054.

[72] Watanabe, M.; Kosaka, Y.; Sanui, K.; Ogata, N. *Macromolecules* **1987**, 20, 452.

[73] Laschewsky, A.; Ringsdorf, H.; Schmit, G.; Schneider, J. *J. Am. Chem. Soc.* **1987**, 109, 788.

[74] Niwa, M.; Hayashi, T.; Higashi, N. *Langmuir* **1990**, 6, 263.

[75] Cox, J. K.; Eisenberg, A.; Lennox, R. B. *Curr. Opin. Colloid Interface Sci.***1999**, *4*, 52.

[76] Goedel, W. A. *Organic Thin Films Structure and Applications*, Frank, C. W. (Ed.), ACS, **1998** Chapter 2 pp10.

[77] Heger, R.; Goedel, W. A. *Macromolecules* **1996**, 29, 8912.

[78] Park, C.; Yoon, J.; Thomas, E. L. *Polymer* **2003**, *44*, 6725.

[79] Hadjichristidis, N.; Pispas, S.; Floudas, G. *Block Copolymers: Synthetic Strategies, Physical Properties, and Applications*, Wiley-interscience, **2003**.

[80] Hamley, I. W. *Developments in Block Copolymer Science and Technology*, Wiley, **2004**.

[81] Hamley, I. W. *Block Copolymers in Solution: Fundamentals and Applications*, Wiley, **2005**.

[82] Hamley, I. W. *Developments in Block Copolymer Science and Technology*, Wiley, **2004**.

[83] Zhu, J.; Eisenberg, A.; Lennox, B. R. *J. Am. Chem. Soc.* **1991**, 113, 5583.

[84] Zhu, J.; Eisenberg, A.; Lennox, R. B. *Langmuir* **1991**, *7*, 1579.

[85] Zhu, J.; Eisenberg, A.; Lennox, R. B. *Macromolecules* **1992**, *25*, 6547.

[86] Meli, M.-V.; Badia, A.; Gru¨tter, P.; Lennox, R. B. *Nano Lett.* **2002**, *2*, 131.

[87] Lu, Q.; Bazuin, C. G. *Nano Lett.* **2005**, *5*, 1309.

[88] Seo, Y.; Paeng, K.; Park, S. *Macromolecules* **2001**, 34, 8735.

[89] Devereaux, C. A.; Baker, S. M. *Macromolecules* **2002**, 35, 1921.

[90] Baker, S. M.; Leach, K. A.; Devereaux, C. A.; Gragson, D. E. *Macromolecules* **2000**, 33, 5432.

[91] Okano, T.; Yamada, N.; Sakai, H.; Sakurai, Y. *J. Biomed. Mater. Res.* **1993**, 27, 1243.

[92] Kanazawa, H.; Yamamoto, K.; Matsushima, Y.; Takai, N.; Kikuchi, A.; Sakurai, Y.; Okano, T. *Anal. Chem.* **1996**, 68, 100.

[93] Huang, X.; Wirth, M.J. *Anal. Chem.* **1997**, 69, 4577.

[94] Fisher. Th.; Läsker, L.; Stumpe, J.; Kostromin, S. G. *J. Photochem. Photobiol. A: Chem.* **1994**, 80, 453

[95] Ikeda, T. *J. Mater. Chem.* **2003**, 13, 2037.

[96] Ichimura, K. *Chem. Rev.* **2000**, 100,1847.

[97] Geue, T.; Ziegler, A.; Stumpe, J. *Macromolecules* **1997**, 30, 5729.

[98] Han, M.*'Photoorientation Behavior of Azobenzene Side Chains Attached to Liquid Crystalline Polymers'* Doctral thesis, Tokyo Institute of Technology, **2000**

[99] Stumpe, J.; Geue, T.; Fishcer, T.; Menzel, H. *Thin Solid Films* **1996**, 284, 606.

[100] Kadota, S.; Aoki, K.; Nagano, S.; Seki, T. *J. Am. Chem. Soc.* **2005**, 127, 8266.

[101] Kadota, S.; Aoki, K.; Nagano, S.; Seki, T. *Coll. and Surf. A Phys. Eng. Asp.*, **2006**, 284-285, 535.

Chapter II

Synthesis and the Molecular Orientation of Liquid Crystalline Polymer Brushes Containing Azobenzene Mesogens

2.1. Introduction

Polymers brushes provide fascinating classes of flexible surfaces with various functionalities. They are defined as dense layers of end-grafted polymer chains confined to a solid surface or interface.[1,2,3] The formation of these tethered chains is generally carried out using either of two techniques; physisorption or chemical bonding of chains to an interface, and called "graft to" or "graft from" technique, respectively. In the "graft to" method, preformed polymer chains containing a suitable end-functionalized group are reacted with a surface to obtain the brush. A "graft from" method is utilized in which the polymer brush layer is generated in situ from a surface immobilized initiator.[4] Recently, high graft density and well defined polymer brush structures have been developed by using the surface initiated controlled/"living" radical polymerization techniques.[5,6,7,8] The advantage of living polymerization is quantitative initiation, which means that polymers are propagated efficiently from the initiator on a substrate. As a result, it is sufficient to afford a high density brush because of the steric hindrance of the growing polymer. The surface density of the polymer chains is so high that the polymer chains are forced to stretch along the direction normal to the graft surface. Atom transfer radical polymerization (ATRP) is one of the several controlled/"living" radical polymerization techniques that have been attracting much attention as a new route to well-defined polymers with low polydisperties.[9,10] The process involves the activation-deactivation processes mediated by halogen transfer is catalyzed by transition metal complex, which occurs repeatedly on the halogenated sites on surface. This situation allows all graft chains to grow almost simultaneously in a controlled fashion. Since ATRP is tolerable to various types of monomers, many functional polymer brushes can be designed.

Introduction of liquid crystal (LC) properties into the surface-graft chains seems of great interest in view of fabrication of "smart" responsive surfaces.[11,12,13,14] Halperin and Williams designed main chain LC polymer brushes that form a nematic LC. The polymer chains stretches and begins to tilt to avoid excluded interaction from the surface when the surface anchoring energy are higher, favoring a homeotropic alignment as a consequence.[11] Peng et al. synthesized side chain-type LC polymer brushes by free radical polymerization aiming to apply for an LC alignment layers.[12] The polymer chains in this case exhibit high polydispersities, and thus planer alignment is not achieved without pretreatment of rubbing on the substrate.[13] On the other hand, Huck et al. synthesized nematic LC polymer brushes by surface-initiated ATRP, and found that their mesogens aligned homeotropically. The orientation control between homeotropic and homogeneous alignment of nematic LC molecules is achieved on a patterned surface of the grafted and non-grafted regions.[14] However, above papers only report the preparation procedures of LC polymer brushes and the behavior of low molecular LC orientation in LC cells. Detailes such as molecular orientation of LC mesogens in the brush chains is not elucidated.

In this chapter, synthesis of novel LC polymer brushes containing Az moiety by surface-initiated ATRP and their molecular orientation of mesogen are investigated. Further, the packing state and molecular orientations were evaluated in comparisons with those of spincast films of the identical LC polymer. Here a unique orientation behavior of a smectic LC state in the thin films prepared by the surface-initiated polymerization is unveiled.

2.2. Experimental Section

2.2.1. Materials

Starting compounds for syntheses were purchased from Tokyo Kasei Kogyo (TCI Inc.), Aldrich Co. and Kanto Kagaku. Copper Bromide (CuBr) was washed with acetic acid and diethyl ether for several times, and dried in vacuum.[15,16] *N*, *N*'-Dimethyl formamide (DMF) as solvent was dehydrated by distillation from calcium hydride. Tetrahydrofuran (THF) and toluene as solvents were dehydrated by distillation from

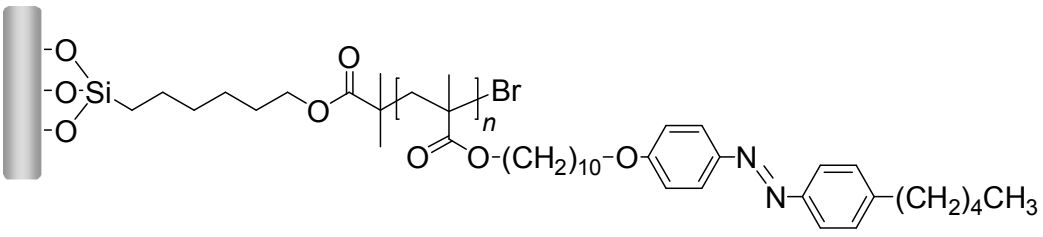

pMA(Az) graft

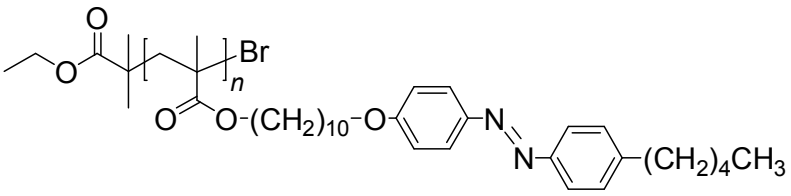

pMA(Az)

Chart 2-1.

sodium with benzophenone. Other compounds were used without further purification.

^{1}H-NMR spectra were recorded on a JEOL 270GXS instrument spectrometer operating at 270MHz using tetramethylsilane as the internal standard for the chloroform solutions. The melting points were measured with a Yanaco MP-S3 melting-point apparatus and are uncorrected.

2.2.2. Synthesis of Azobenzene Monomer

The synthetic strategy is shown in **Scheme 2-1**. Enormous methacrylate analogs bearing azobenzene moieties were synthesized previously.[17,18,19] The compounds employed in this work were also synthesized in the same manners.

2.2.2.1. 4-[(4'-Pentylphenyl)azo]phenol (5AzOH)

4-Pentylaniline (25.8 g, 158 mmol) was dissolved in a mixture of concentrated hydrochloric acid (25 mL) and water (150 mL). Sodium nitrate (15.9 g, 230 mmol) in water (80 mL) was added dropwise to the above solution at 5 °C. An aqueous solution (800 mL) dissolving phenol (22.0 g, 234 mmol), sodium hydroxide (9.30 g, 233 mmol), and urea was then added dropwise under vigorous stirring. The solution was stirred for 2 h at 5 °C and 3 h at room temperature. After this solution was neutralized with a diluted hydrochloric acid aqueous solution, the precipitate was filtered off and dissolved in ethyl acetate. The solution was washed with a NaCl aqueous solution, and then, dried over anhydrous magnesium sulfate. The precipitate was recrystallized from hexane twice to give yellow platelet crystals.

Yield: 25.1 g (59.1 %), m. p.: 72–73 °C, ^{1}H NMR(δ [ppm], $CDCl_3$): 0.89 (3H, t, J = 7 Hz, $\underline{CH_3}$–), 1.24–1.35 (4H, m, –$\underline{CH_2}$–), 1.64 (2H, t, J = 7 Hz, –$\underline{CH_2}$–), 2.65 (2H, t, J = 8 Hz, –$\underline{CH_2}$–Ph), 5.27 (1H, s, –OH), 6.90 (2H, d, J = 9 Hz, Ph–H), 7.28 (2H, d, J = 9 Hz, Ph–H), 7.77–7.84 (4H, m, Ph–H).

2.2.2.2. 4-(10-Hydroxydecyloxy)-4'-pentylazobenzene (5Az10OH)

Potassium carbonate (10.3 g, 74.5 mmol) and potassium iodide (1.24 g, 7.47 mmol) were added to 5AzOH (10.0 g, 37.3 mmol) in dry DMF (60ml), and then mixture

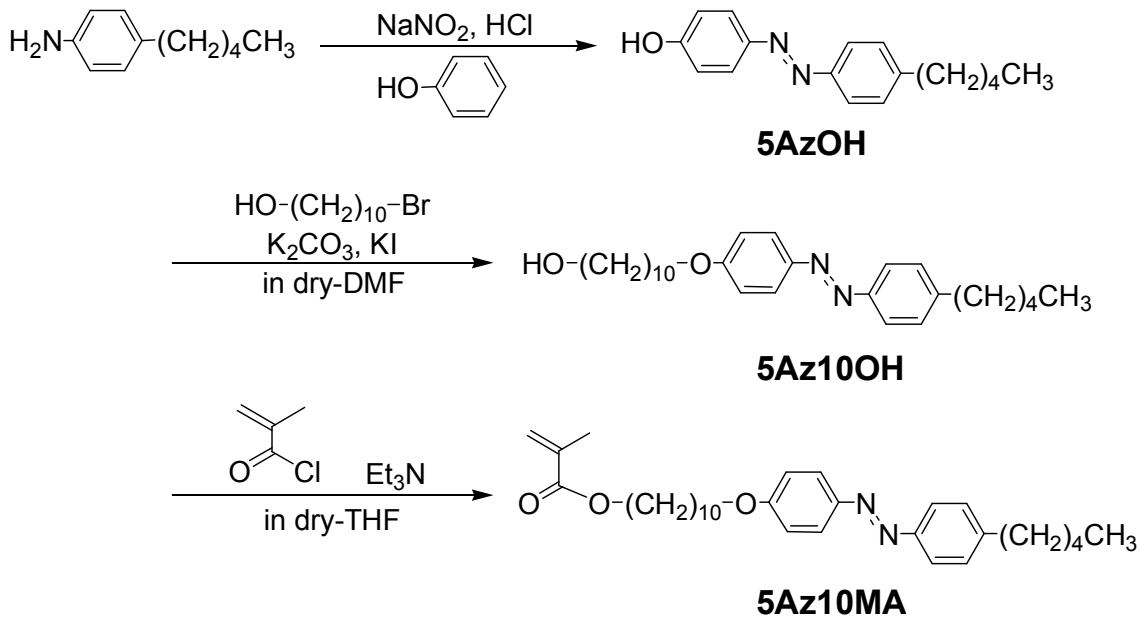

Scheme 2-1. Synthetic scheme of methacrylate monomer containing azobenzene derivative used in this work

was stiired for 30 min at 70 °C. 10-Bromodecanol (13.3 g, 56.1 mmol) in dry DMF (40ml) was added dropwise to the solution. The mixture was stirred for 6h at 70 °C. The reaction mixture was pored into water. A precipitated yellow solid was filtered, washed with water for several times, and dried in vacuum. The solid was recrystallized from methanol.

Yield: 14.7 g (84.1 %), m. p. : 81–82 °C, ^{1}H NMR(δ [ppm], $CDCl_3$): 0.87 (3H, t, J = 7 Hz, CH_3–), 1.32–1.65 (8H, m, –CH_2–), 2.67 (2H, t, J = 8 Hz, –CH_2–Ph), 5.27 (1H, s, –OH), 6.94 (2H, d, J = 9 Hz, Ph–H), 7.30 (2H, d, J = 9 Hz, Ph–H), 7.77–7.88 (4H, m, Ph–H).

2.2.2.3. 4-(10-Methacryloydecyloxy)-4'-pentylazobenzene (5Az10MA)

Trietylamine (4.54 g, 4.82 mmol) was added to 5Az10OH (14.0 g, 29.9 mmol) in dry THF solution. A dry THF solution of methacryloyl chloride (4.69 g, 4.82 mmol) was added dropwise to the solution at 0 °C. The mixture was stirred for 30 min at 0 °C and 12 h at room temperature. The reaction mixture was evaporated, and ethyl acetate was added. The solution was washed with water, and brine, and then, dried over anhydrous magnesium sulfate. The solvent was evaporated and the residue was recrystallized from methanol twice. Yellow solid was obtained.

Yield: 9.34 g (63.5 %), m. p.:75 –76 °C, ^{1}H NMR(δ [ppm], $CDCl_3$): 0.87 (3H, t, J = 7 Hz, CH_3–), 1.32–1.65 (8H, m, –CH_2–), 2.67 (2H, t, J = 8 Hz, –CH_2–Ph), 5.27 (1H, s, –OH), 6.94 (2H, d, J = 9 Hz, Ph–H), 7.30 (2H, d, J = 9 Hz, Ph–H), 7.77–7.88 (4H, m, Ph–H).

2.2.3. Preparation of ATRP initiator Modified Substrates.

The synthesis route displays in **Scheme 2-2**. Silane coupling reagent bearing ATRP initiated group was synthesized according to previous literature.[20] Modified surface was prepared by chemical vapor adsorption (CVA) method.[21]

2.2.3.1. 1-(2-Bromo-2-methyl) propionyloxy-5-hexene (BPH)

2-Bromoisobutyrryl bromide (4.40 mL, 36.0 mmol) was added dropwise to a THF solution of 5-hexene-1-ol (3.00 g, 30.0 mmol) with triethylamine (3.60g, 35.6

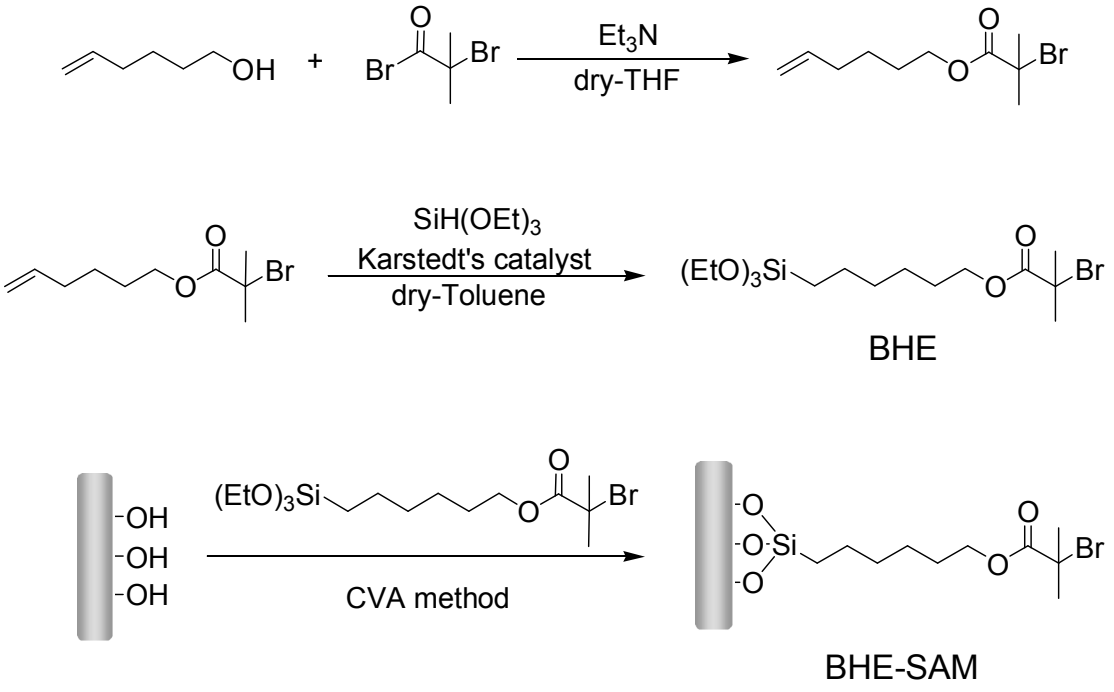

Scheme 2-2. Synthetic scheme of the surface initiator, used in this study.

mmol) at 0 °C. The mixture was stirred for 1h and 15h at room temperature. The mixture was filtrated and evaporated to dryness under reduced pressure. The residue was extracted with chloroform and washed with 1N HCL aq., conc. $NaHCO_3$ aq. solution, and brine, and then, dried over anhydrous magnesium sulfate. The removal of the solvent gave a brown oil, which was purified by column chromatography of silica gel with a mixture of hexane / ethyl acetate = 15/1 as an eluent. Transparent oil was obtained.

Yield: 6.11 g (82.2 %), ^{1}H NMR(δ [ppm], $CDCl_3$): 1.37 - 1.69 (4H, m, –$\underline{CH_2}$–), 1.87 (6H, s, C($\underline{CH_3}$)$_2$), 2.04 (2H, q, J = 7 Hz, CH_2=CH$\underline{CH_2}$), 4.11 (2H, t, J = 7 Hz, –$\underline{CH_2}$O–), 4.88 - 4.98 (2H, m, –$\underline{CH_2}$=CH–), 5.65 - 5.80 (1H, m, –CH_2=$\underline{CH}$–)

2.2.3.2. (2-Bromo-2-methyl) propionyloxyhexyltriethoxysilane (BHE)

This reaction was curried out in globe box. BPH (2.87 g, 11.6 mmol) was dissolved in toluene (10 mL). Triethoxysilane (10.0g, 60.9 mmol) was added into flask, and subsequently Karstedt's catalyst solution (40 μL) was added with a microsyringe. The reaction mixture was stirred for 15h at room temperature. Complete disappearance of BPH, and hence the completion of reaction was confirmed by ^{1}H NMR spectroscopy. Mixture was passed through silica gel column with a toluene as an eluent to remove catalyst. Unreacted triethoxysilane and toluene were completely removed under vacuum at 60 °C.

Yield: 4.16 g (87.3 %), ^{1}H NMR(δ [ppm], $CDCl_3$): 0.56 (2H, t, J = 8 Hz, Si$\underline{CH_2}$–), 1.16 (9H, J = 8 Hz, ($\underline{CH_3}CH_2O)_3$Si), 1.18 - 1.61 (8H, m, –$\underline{CH_2}$–), 1.86 (6H, s, C($\underline{CH_3}$)$_2$), 3.74 (6H, q, J = 7 Hz, –($\underline{CH_2}$)$_3$OSi–), 4.09 (2H, t, J = 7 Hz, –$\underline{CH_2}$O–)

2.2.3.3. Modification of ATRP Initiator onto Solid Substrates (BHE-SAMs)

Quartz plates (1 cm ×1.5 cm) were washed with a saturated potassium hydroxide ethanol solution, and pure water under ultrasonic wave treatment. The static contact angle of water on this surface measured with a FACE CA-XP (Kyowa Interface Science) was 8 ± 2 ° (hydrophilic plates). Silicon wafer substrates (1 cm × 1.5 cm) were washed with acetone under ultrasonic wave treatment fro 5 min. Both substrates were cleaned

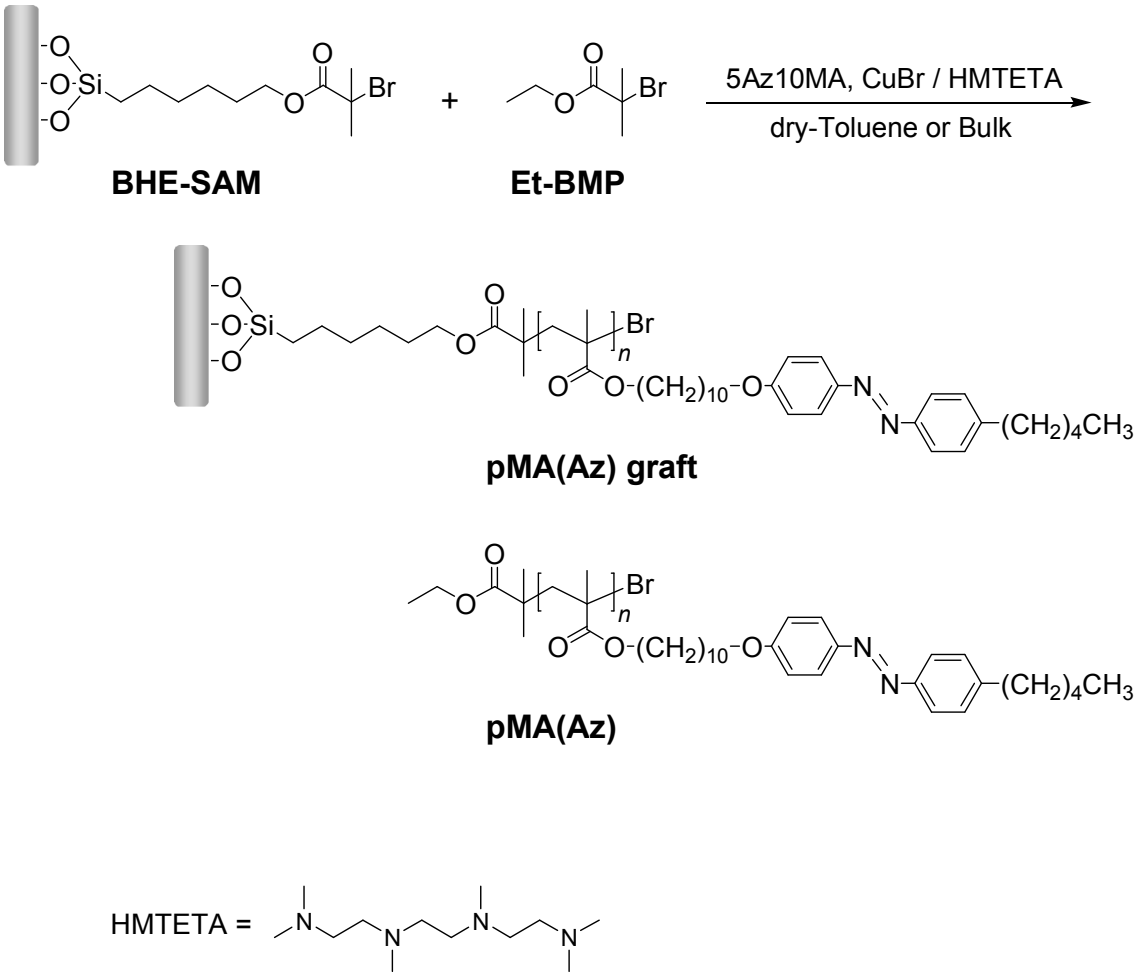

Scheme 2-3. Synthetic scheme of pMA(Az) chains by "graft-from" surface-initiated atom transfer radical polymerization.

by exposure to UV ozone for 45 min using a ozone cleaner (Nippon Laser & Electronics) before surface modification reaction.

Cleaned silicon wafer or quartz substrates were placed into a Teflon container. The container was sealed and placed in an oven maintained at 150 °C for 1 hour. Then, a glass cup filled with BHE liquid (about 50mg) was put together, and maintained at 150 °C for 3 h. The BHE liquid in the vessel vaporized and reacted with the hydroxyl groups on the sample surface. Subsequently, the container was opened and placed at 150 °C for 1h. After the surface reaction, the samples treated with BHE were dipped into dehydrated toluene and ethanol successively and washed by ultrasonic bath for 5 min. Finally, the samples were dried under vacuum and stored in nitrogen atmosphere.

2.2.4. Surface-initiated Atom Transfer Radical Polymerization

A typical synthesis shows follow. 7 mg (0.05 mmol) of Cu(I)Br, 492 mg (1.0 mmol) of the Az containing monomer 5Az10MA, 1 mg (0.005 mmol) of ethyl 2-bromoisobutyrate as a free initiator, and 11.5 mg (0.05 mmol) of 1,1,4,7,10,10-hexamethyltriethylentetraamine as a ligand were dissolved in 1.25 ml of dry toluene and filled with nitrogen. The mixture was degassed by freeze-pomp-thaw cycle for three times. In a glove box, initiator-modified quartz or silicon substrates were added in polymerization solution and sealed. The flask was placed in the preheated 80°C oil bath for several hours. After the polymerization, polymer grafted substrates were washed with tetrahydrofuran (THF) for several times to remove unreacted monomer and free polymer, and dried at room temperature.

2.2.5. Synthesis of Free Polymer PMA(Az) and Preparation of Spincast Films

Free polymer PMA(Az) were synthesized by using the analogous procedure of the grafted substrates except for BHE-SAMs. The number-average molecular weight (M_n) was ca. 9800, with polydispersity (M_w / M_n) of 1.14. This polymer exhibited a smectic LC property. Thermal phase properties were as follows, glass transition (T_g) to smectic phase: 51 °C, smectic phase to isotropic: 108 °C (Figure 2-1). Spincast films were obtained from a 2 wt% toluene solution using a spin-coater at 2000 rpm for 30 s,

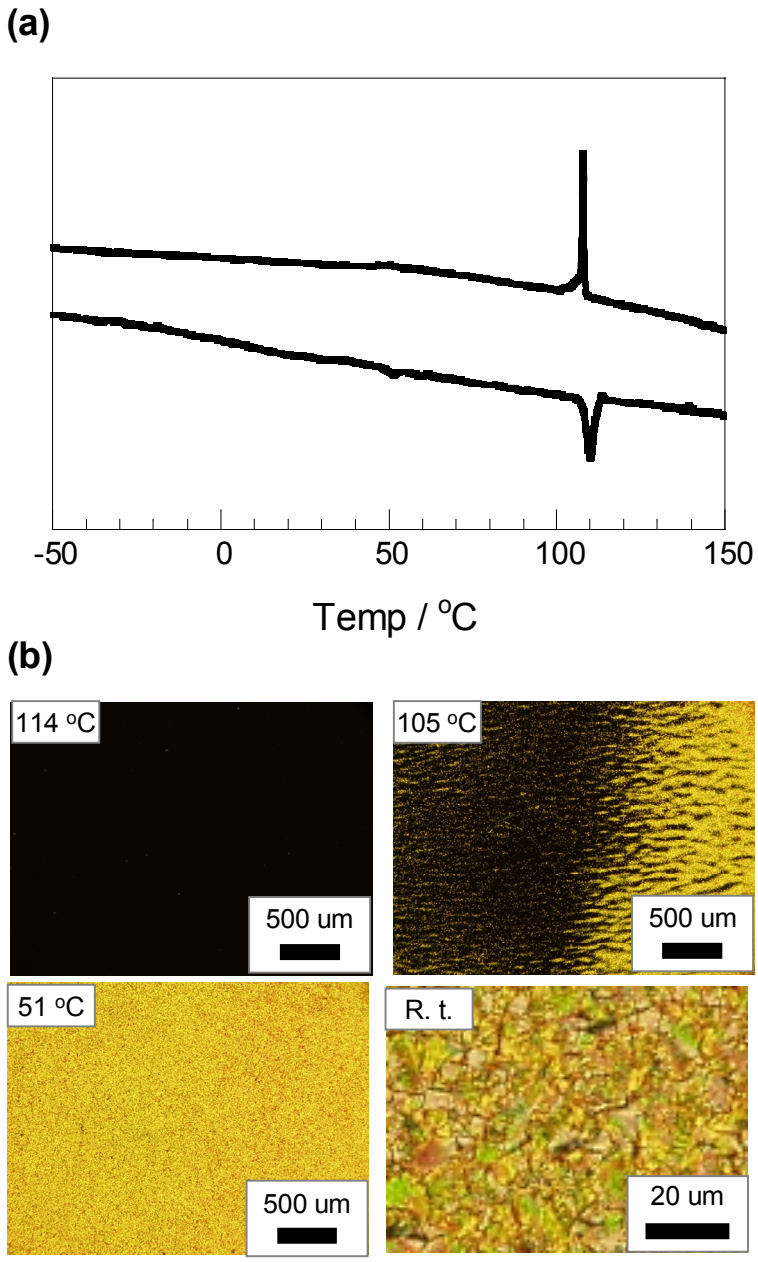

Figure 2-1. DSC curves of the PMA(Az) on the first cooling and second heating process (a), and typical polarized optical microscopic images (b).

and annealed at 100 °C for 10 min. Their film thickness was ca. 40 nm by ellipsometry and AFM measurements. For investigate film thickness dependency, the thin films of thicknesses 5 - 40 nm were prepared from toluene solution of various polymer concentration.

2.2.6. Measurements

2.2.6.1. Immobilizations of the Initiator on the Substrates

X-ray photoelectron spectroscopy (XPS) was measured by ESCA-3300 (Shimadzu) and operating to confirm the formation of the initiator monolayer with an Mg_{α} X–ray at 10 mA and 30 kV. All binding energies were referenced to Si2p at 99.34 eV. Atomic force microscopy (AFM) was carried out on a SPA400/SPI3800N system (Seiko Instruments) to observation surface morphologies of initiator modified substrates and roughness. The static contact angle of water on this surface was measured with a FACE CA-XP (Kyowa Interface Science). The contact angles were obtained by averaging the results of 5 points of measurements.

2.2.6.2. Characterization of Grafted Substrates

Molecular weights and polydispersites of synthesized polymers or free polymers on graft polymerizations were determined by gel permeation chromatography (GPC) analysis was carried out on a Shodex liquid chromatography system equipped with a guard column (Shodex GPC KF-G), two columns (Shodex KF-803L and Shodex KF-805L), UV (Shodex UV-41) and RI (Shodex RI-101) detectors which was calibrated with standard polystyrene. THF was used as an eluent at a flow rate of 1.0 mL / min.

UV–visible absorption spectra for the graft substrates and spincast films at room temperature were measured with an Agilent 8453 spectrometer (Agilent Technology).

Layer thickness was measured by an ellipsomater (Philips PZ2000) equipped with He-Ne laser (632.8 nm). The incident angle was 70 °. The refractive index of the graft layer was assumed to be 1.561, the value for a spincast films.

2.2.6.3. Investigation of LC Properties

Grazing angle-incidence X-ray diffraction (GI–XRD) measurements were Rigaku NANO-viewer and Rigaku RINT-2100 operating with CuK_{α} radiation (0.154 nm). Their scattering profiles recorded on imaging plates.

UV-vis spectroscopic study at various temperatures was performed on an MCPD-2000 UV-vis spectrometer (Ohtsuka Electronics) combined with a deuterium-halogen lamp MC-2530 (Ohtsuka Electronics) equipped with a Mettler FP82HT hot stage at a heating or cooling rates of ±1 °C/min.

POM observations were used Olympus BH-2 equipped with a Mettler FP82HT hot stage for visual observation and observed at cooling process from 120^{o}C.

2.3. Results and Discussion

2.3.1. Immobilization of the Initiator on Substrates

The CVA method is often used to prepare smooth monolayered films of organosilane compounds without 3D aggregation.[22,23] Inpreparation of the polymer brushes, their surface roughness are very influential, therefore, this method was employed in this study. The typical water contact angle of silicon wafer and quartz cleaned by UV/O^3 cleaner is lower than 5 °. In contrast, the contact angles after modification with BHE by CVA were significantly different from that of the inherent hydrophilic properties of the silicon wafer before the treatment. The contact angles of water were 54.8 ° (silicon wafer) and 58.7 ° (quarts) when treated at 100 °C, and 70.8 ° (silicon wafer) and 66.1 ° (quarts) at 120 °C, respectively. The contact angles of water was 79 ° in average on the Br-terminated SAMs.[24,25] Thus, the surface treated at 100 °C and 120°C are not fully covered with BHE. On the other hand, substrates treated at 150°C gave the contact angle values of 79.7 ° (silicon wafer) and 75.2 ° (quartz), respectively, which exactly agree with that reported in previous literatures.[21,22]

The surface morphologies of BHE-SAM treated at 100, 120 and 150 °C evaluated by AFM are shown in Figure 2-2. The morphologies on the silicon wafer show that the surface was almost uniform at a molecular level. A root mean square

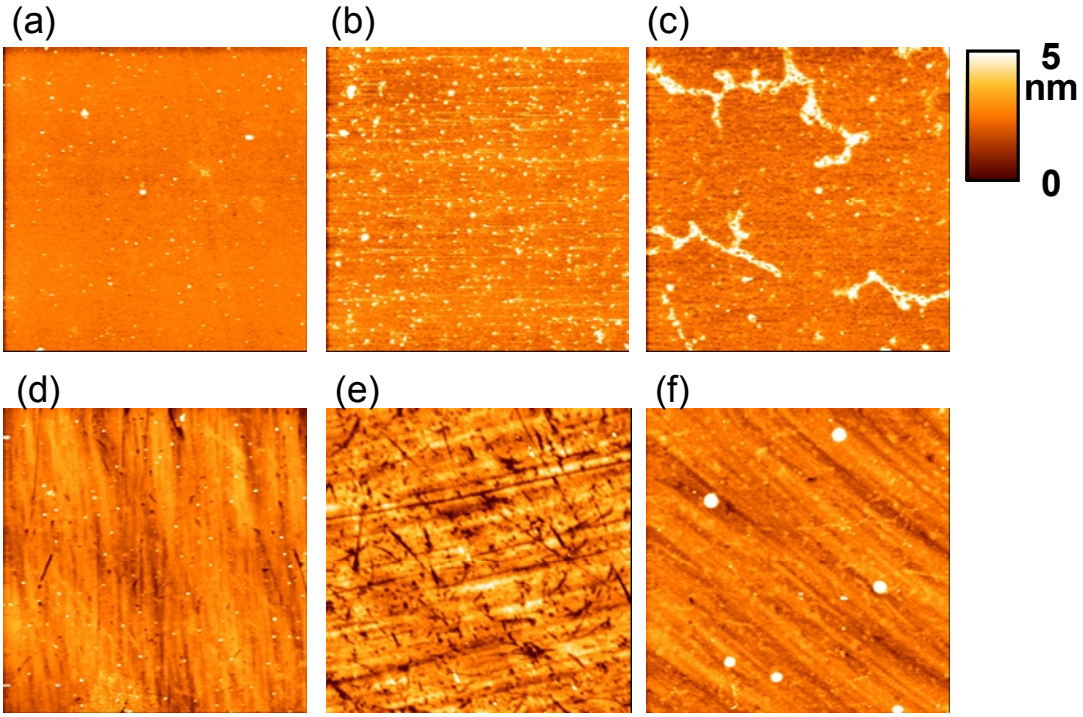

Figure 2-2. Topographical AFM images of BHE-SAMs on silicon wafer (a, c and e) and quartz (b, d and f) obtained after treatment at 100 (a and d), 120 (b and e), and 150 °C (c and f). The scan area is 5 μm^2.

Table 2-1. contact angles of water and a root mean square roughness (*Rrms*) on silicon wafer and a quart plate prepared at various treatment temperatures

	Silicon wafer		Quartz	
Temperature / °C	C. A. / °	*Rrms* / nm	C. A. / °	*Rrms* / nm
100	54.8	0.79	58.7	0.99
120	70.8	0.65	66.1	0.71
150	79.7	0.83	75.2	1.8

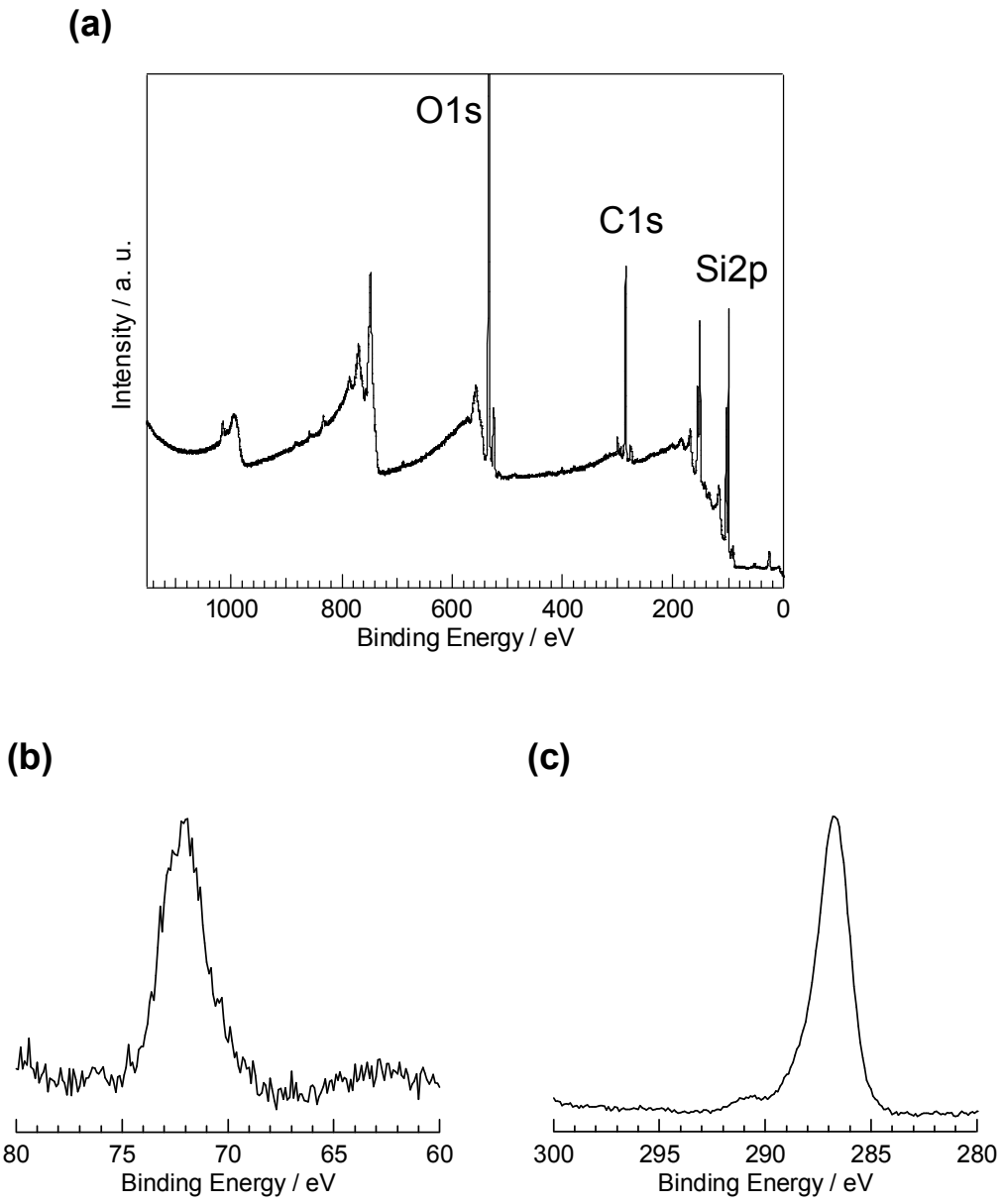

Figure 2-3 XPS spectra of the ATRP-initiator modified substrate at wide region (a), Br 3d (b), and C1s (c). The CVA condition is at 150 oC for 3 h.

roughness (*Rrms*) in the scan area of 5 μm^2 is 0.79, 0.65, and 0.83 nm, respectively. On the quartz surface, the *Rrms* was larger than on the silicon wafer. This can be interpreted as the roughness of the silicon wafer is smoother than the quartz before the CVA treatment, and therefore, the morphology of the BHE-SAMs is reflected bythem. The contact angles and *Rrms* were summarized in Table 2-1. In further experiments, CVA treatment was performed at 150 °C.

After the surface modification at 150 °C, XPS measurements were achieved to confirm the formation of the initiator monolayer. Figure 2-3 shows the XPS spectra of the initiator layers on silicon wafer treated at 150 °C. In the wide range measurement, the peak intensity derived from bromine 3d was very small in comparison with other peaks such as carbon or oxygen. This phenomenon is explained that the loss of the bromine under a prolonged X-ray irradiation occurred.[22] The bromine 3d peak and the carbon 1s peak were observed in the narrow scan mode around 70 eV and 286 eV, respectively. The carbon 1s signals attributed to C=O and C–O bonds were also observed (Figure2-3c). These results are indicative of formation of a BHE-SAM on the silicon wafer.

2.3.2. Characterization of Graft Substrates

Figure 2-4a shows the absorption spectra of the PMA(Az) graft films on quartz substrates with various polymerization durations. The peaks around 244 nm and 340 nm were assigned to the ϕ–ϕ* transition and π–π* long-axis transition of the Az unit, respectively. All samples exhibited similar absorption spectra and the absorbance was unchanged by repeated washing with THF. Thus, the polymer chains were not physically adsorbed but chemically tethered onto the substrates. The absorbance gradually increased with the increase in polymerization time. Figure 2-4b displays the plot of the M_n of the free polymer produced in polymerization solution and the absorbance on quartz substrates as a function of polymerization time. The M_n value increased with polymerization time and reached 40000 after 6 h, and also the absorbance also increased. However, after 8 h, the absorbance the similar value to that after 6 h. Thus the absorbance increment was saturated in several hours. Figure 2-5a displays the

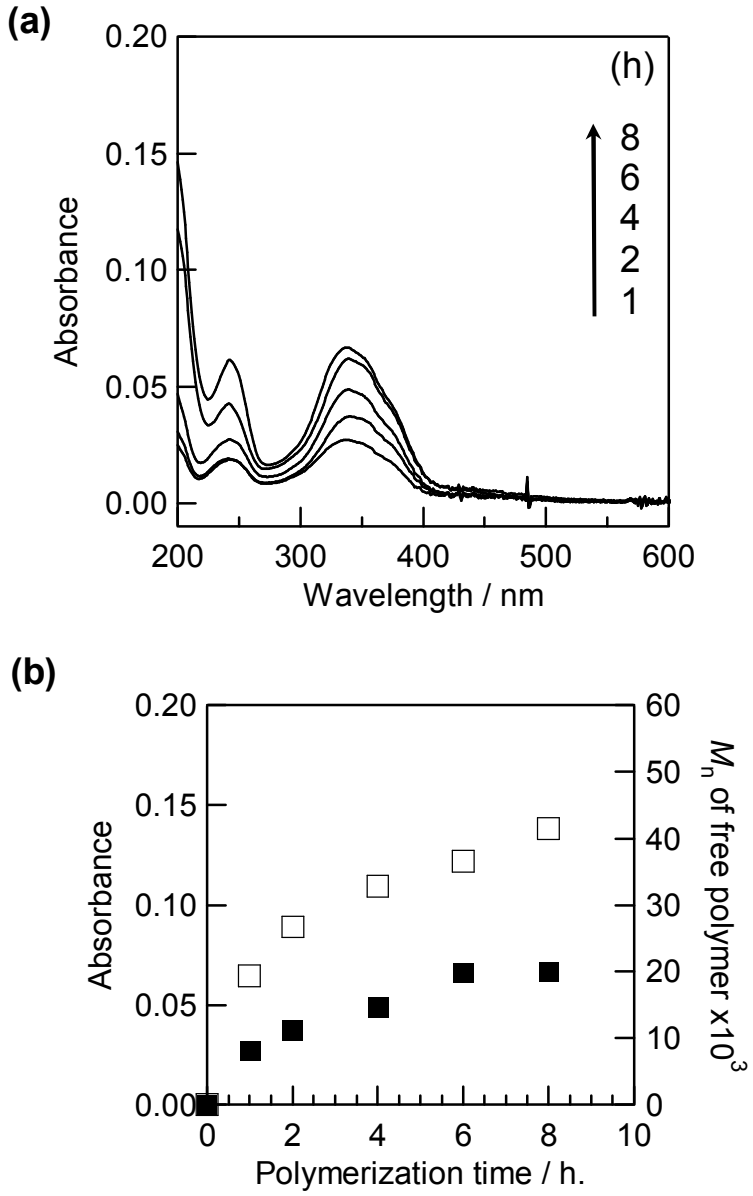

Figure 2-4. UV-Visible absorption spectra of the grafted polymer film obtained at various polymerization times (a) and the relationship between the absorbance (■) or M_n of free polymers (□), and polymerization times (b). The reaction condition: $[M]_0$ = 0.5 mol dm^{-3}, [M]/[I] = 200/1.

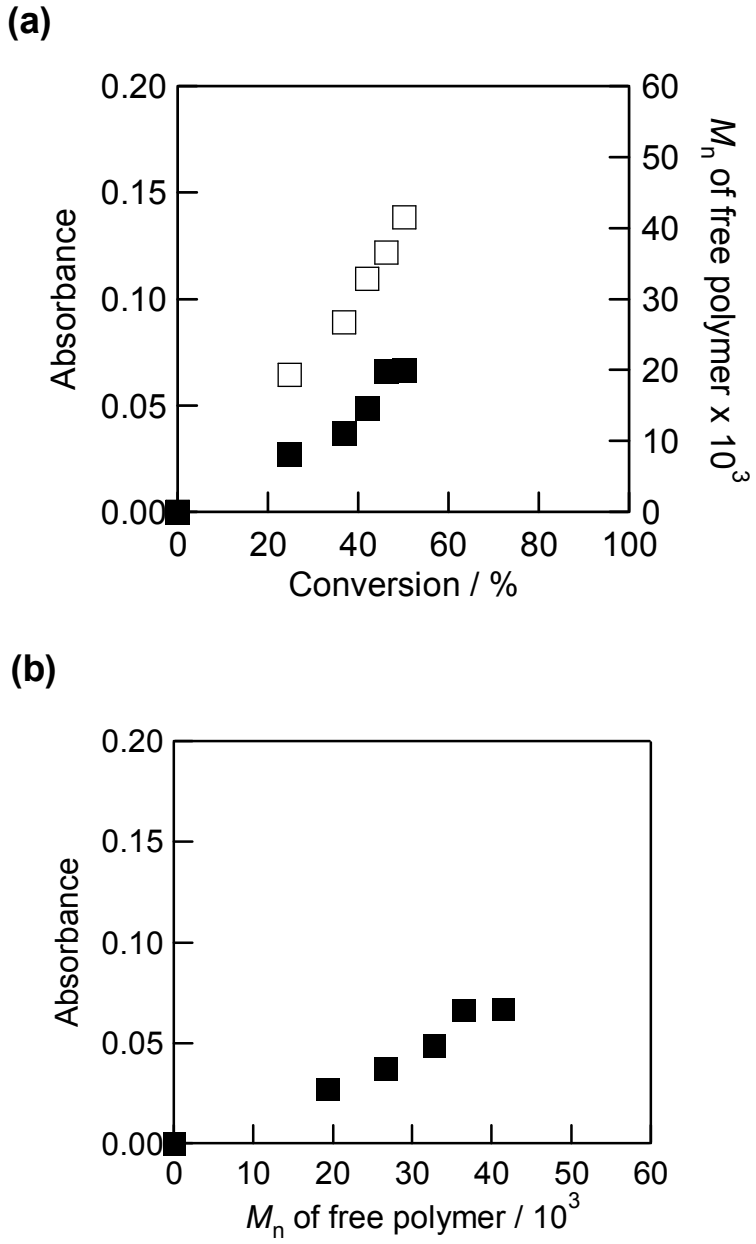

Figure 2-5. Plots of absorbance on quartz (■) and *M*n of free polymers (□) vs polymer conversion for free initiator (a), and relationship between absorbance and *M*n of free polymer (b).

plots of absorbance on the quartz substrate and M_n of free polymers vs polymerization conversion for the free initiator. M_n of free polymers constantly increased, despite the fact that the increase of absorbance was ceased. The above results show that the living polymerization continues in solution, nevertheless only free initiator on the substrate contributes to the polymerization after a certain stage. This situation can be also indicated by a plot of absorbance vs M_n (Figure 2-5b). Similar tendencies were observed for other polymerization conditions changing monomer concentration, reaction temperature, and the molar ratio of monomer to the free initiator.

On the other hand, the increase in absorption, corresponding to the graft chain length was constantly observed when polymerization was carried out at higher monomer concentrations (data not shown). This fact suggests that the graft chain length on substrates is ceased at some stage when the monomer concentration is lowered to a certain level. Therefore, to control the graft chain length, variations of the initial monomer concentration should be more effective and reproducible. Figure 2-6a displays the absorption spectra of the PMA(Az) graft films on a quartz substrate when the initial monomer concentration is varied. Here, the polymerization conditions of all samples are the same ($[M]_0/[I]_0$ = 200/1, reaction time: 12 h) except monomer concentration. The absorbance constantly increased with the initial monomer concentration. Figure 2-6b shows the absorbance at absorption maximum (λ_{max}) of the π–π^* long-axis transition of Az as a function of initial monomer concentration. A nearly proportional relationship was obtained between them. This implies that surface-initiated ATRP is a non-homogeneous reaction system in which the apparent concentration of initiator is extremely small. Thus, the concentration of monomer is directly reflected to the chain length. The film thickness was evaluated to be 20 nm from an ellipsometric measurement and AFM observations. In the above manners, the PMA(Az) brushes on solid substrate were successfully synthesized by surface-initiated ATRP, and the method to control the thickness of a graft film is found.

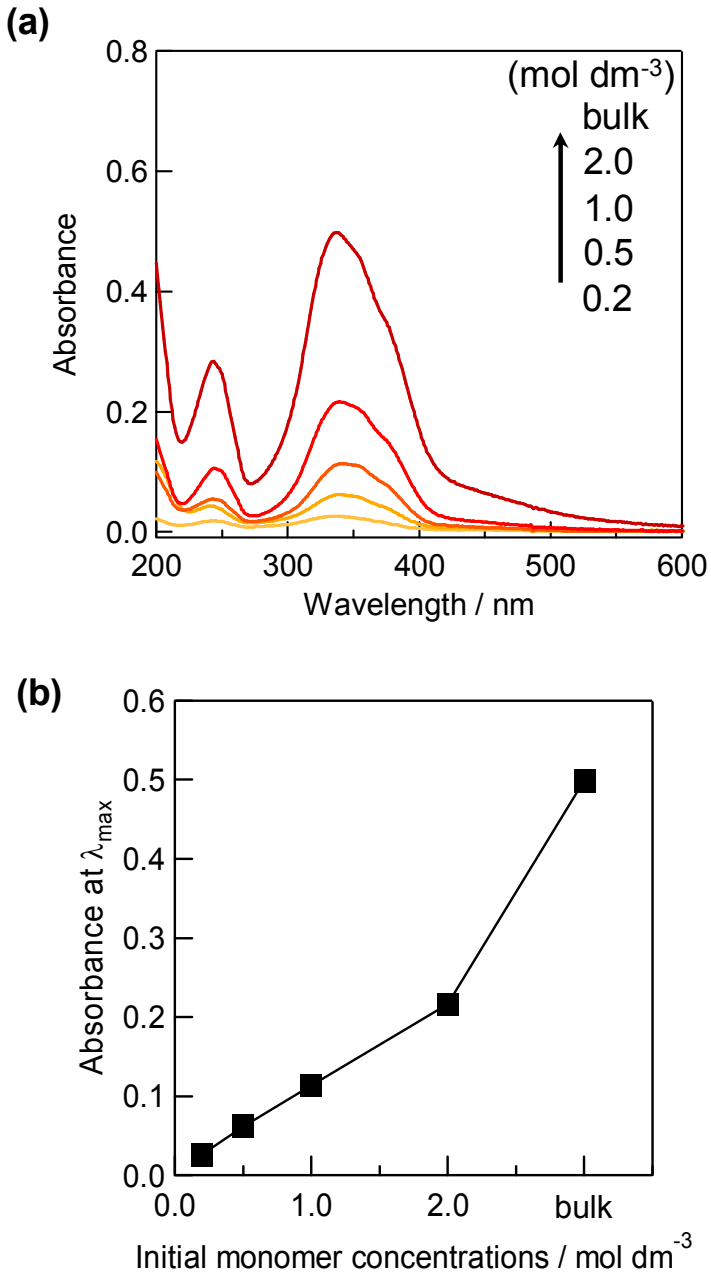

Figure 2-6. UV-Visible absorption spectra of the grafted polymer film obtained by the polymerization at various initial monomer concentration [M]0 (a), and the absorbance as a function of [M]0 (b).

2.3.3. Molecular Orientation of Azobenzene Units

2.3.3.1. UV-visible Spectroscopic Measurements

Figure 2-7 shows the typical UV-visible absorption spectra of a PMA(Az) grafted film (a) and a spincast film prepared from 2 wt% toluene solution (b) on a quartz substrate before and after annealing. Absorption maximum (λ_{max}) of the π–π* long-axis transition of Az in THF solution was positioned at 352 nm, whereas that of the graft substrates showed around 338 nm, indicative of the formation of H-type aggregates of Az units. The molecular orientation of Az units in side chain is roughly estimated by the ratio of absorption intensities at the π–π* to ϕ–ϕ* band, since the π–π* transition is directional dependent while the ϕ–ϕ* transition at 244 nm is insensitive to the chromophore orientation. For the grafted polymer film, the ratio of $A_{\phi-\phi^*}/A_{\pi-\pi^*}$ was ca. 0.61 and essentially unchanged by annealing. This indicates that the Az units exhibit a homogeneous (parallel) orientation to the substrate. Interestingly, the spectral features were essentially unchanged even after dipping into organic solvents (good solvents) such as THF and chloroform.

In sharp contrast, large spectral changes were observed for the spincast film by annealing (Figure 2-7b). The absorbance of the π–π* transition significantly decreased from 0.24 to 0.08 accompanied by a hypsochromic shift from 334 nm to 320 nm by annealing. This orientational change occurred only within 1 min of the thermal treatment. The $A_{\phi-\phi^*}/A_{\pi-\pi^*}$ ratio became 0.71 from 1.85 after this procedure. Thus, stronger H-type aggregation was formed with orientational change to a more perpendicular state to the substrate. Such normal orientation of the mesogenic groups are commonly observed for the spincast films of smectic LC Az polymer.[26,27]

In smectic LC polymer films, their orientation is depended on film thickness. Stamm et al. reported that the orientation of mesogens alters around several nanometer thicknesses by X-ray analysis.[28,29] Moreover, LC diblock copolymers containing Az unit thin films also depends on film thickness; the orientation Az chromophores changed from perpendicular to parallel on thickness boundary between 60 and 70 nm.[30] The thickness of PMA(Az) grafted films are below 50 nm. The Az mesogens may be lied on the substrate in block copolymer film.[27] So, thickness dependency was evaluated in

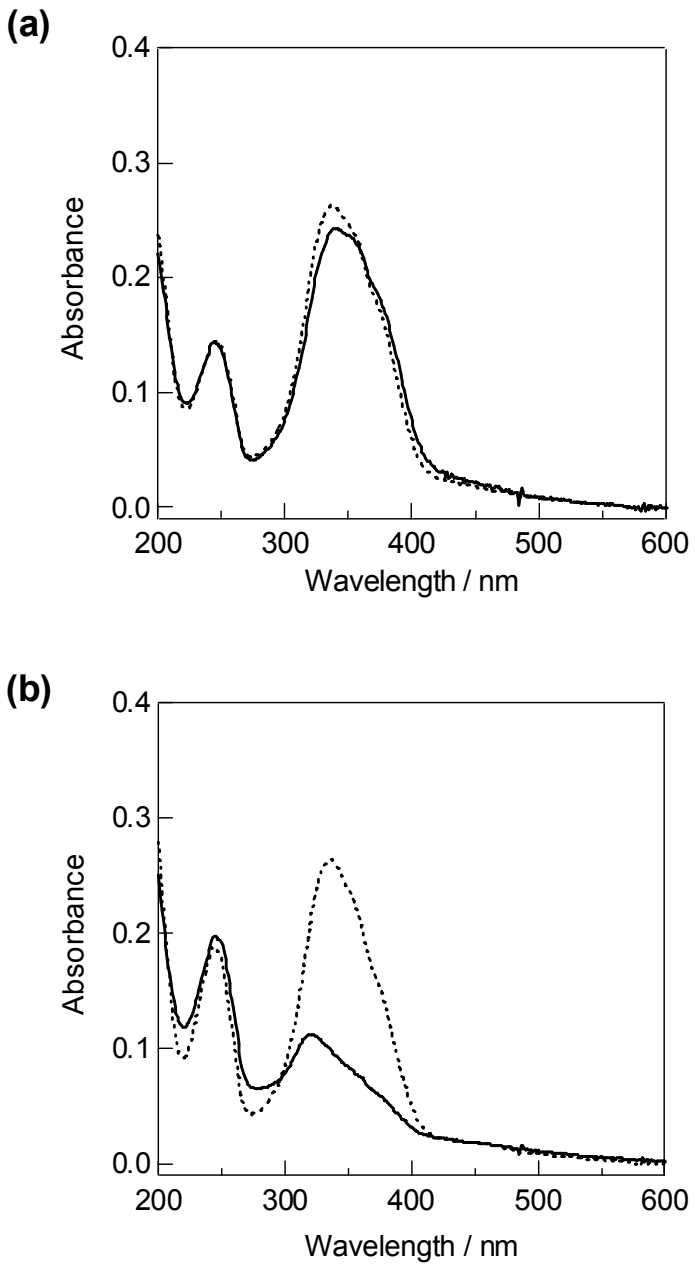

Figure 2-7. UV-vis absorption spectra of the Az grafted polymer film (a), and spincast film (b) before (dashed line) and after thermal annealing (solid line). Thermal annealing was achieved at 140 oC for 2 h (grafted chains) and at 100 oC for 10 min (spincast film)

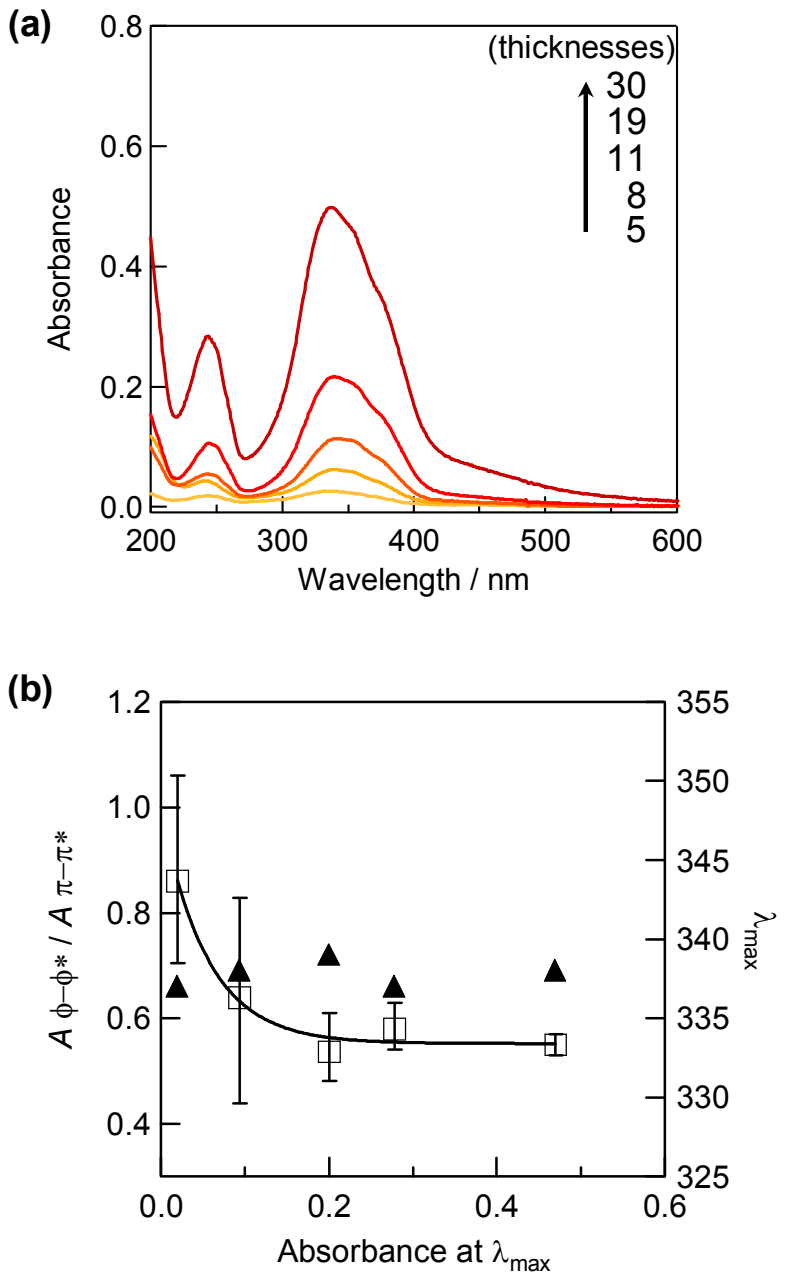

Figure 2-8. UV-vis absorption spectra of Az-polymer grafted substrates obtained at various polymerization conditions (a), and the ratio of $A_{\phi-\phi^*}/A_{\pi-\pi^*}$ (□) and wavelength of λ_{max} (▲) vs absorbance at λ_{max} (b).

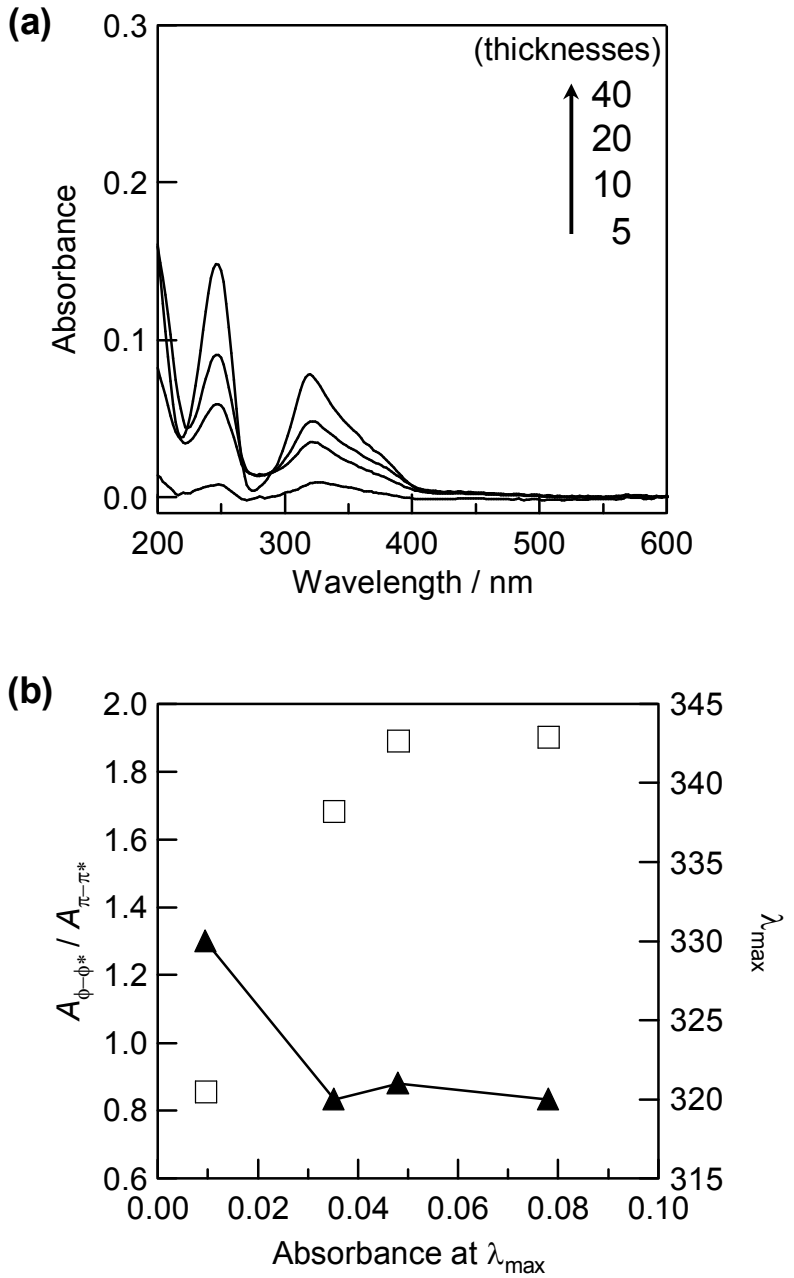

Figure 2-9 UV-vis absorption spectra of spincast films of various thicknesses after annealing (a), and the ratio of $A_{\phi-\phi^*}/A_{\pi-\pi^*}$ (□) and wavelength of λ_{max} (▲) (b).

both films.

Figure 2-8 shows the ratio of $A_{\phi-\phi^*}/A_{\pi-\pi^*}$ as a function of the absorbance at λ_{max} in polymer-grafted substrates. When the absorbance is small, namely the grafted chain lengths were short, $A_{\phi-\phi^*}/A_{\pi-\pi^*}$ were around 1.0. With increasing the absorbance, the ratio of $A_{\phi-\phi^*}/A_{\pi-\pi^*}$ were gradually reduced down to ca. 0.6. The λ_{max} did not show shifts with change in the absorbance. With above knowledge, mesogen orientations in the grafted chains were interpreted as follows. In the initial stage of polymerization, Az mesogens oriented randomly because the polymer chains were short and mesogens possess high flexibility. This situation is implied by the range of error bar. With increasing the length of polymer chains, they start to orient perpendicular to the substrate because of a spatial confinement. Thus, Az mesogens are oriented perpendicular to the main chain, leading to the parallel orientation to the substrate.

In contrast, thickness dependency was not observed in spincast films (Figure 2-9). The spectral shapes are essentially the same exhibiting large spectral changes and H-aggregation. The relationship between the ratio of $A_{\phi-\phi^*}/A_{\pi-\pi^*}$ and the absorbance at λ_{max} were unchanged. It is concluded that the parallel molecular orientation of Az groups in the grafted chain system is attained by anchoring the terminal the substrates, and not by the film thickness change.

2.3.3.2. Grazing-incidence X-ray Diffraction Measurements

The LC state and orientation of the mesigonic Az groups in the grafted polymers on the substrate were investigated in more detail by GI-XRD measurements. Figure 2-10a shows 2-dimensional GI-XRD profile of the grafted polymer film recorded on an imaging plate. An intense comet-tail-like image running orthogonal to the substrate is an artifact of specular reflection. Diffraction patterns were only observed in the in-plane direction, i. e., the periodic structures derived from the smectic LC phase were formed perpendicular to the substrate plane, and LC mesogen being aligned parallel to substrates. This result is in agreement with the data indicated by the UV-vis absorption spectra. In-plane orientation of mesogens is often observed in a microphase separated state of LC block copolymers[3132]. However in this case, such orientation is observed for

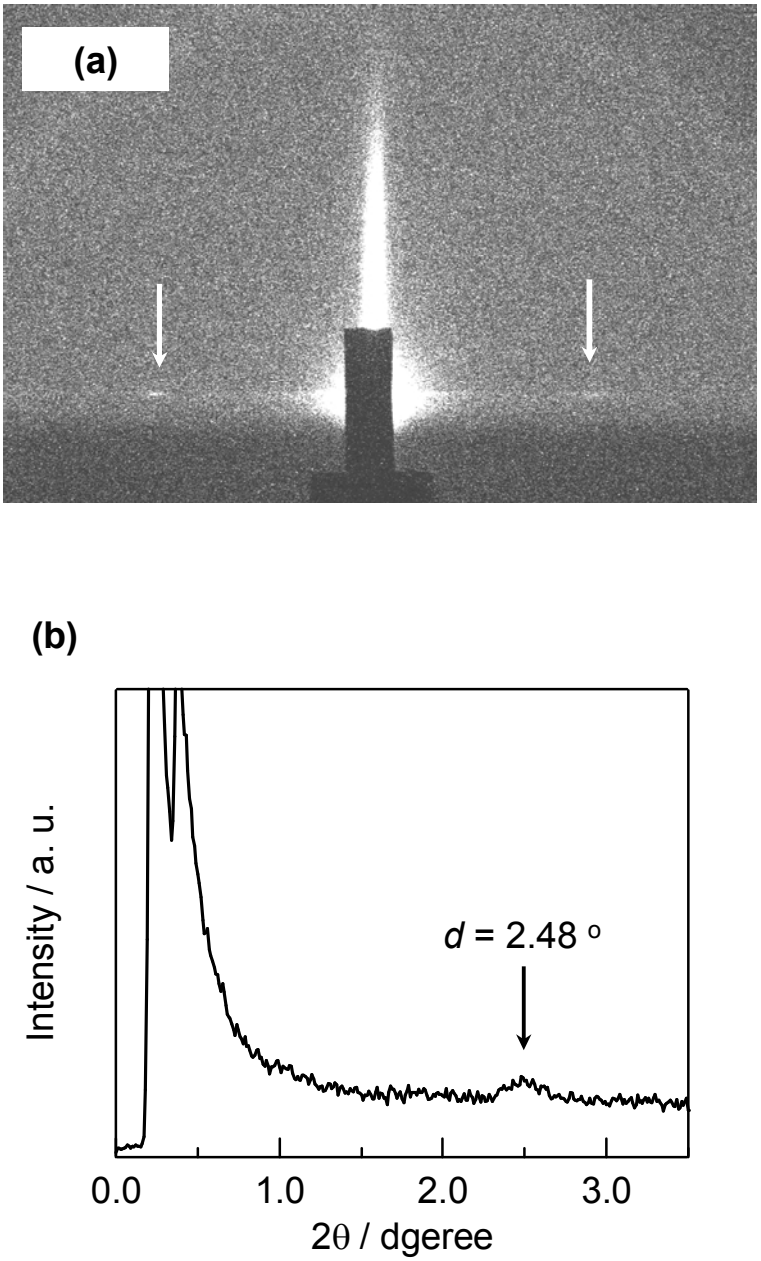

Figure 2-10. 2D GI-XRD pattern of the grafted polymer film recorded on an imaging plate (a), and 1D profile in the in-plane direction extracted from the 2D XRD pattern (b). The in-plane diffraction spots are indicated by arrows in (a). A strong comet-tail-like line running in the perpendicular direction is a specular reflection.

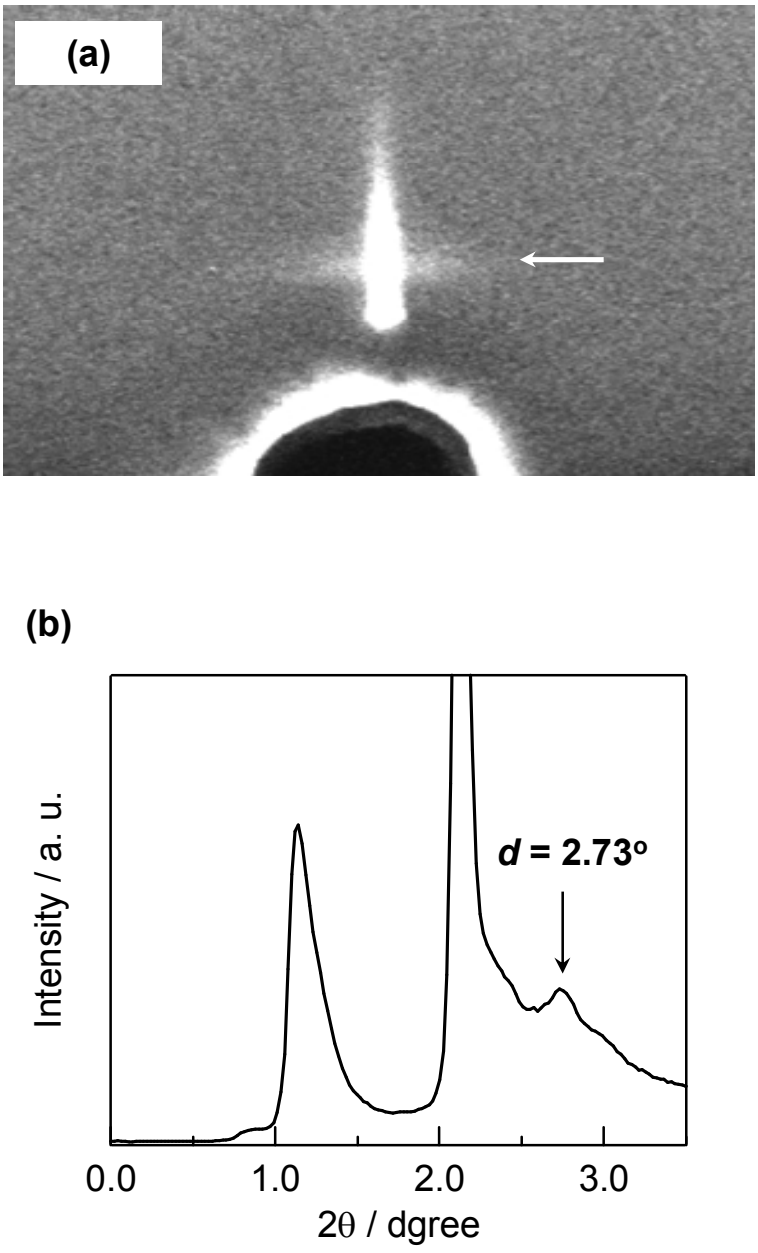

Figure 2-11. 2D GI-XRD pattern of the spincast film recorded on an imaging plate (a), and 1D profile in the out-of-plane direction extracted from the 2D XRD pattern (b). The out-of-plane diffraction spots are indicated by an arrow in (a). A strong comet-tail-like line running in the perpendicular direction is a specular reflection.

the first time in the homopolymer system by grafting from the surface. Figure 2-10b shows 1-dimensional SAXS pattern monitored in the in-plane direction. A clear peak was observed at $2\theta = 2.48$ °, which corresponds to a layer spacing of 3.56 nm. This spacing corresponds to a long-range ordering of approximately the length of the fully extended Az side chain, suggesting a formation of interdigitated structures of Az side chains.

In contrast, a diffraction pattern on the spincast films of PMA(Az) was observed only in the out-of-plane direction at $2\theta = 2.73$ ° ($d = 3.26$ nm), derived of smectic LC phase (Figure 2-11). Thus, virtually identical smectic structure is formed both in the grafted polymer film and spincast film, only with contrasting orientations.

2.3.4. Evaluation of LC Properties of Grafted Polymer Films

In general, thermal properties of the LC polymers were investigated by using differential scanning calorimetry (DSC), polarizing optical microscopy (POM), and X-ray diffraction (XRD). In this graft substrates, layer structures derived of smectic LC phase are observed by GI-XRD measurements. The elucidation of thermal properties of the graft chains is a difficult task, because the LC phase transition enthalpy is very small. For investigation of LC properties on the grafted chains, the change of LC phase - isotropic phase transitions is evaluated by UV-vis absorption spectroscopy and POM observations.

2.3.4.1. UV-visible Absorption Spectroscopy at Various Temperatures

Figure 2-12 displays UV-vis absorption spectra taken in a cooling process from 150 to 40 °C. The spectral shape and λ_{max} around 350 nm above 120 °C indicate that no aggregates of Az units were formed. On cooling, λ_{max} shifted toward shorter wavelengths from 350 to 338 nm at 115 – 108 °C, showing H-aggregate formation at lower temperatures. On heating process, this spectral shift was observed in the same temperature range. Thus, this spectral change occurred reversibly on repeated temperature changes. The plot of λ_{max} and absorbance at λ_{max} vs temperature are shown in Figure 2-12. This temperature range corresponds to the smectic LC-isotropic phase

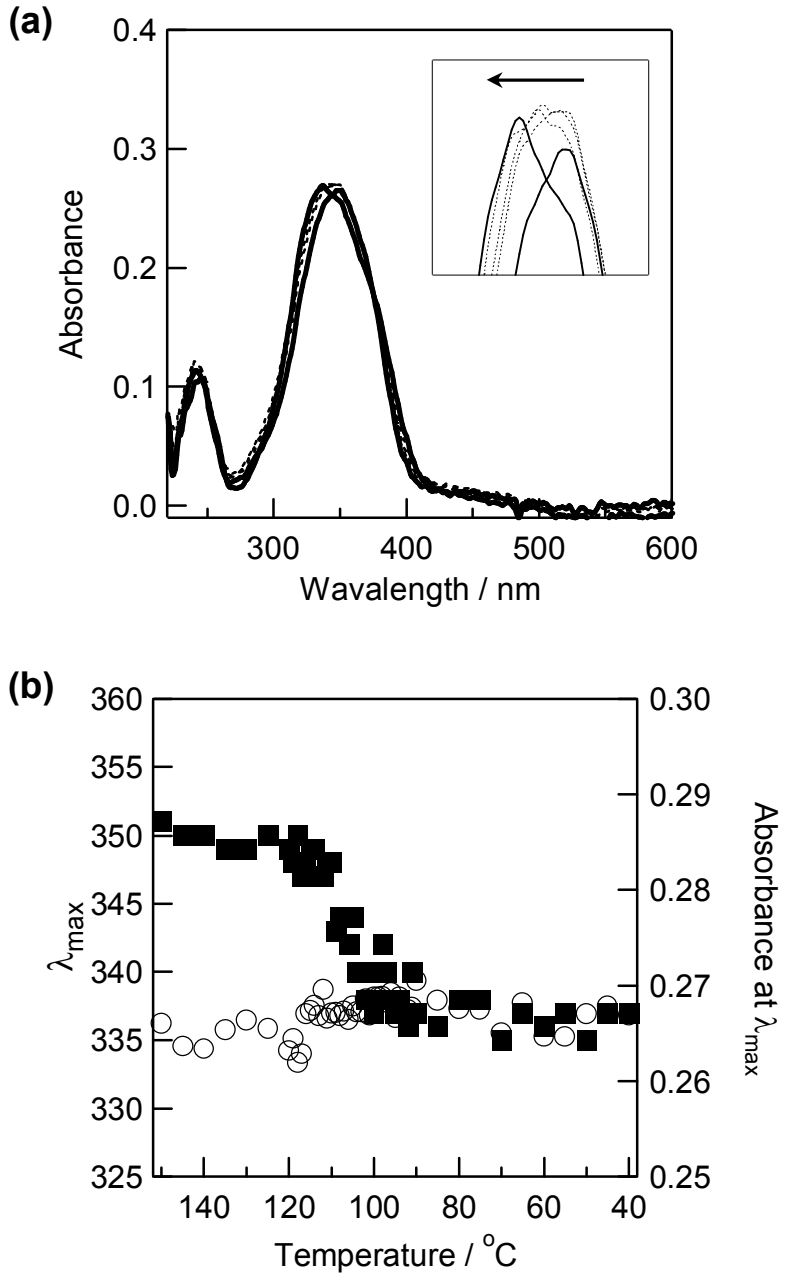

Figure 2-12. UV-vis absorption spectra of the grafted polymer film at various temperatures on cooling process (a), and the relationship between λ_{max} or absorbance at λ_{max} vs temperatures (b).

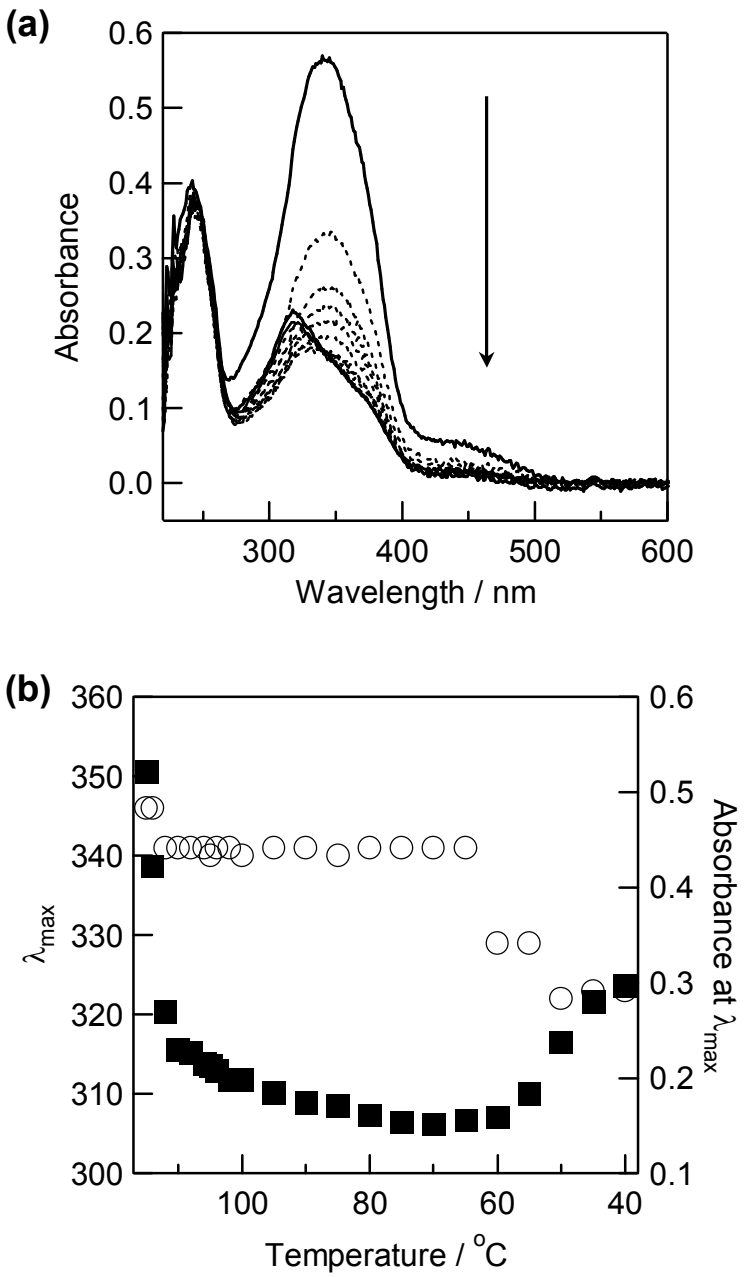

Figure 2-13. UV-vis absorption spectra of the spincast film at various temperatures (a), and the relationship between λ_{max} and absorbance at λ_{max} vs temperature (b).

transition of free polymer PMA(Az) evaluated by DSC. Thus, the smectic LC-isotropic phase transition of the grafted polymer can be detected as aggregation changes of the Az mesogenic groups. In other words, the thermophysical properties of the free polymer are maintained in the grafted state. The absorbance values were not changed in the cooling and heating processes, suggesting that absorptivity in the aggregated and non-aggregated states are almost the same. A slight enhancement of the transition temperature should be worth mentioning. The higher point to the isotropic transition estimated by the spectral data was 115 °C, 7 °C higher than that observed for PMA(Az) in the DSC analysis (Figure 2-1). Tsujii and co-workers reported that the T_g of high density poly(methyl methacrylate) brushes becomes higher than that of corresponding cast films.[33] A similar effect is admitted for the LC to isotropic transition temperature.

Figure 2-13 displays the UV-vis absorption spectra of a spincast film at various temperatures on cooling process. The absorbance of the π–π* transition band gradually decreased concomitantly with hyprochromic shifts of λ_{max}, but that of the ϕ–ϕ* band stayed unchanged. Below 60 °C, λ_{max} was shifted to 320 nm and formed stronger H-aggregate. Such change in absorbance should be ascribed to the change in the molecular orientation from random to perpendicular state on substrate. Furthermore, this spectral change was only observed 1st cooling process, and not reversible.

2.3.4.2. Polarized Optical Microscopic Observation

Figure 2-14 illustrate the POM images of a thick grafted polymer film. At 120 °C where no aggregation state of Az units was observed in the UV-vis spectrum, no transmitted light was observed, indicating that the mesogenic groups of the grafted polymer were in an isotropic state (a). On cooling, an LC texture ascribed to appearance of optical anisotropy was observed at 113.1 °C (b). At 111°C, an LC texture due to the optical birefringence appeared. This temperature range just corresponds to that of the blue shift in the UV-vis spectrum. Together with the results obtained by GI-SAXS measurements and UV-vis spectroscopy, it is concluded that the thermophysical properties of the graft chains on substrate are almost similar as those of spincast films. Only the molecular orientation is different.

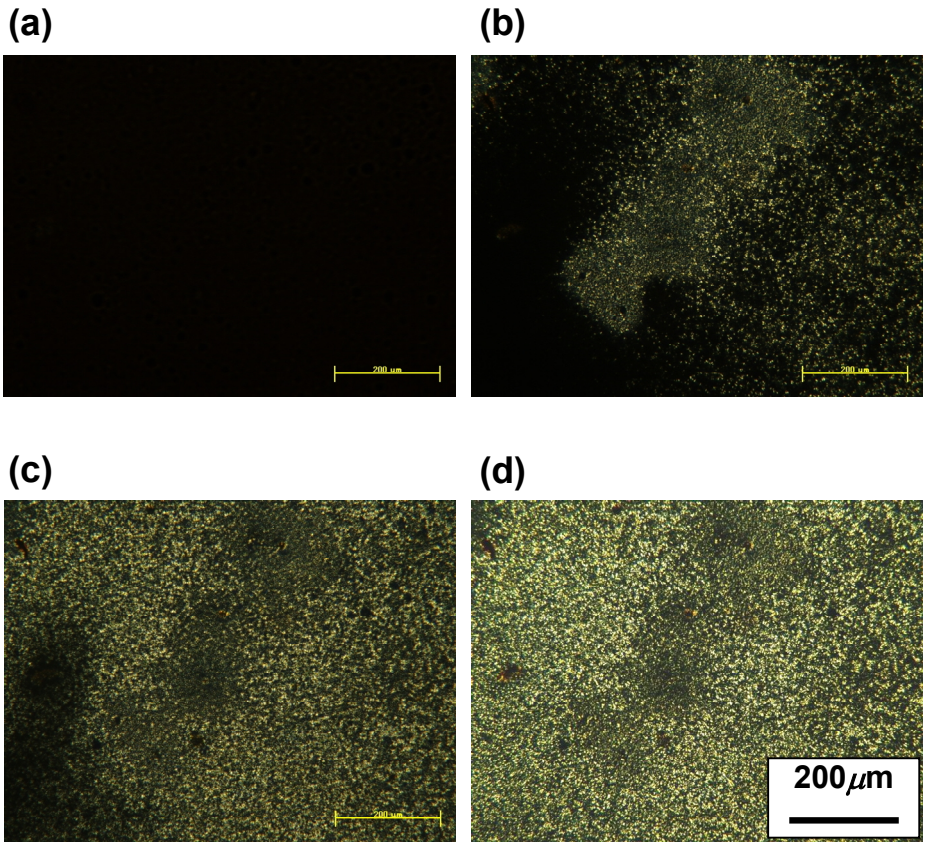

Figure 2-14. POM images of grafted films at 120 ºC (a),113.1 ºC (b), 113ºC, and 111ºC (d) on the cooling process.

2. 4. Conclusions

This chapter described the fabrication of Az grafted polymer films and evaluations of the molecular orientations. Grafted polymer films containing Az mesogenic groups tethered on a solid substrate were successfully synthesized by surface-initiated ATRP method. The chain length of graft film was controlled by polymerization time and initial monomer concentration.

The molecular orientation of LC mesogens was evaluated by UV-vis spectra and GI-XRD measurements, their structural properties were compared with those of conventional spincast films. In the grafted film, LC orientation is fully different from those of a spincast film. The LC orientations in the Az grafted films and spincast films are illustrated in Figure 2-15. In spincast films, Az mesogens adopt a homeotropic alignment to the substrate plane by annealing. In contrast, parallel alignment of Az units is attained in the films obtained by surface-initiated grafting polymerization. To our knowledge, this type of smectic LC orientation in a polymer film is observed for the first time.

In the grafted LC polymer film, thermophysical properties almost coincide with those of a spincast film. The temperature of a smectic LC phase-isotropic phase transitions of grafted film agrees with that of the spincast film as revealed by UV-vis spectroscopy and POM. In viewpoint of chemical structures, both polymers are identicalexcept for that the anchoring architecture onto the substrate surface exists or not. Consequently, by tethering on the substrate surface, the orientation of polymer chains and mesogens can be altered without losing their characteristics.

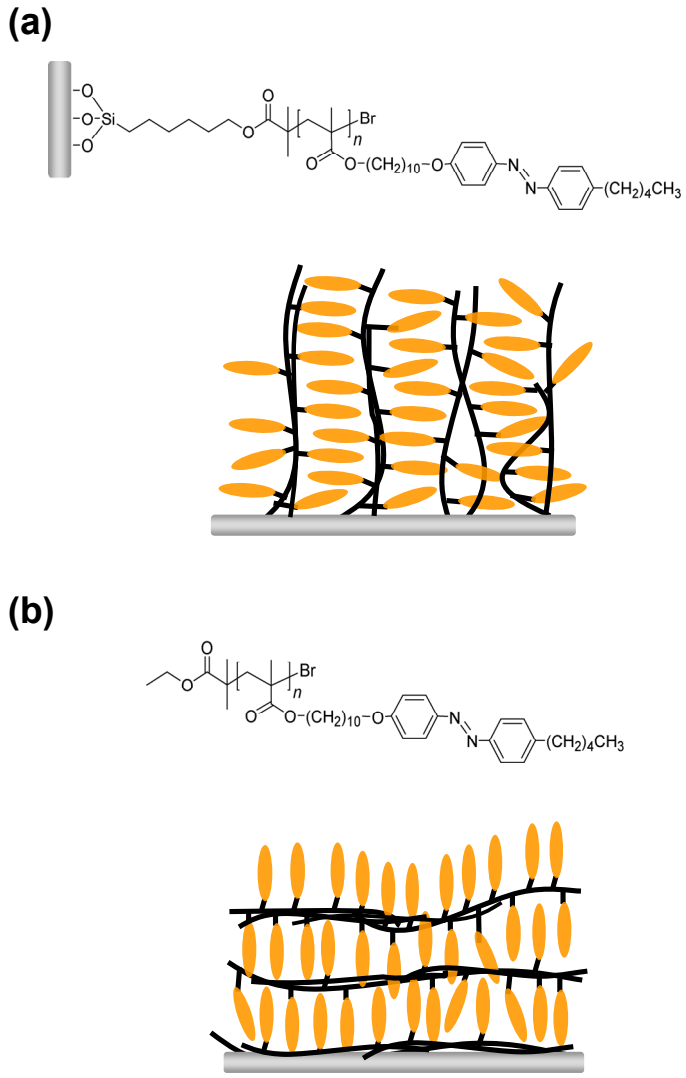

Figure 2-15. Schematic illustration of the orientation of mesogenic Az groups in the grafted polymer on substrate (a) and spincast film (b).

Reference

[1] Advincula, R. C.; Brittain, W. J.; Caster, K. C.; Rühe, J. (Ed.) *Polymer Brushes*, WILEY-VCH, **2004**.

[2] Zhao, B.; Brittain, W. J. *Prog. Polym. Sci.*, **2000**, 25, 677.

[3] Milner, S. T. *Science*, **1991**, 251, 905

[4] Mansky, P.; Liu, Y.; Huang, E.; Russell, T. P.; Hawker, C. *Science* **1997**, 275, 1458.

[5] Ejaz, M.; Yamamoto, S.; Ohno, K.; Tsujii, Y.; Fukuda, T. *Macromolecules*, **1998**, 31, 5934.

[6] Zhao, B.; Brittain W. J. *J. Am. Chem. Soc.*, **1999**, 121, 3557.

[7] Matyjaszewski, K.; Miller, P. J.; Shukla, N.; Immarapom, B.; Gelman, A.; Luokala, B. B.; Siclovan, T. M.; Kickelbick, G.; Vallant, T.; Hoffmann, H.; Pakula, T. *Macromolecules*, **1999**, 32, 8716.

[8] Husseman, M.; Malmström, E.; McNamara, M.; Mate, M.; Mecerreyes, D.; Benoit, D. G.; Hedrick, J. L.; Mansky, P.; Huang, E.; Russell, T. P.; Hawker, C. J. *Macromolecules*, **1999**, 32. 1424.

[9] Matyjaszewski, K.; Xia, J. *Chem. Rev.* **2001**, 101, 2921.

[10] Kamigaito, M.; Ando, T.; Sawamoto, M. *Chem. Rev.* **2001**, 101, 3689.

[11] Halperin A.; Williams, D. R. M. *J. Phys. Condens. Matter.*, **1994**, 6, A297.

[12] Peng, B.; Johannsmann, D.; Rühe, J. *Macromolecules*, **1999**, 32, 6759.

[13] Peng, B.; Rühe, J.; Johannsmann, D. *Adv. Mater.*, **2000**, 12, 821.

[14] Hamelinck P. J.; Huck, W. T. S. *J. Mater., Chem.*, **2005**, 15, 381.

[15] Börner, H. G.; Beers, K.; Matyjaszewski, K.; Sheiko, S. S.; Möller, M *Macromolecules* **2001**, 34, 4375.

[16] Keller, R. N.; Wycoff, W. M. *Inorg. Synth.* **1946**, 2, 1.

[17] Tian, Y.; Watanabe, K.; Kong, X.; Abe, J.; Iyoda, T. *Macromolecules* **2002**, 35, 3739.

[18] Kadota, S.; Aoki, K.; Nagano, S.; Seki, T. *Trans. Mater. Res. Soc. Jpn.* **2005**, 30,659.

[19] Kadota, S.; Aoki, K.; Nagano, S.; Seki, T. *Coll. and Surf. A Phys. Eng. Asp.*, **2006**, 284-285, 535.

[20] Ohno, K.; Morinaga, T.; Koh, K.; Tsujii, Y.; Fukuda, T. *Macromolecules* **2005**, 38, 2137.

[21] Sugimura, H.; Hozumi, A.; Kameyama, T.; Takai, O. *Surf. Interface Anal.*, **2002**, 34, 550.

[22] Hayashi, K.; Saito, N.; Sugimura, H.; Takai, O.; Nagagiri, N. *Langmuir* **2002**, 18, 7469.

[23] Hozumi, A.; Yokogawa, Y.; Kameyama, Y.; Sugimura, H.; Hayashi, K.; Shinohara, H.; Takai, O. *J. Vac. Sci. Techno. A* **2001**, 19, 1812.

[24] Kong, X.; Kawai, T.; Abe, J.; Iyoda, T. *Macromolecules* **2001**, 34, 1837.

[25] Rieko, P. C.; Baer, D. R.; Fryxell, G. E.; Engelhard, M. H.; Porter, M. S. *J. Vac. Sci. Technol. A* **1993**, 11, 2292.

[26] Geue, T.; Zieglar, A.; Stumpe, J. *Macromolecules*, **1997**, 30, 5729.

[27] Han, M.; Morino, S.; Ichimura, K. *Chem. Lett.*, **1999**, 645.

[28] Mensinger, H.; Stamm, M.; Boeffel, C. *J. Chem. Phys.* **1992**, 96, 3183.

[29] Henn, G.; Stamm, M.; Poths, H.; Rücher, M.; Rabe, J. P. *Physica B*, **1996**, 221, 174.

[30] Morikawa, Y.; Nagano, S.; Watanabe, K.; Kamata, K.; Iyoda, T.; Seki, T. *Adv. Mater.*, **2006**, 18, 883.

[31] Fischer, H.; Poser, S. *Acta Polymerica*, **1996**, 15, 949.

[32] Mao, G.; Wang, J.; Clingman, S. R.; Ober, C. K.; Chen, J. T.; Thomas, E. L. *Macromolecules*, **1997**, 30, 2556.

[33] Yamamoto, S.; Tsujii, Y.; Fukuda, T. *Macromolecules*, **2002**, 35, 6077.

Chapter III

Photo-alignment Behavior of Liquid Crystalline Azobenzene Side Chains in the Polymer Brushes

3.1. Introduction

High density polymer brushes have attracted a great deal of interest due to the derived properties in the thermophysical properties,[1] tribological properties,[2,3,4] adhesion,[5] and wettability.[6] Such deviations are originated from the anisotropy of the polymer chains. This structure has been synthesized by using surface-initiated controlled/"living" polymerization techniques such as atom transfer radical polymerization (ATRP).[7,8] Since ATRP is available with various functionalized monomers, many researchers have been investigating the surface properties of functional polymer brushes introducing the ionic groups,[9,10] thermo-responsive molecules,[11,12] photo-functional units,[13,14] electrochemical units,[15] and liquid crystalline groups[16] and so on.

Chapter II described that the novel liquid crystalline (LC) polymer brushes containing azobenzene (Az) moiety in the side chains were synthesized by surface-initiated grafting polymerization, and that the LC orientation in the side chains showed a parallel alignment in the films with retention of the thermophysical properties of a conventional spincast film. The Az mesogens are anticipated to be more effectively controlled with irradiation of ultraviolet light (UV) or visible light (Vis), since they are oriented parallel to the substrate plane. Additionally, it seems that Az groups in the grafted polymer film respond to light in a different manner from that in spincast films. Therefore, this chapter investigated the photo-alignment behavior of the Az-polymer grafted on the substrates.

Photoinduced optical anisotropy in polymer films has been extensively studied from fundamental interest relating to polymer physics and also from practical viewpoints in the applications to optical data storages and processing.[17] The optical anisotropy is

induced by irradiation with linear polarized light in polymer films. The reorientation of Az is caused by repeated photoisomerizations in such a way that the chromophore orient perpendicularly to the polarization plane of the light. Stumpe et al. reported that the storage stability of photoinduced optical anisotropy in spincoated films[18,19,20] and Langmuir-Blodgett multilayers[21] of liquid crystalline polymers bearing an Az group in the side chain. They found that in spincoated films, the photoinduced optical anisotropy is enhanced by thermal annealing above the T_g.[17] Han et al. studied of the photomanipulation of two and three dimensional orientations of liquid crystalline polymers attaching Az molecules in the side chains by irradiation with linearly polarized 436 nm light,[22] non-polarized 436 nm light,[23] and polarized 365 nm light.[24]

Furthermore, reversible photochemical alignment control of nematic LC by using photochromic command layers have been reported by Ichimura et al. in 1988.[25] Since each photochromic unit brings about the reversible alignment alteration of about 10^4 LC molecules, this system is called "command surface". Systematic studies allowed the application to other types of LCs such as smectic,[26] cholesteric,[27] discotic,[28] and lyotropic LCs.[29] Furthermore, by using command surface process, photoalignment of dye aggregates,[30] poly(di-n-hexylsilane) main chain,[31,32,33] and mesoporous materials[34,35] are reported.

The research background as mentioned above motivated to evaluate photoorientation behavior on the Az-polymer grafted substrates under investigation. This chapter demonstrates the photoalignment behavior of LC mesogens in the grafted polymer. The photoinduced molecular orientation and reorientation are investigated by UV-vis absorption spectroscopy and grazing-incidence X-ray diffraction (GI-XRD) measurements.

3.2. Experimental Section

3.2.1. Materials

The chemical structures used here are shown in Chart 3-1. The Az-polymer grafted substrates (PMA(Az) graft) were synthesized by surface-initiated ATRP. Details about syntheses were described in chapter II. Their thicknesses were ca. 5 - 30 nm as

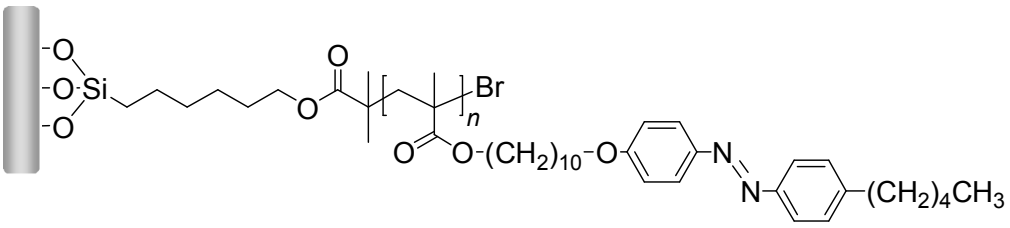

pMA(Az) graft

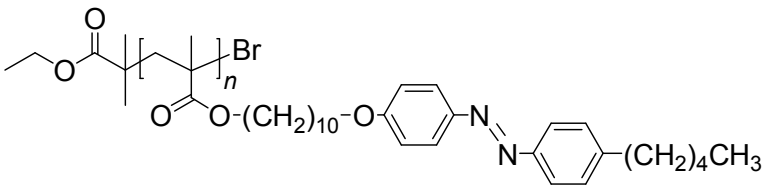

pMA(Az)

Chart 3-1.

measured by ellipsometory (Philips PZ2000 equipped with 632.8 nm He-Ne laser). The samples were annealed at 140 °C for 1 h before subjecting to various measurements.

A free polymer of PMA(Az) were also synthesized by ATRP. The number average molecular weight (M_n) was ca. 9800, with polydispersity (M_w/M_n) of 1.14. Spincast films were achieved from a 2 wt% toluene solution of PMA(Az) on quartz plates cleaned in KOH/ethanol by using a spin-coater at 2000 rpm for 30 s. Samples were annealed at 100 °C for 10 min to remove residual solvent. The film thickness was ca. 40 nm as evaluated both by ellipsometory and AFM measurements (Seiko Instruments NanoPics2100/NPX200 system).

3.2.2. Measurements

UV–vis absorption spectra for the grafted substrates and spincast films at room temperature were taken with a Hewlett-Packard diode array spectrometer 8452A and an Agilent Technology 8453 spectrometer. For polarized spectra, a polarizer mounted in a rotating holder was placed in front of the sample.

The UV and visible light irradiation of the samples was performed using a Hg-Xe lamp (SAN-EI Electric UVF-203S) equipped with an appropriate set of color filters (Toshiba glass: UV-35 + UV-D36A and V-44 + Y-43 for 365 nm and 436 nm light, respectively). Linearly polarized light (LPL) was obtained by passing through a polarizer. Light intensity was measured by an optical power meter (Advantest TQ8210). A hot stage was employed to control heating temperatures.

Grazing-angle incidence X-ray diffraction (GI-XRD) measurements were obtained with a Rigaku RINT-2100 operating with CuK_α radiation (0.154 nm). Their scattering profiles were recorded on a imaging plate.

3.3. Results and Discussion

3.3.1. Photoisomerization

Spectral changes on UV and visible light irradiation were followed in Az polymer grafted films and spincast films, and the results are shown in Figure 3-1 and 3-2, respectively. Before irradiation, the absorption maximum (λ_{max}) centered at 337 nm,

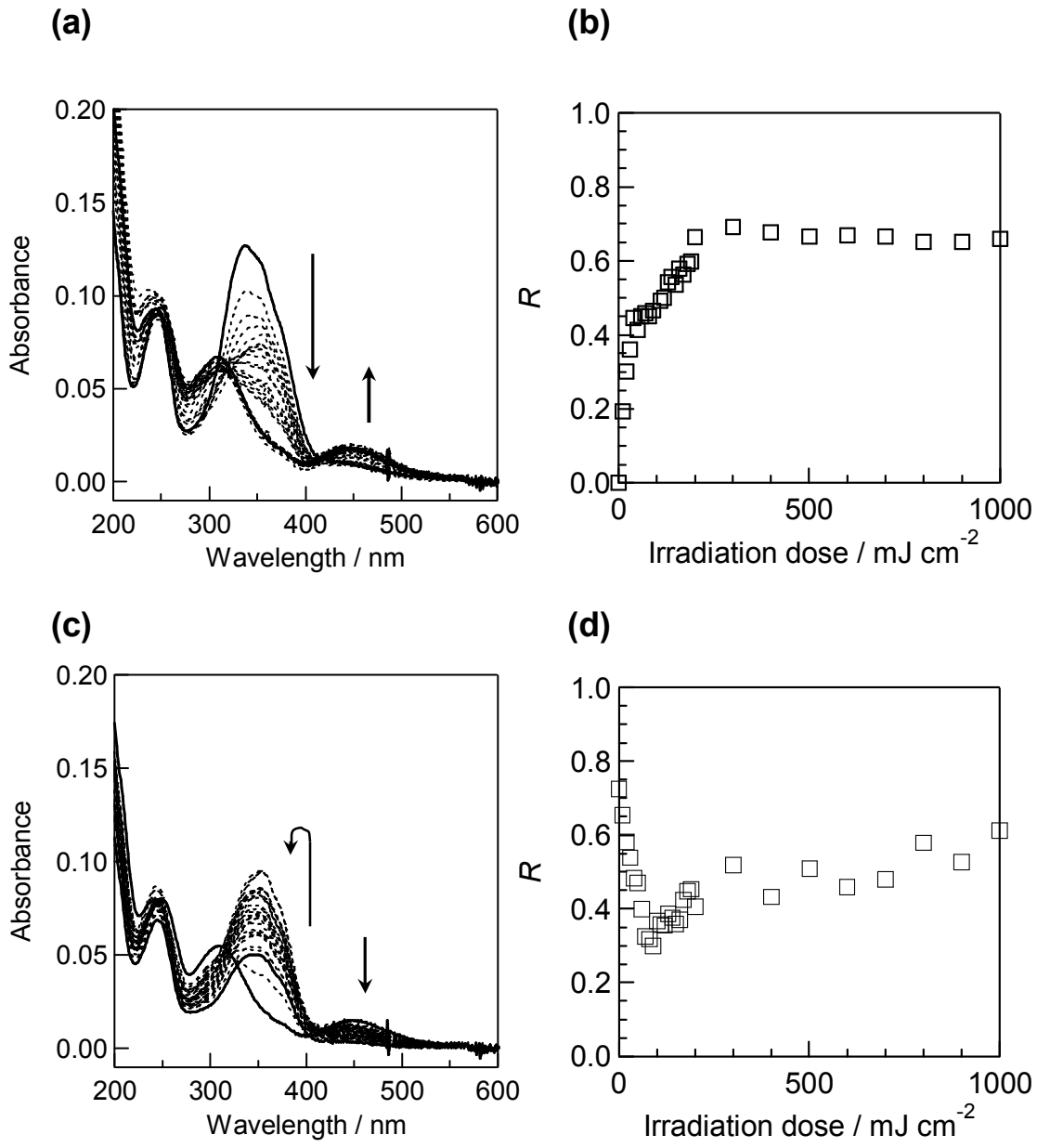

Figure 3-1. UV–vis absorption spectra of Az polymer grafted substrate, (a) upon 365 nm UV irradiation (2 mW cm-2) and (c) upon 436 nm Vis irradiation (1 mW cm-2). (b) and (c) show the changes in R defined in the text, which can be a rough measure of cis-content.

and 320 nm, respectively. In grafted films, the Az side chains formed H-aggregate and oriented parallel to the substrate plane, whereas a perpendicular orientation was formed in the spincast films. This photochemical process in the Az-polymer grafted film was similar to that in a tetrahydrofuran (THF) solution. Upon 365 nm UV irradiation, the absorbance of the π–π* long-axis transition band of the trans-isomer at 337 nm gradually decreased and the n–π* absorption band at 455 nm enhanced concomitantly, indicating formation of the cis-isomer. The isomerization states were estimated by the changes in the normalized absorption intensities at 337 nm in the trans–cis photoisomerisation. A measure of cis-content (R) is defined as follows.

$$R = 1\text{-}\{A_{\lambda\max} / A_{\lambda\max}(0)\},$$

where $\lambda_{\max}$ and $A_{\lambda\max}(0)$ denote the absorbances at $\lambda_{\max}$ before and after irradiation of 365 or 436 nm light, respectively. Figure 3-1b and 1d shows the changes in the R values with irradiation dose. When the 365 nm light was irradiated, R values increase gradually and reached a saturation level by about 100 mJ cm^{-2}. This exposure energy was almost the same as that observed in THF solution. The reverse spectral changes were observed by irradiation of 436 nm visible light. This indicates that the photoisomerization process of Az-polymer grafted films occurred as efficiently as that in solution. It is assumed that such effective photoisomerization is caused by the parallel orientation of Az chromophores. On the other hand, upon 436 nm light irradiation, absorbance at 352 nm R gradually increased until 80 mJ cm^{-2}. However, upon further irradiation, R progressively reduced to reach a saturated state (the photostationary state). The absorption spectral shape of the initial trans state and the final one via the cis form were different. $A_{\lambda\max}$ decreased from 0.13 to 0.05 for the former and the latter, respectively. This behavior should be attributed to the change in the orientation of Az unit. After a thermal treatment at 140 °C for 10 min, the absorbance at the photostationary state immediately increased and became congruent with that of the initial trans form.

Figure 3-2 displays the photo-isomerization behavior of a spincast film after the

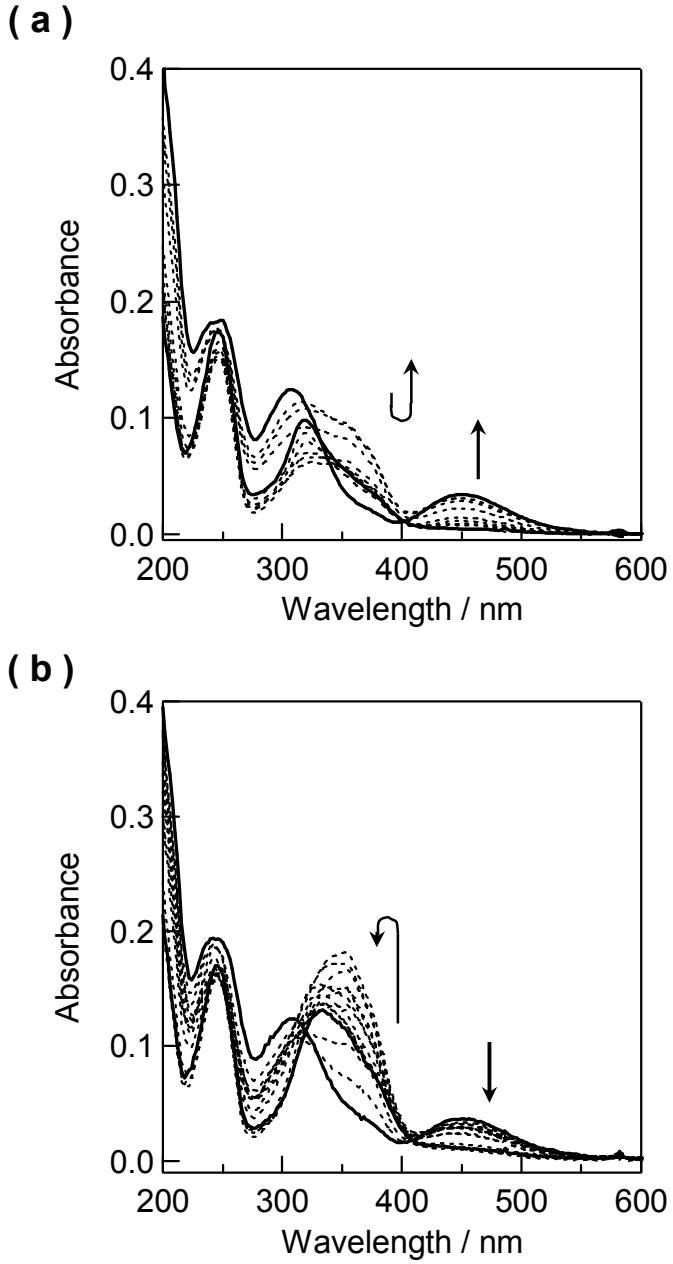

Figure 3-2. UV–vis spectra of spincast film. (a) upon 365 nm UV irradiation (2 mW cm-2) and (b) upon 436 nm Vis irradiation (1 mW/cm-2).

thermal treatment. The spectral changes are quite different from those of the grafted films. Complicated changes were observed when the annealed spincast film was irradiated with 365 nm light. In an early stage of the irradiation until 100 mJ cm^{-2}, the absorbance at 320 nm decreased accompanying λ_{max} shifts from 320 nm to 326 nm. Spectral shape became broader around 350nm. This indicates that the H-type aggregate is dissociated and the Az groups became in a monomeric state. With further irradiation, the absorbance increased monotonously and finally the n–π* absorption band at 455 nm indicating the formation of cis-isomer enhanced. The back-reaction process on the irradiation of visible light at 436 nm was also different. The absorbance derived from the monomeric state at 352 nm was clearly observed at an earlier stage, which gradually increased until 60 mJ cm^{-2}. By further irradiation, the absorbance reduced and λ_{max} was shifted to 330 nm. This tendency is in agreement with that of other previous LC polymers containing Az molecules.[36,37]

Therefore, the above results clearly show that the Az-grafted films and spincast films exhibit quite different photophysical and photochemical properties. Such different behaviors may be related to the photoinduced orientations.

3.3.2. In-plane Photoalignment by Irradiation of Linearly Polarized Visible Light

3.3.2.1. Photoinduced Dichroism

Figure 3-3 shows polarized UV-vis absorption spectra of Az graft substrates before irradiation with 436 nm linearly polarized visible light. Polarized direction: A_1 and A_2 were taken as illustrated in Figure 3-3a. The π-π* band of Az were observed around 338 nm. Essentially the same spectra in the directions of A_1 and A_2 were obtained. Thus, the in-plane dichroism was not observed before exposure to 436 nm LPL. Probably, the mesogens formed polydomains. Also, the dichroism was not observed in spincast films before irradiation with LPL. The Az molecules were highly oriented perpendicular to the substrates by thermal annealing, therefore, the chromophores hardly absorbed the LPL.

Figure 3-4 displays polarized UV-vis spectra of the Az-polymer grafted film, which was irradiated with 436 nm LPL at room temperature. The exposure energy was

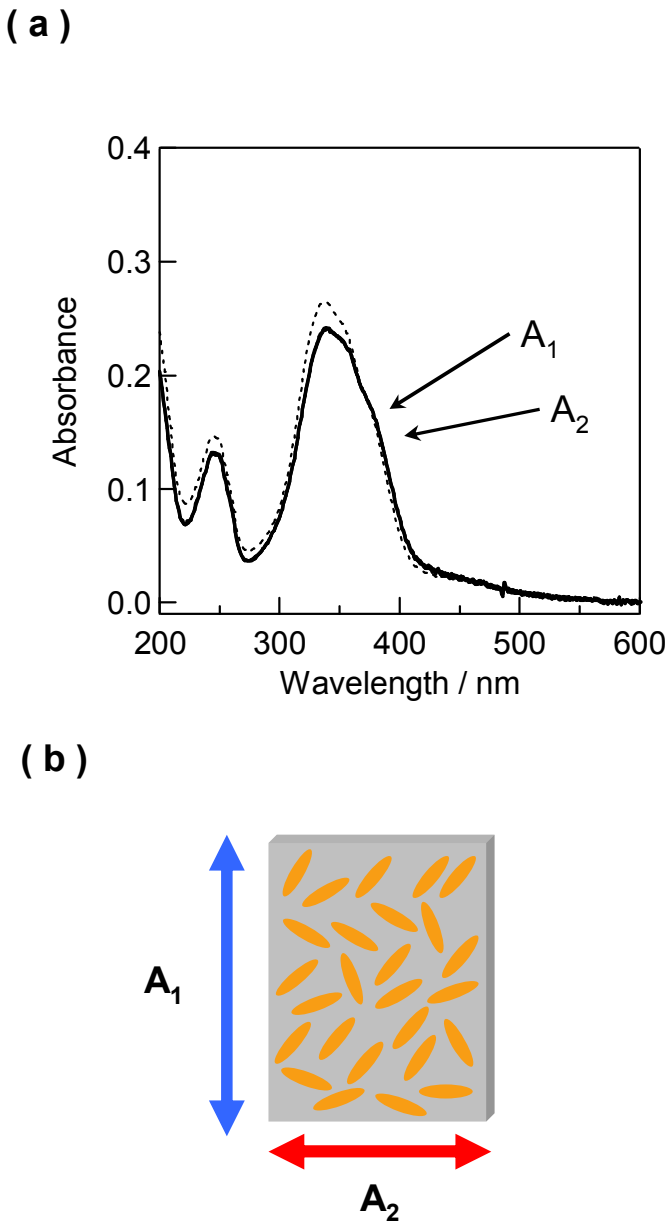

Figure 3-3. Polarized UV–vis spectra of Az-polymer grafted film before exposure to linearly polarized light (a). Dashed line is a spectrum taken with non-polarized beam. A1 and A2 indicate the direction of polarization of the probing light (b).

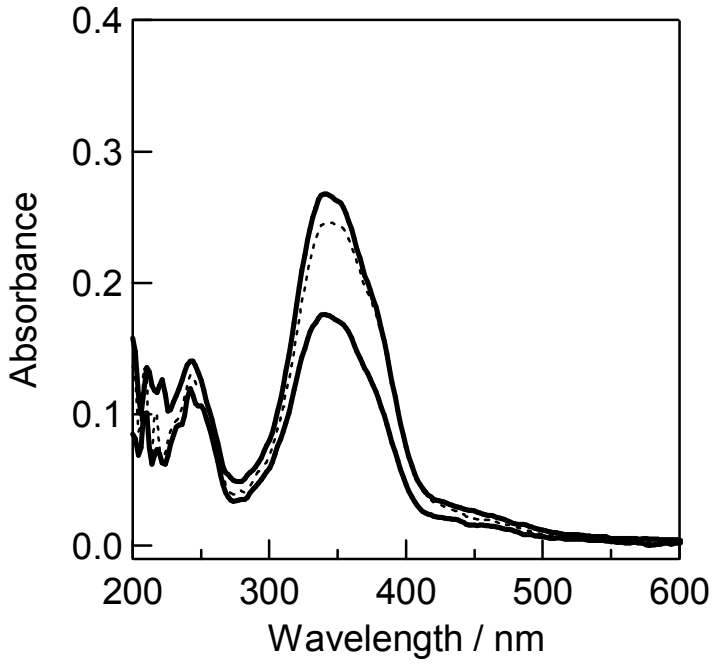

Figure 3-4. Polarized UV–vis absorption spectra of grafted substrates upon 436 nm LUV irradiation at room temperature. Dashed line shows a spectrum taken with non-polarized beam before irradiation of LPL.

approximately 2 J cm^{-2}. The absorbance of the π-π* transition band for the polarized probing light set orthogonal to the electric vector of the actinic LPL ($A_{\perp}$) was larger than that in parallel with that ($A_{//}$). The level of photoinduced in-plane optical anisotropy of films was estimated by order parameters (S) of the azobenzene as follows equation.

$$S = (A_{\perp} - A_{//}) / (A_{\perp} + 2A_{//})$$

where $A_{\perp}$ and $A_{//}$ denote absorbances at λ_{max} (=338 nm for grafted films after annealing) obtained by measurements using polarized light with the electric vectors perpendicular and parallel to that of actinic polarized light. S was ca. 0.14 and this value was slightly higher than that of spincast films or other smectic liquid crystalline polymers reported (S < 0.1).[22] From previous literatures, the order parameters of smectic LC polymer increased with irradiation of LPL above T_g.[22] Therefore, the order parameter of grafted films was expected to be increased at elevated temperatures.

3.3.2.2. Effect of Temperature

It was reported that the annealing of spin-coated films of liquid crystalline polymers leads to marked enhancement of the optical anisotropy generated by irradiation with linearly polarized light.[38] Han et al. reported that S of spincast films of smectic LC Az-polymers were increased and reached 0.2 at smectic LC temperatures.[22]

The Az grafted films were exposed to linearly polarized 436 nm light at room temperature and elevated temperatures near the T_g or above T_g to explore the effect of temperature on the photoinduced orientation behavior of the azobenzene molecules. Figure 3-5 shows the generation of photodichroism at various film temperatures; room temperature (25 °C), 60 °C (above T_g of free polymer; PMA(Az)), and 100 °C (above T_g and near the isotropic temperature of PMA(Az)). When the 436 nm LPL was irradiated at room temperature, S values increased gradually and reached a saturation level at approximately 400 mJ cm^{-2}. The photoirradiation of grafted films with the linearly polarized 436 nm light at elevated temperatures displayed photoorientational behavior dramatically different from the results carried out at room temperature. The

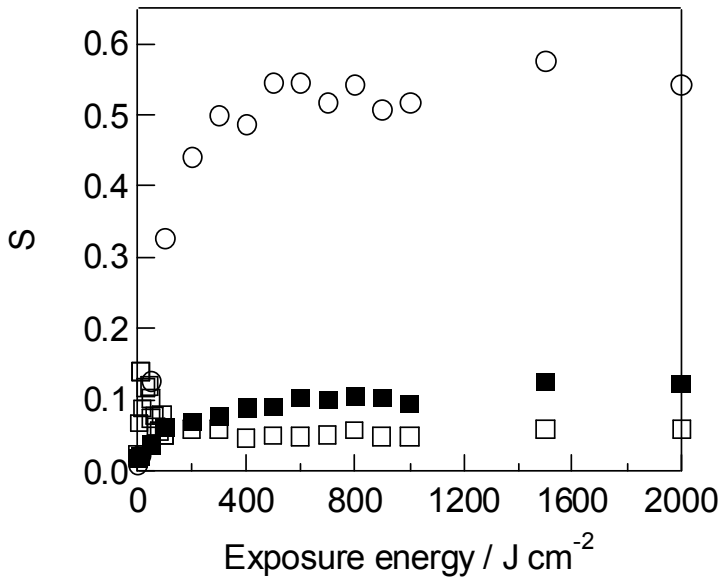

Figure 3-5. Changes in order parameters (S) of Az-polymer grafted substrates during irradiation with linearly polarized 436 nm light at room temperature (■), 60 oC (○), and 100 oC (□).

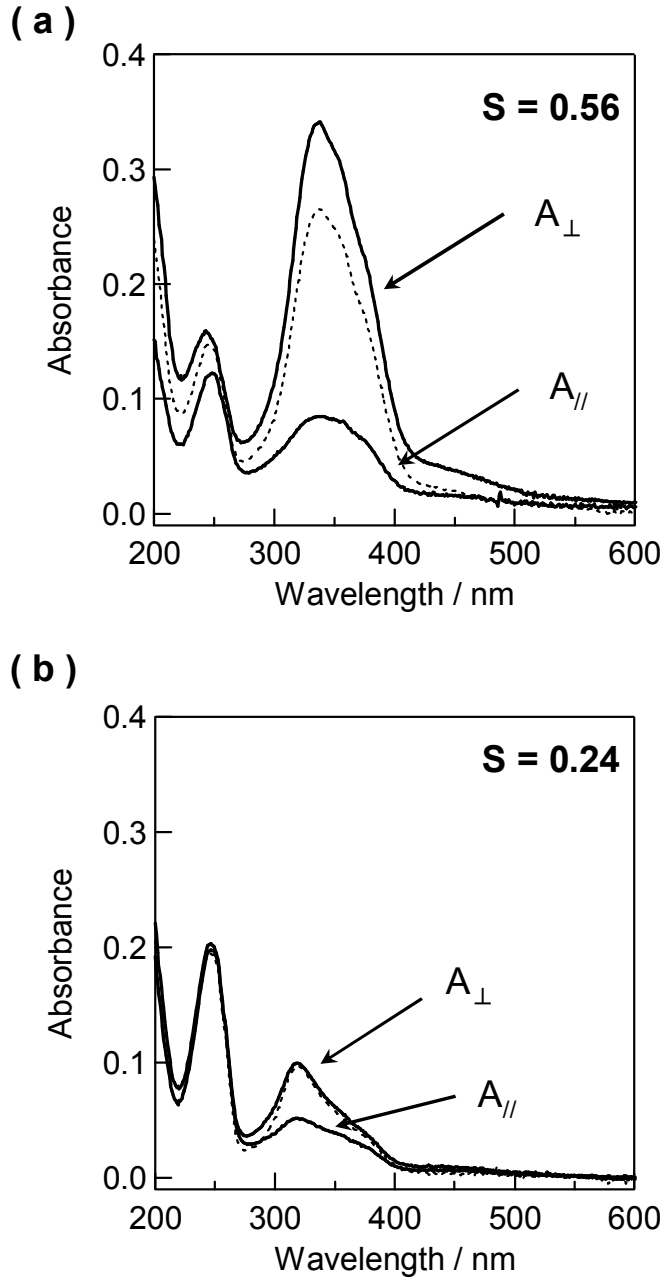

Figure 3-6. Polarized UV–vis absorption spectra of grafted substrate (a) and spincast film (b) upon 436 nm LPL irradiation at 60 oC. The exposure energy was 2 J cm-2.Dashed line is a non-polarized UV-vis spectrum before irradiation of LPL.

photo-irradiation was performed at elevated temperatures, followed by immediate cooling to ambient temperature to achieve absorption spectral measurements. The profile of the photoinduced orientation of S at 60 °C, higher than T_g of PMA(Az) (51 °C) exhibited a rapid appearance of the photodichroism and reached a saturation value at about 200 mJ cm^{-2} (open circle in Figure 3-5). Figure 3-6a shows polarized UV-vis spectra of Az-polymer grafted substrates whose film thickness was about 20 nm after exposure with at 60 °C. It is noteworthy that the final value of S (= 0.56) is much higher than that obtained at room temperature. In contrast, S of the spincast film obtained after LPL irradiation at 2 J cm^{-2} and 60 °C was ca. 0.24 (Figure 3-6b). Above the results, S of grafted films was much higher than that of spincast films. The smaller induction of in-plane anisotropy can be explained as follows. The Az mesogones are highly oriented perpendicular to the substrate by thermal annealing, and therefore, can absorb light only slightly. In other words, the large absorption of LPL caused the large in-plane anisotropy for the grafted film because the Az chromophores are oriented parallel to the substrate.

Changes in S at 100 °C were quite different from that at room temperature and 60 °C. The S values increased abruptly at the early stage of the photoirradiation, however, a rapid reduction in S was observed through a maximum value at approximately 50 mJ cm^{-2} to be leveled off above approximately 150 mJ cm^{-2}. The reduction in S at the later stage should be caused by the segmental relaxation of the polymer chains at the temperature higher than T_g.

This photoinduced dichroism can be erased by thermal annealing at 140 °C, above the isotropidization temperature, and rewritten with another LPL of different direction. The randomized orientational state after annealing at 140 °C was thermally stable with no memory effect of the precious state. Thus in-plane orientation was fully rewritable, and any in-plane anisotropy can be produced with any polarization direction given.

3.3.2.3. Effect of Graft Length

Before irradiation with LPL, film thicknesses became larger when the

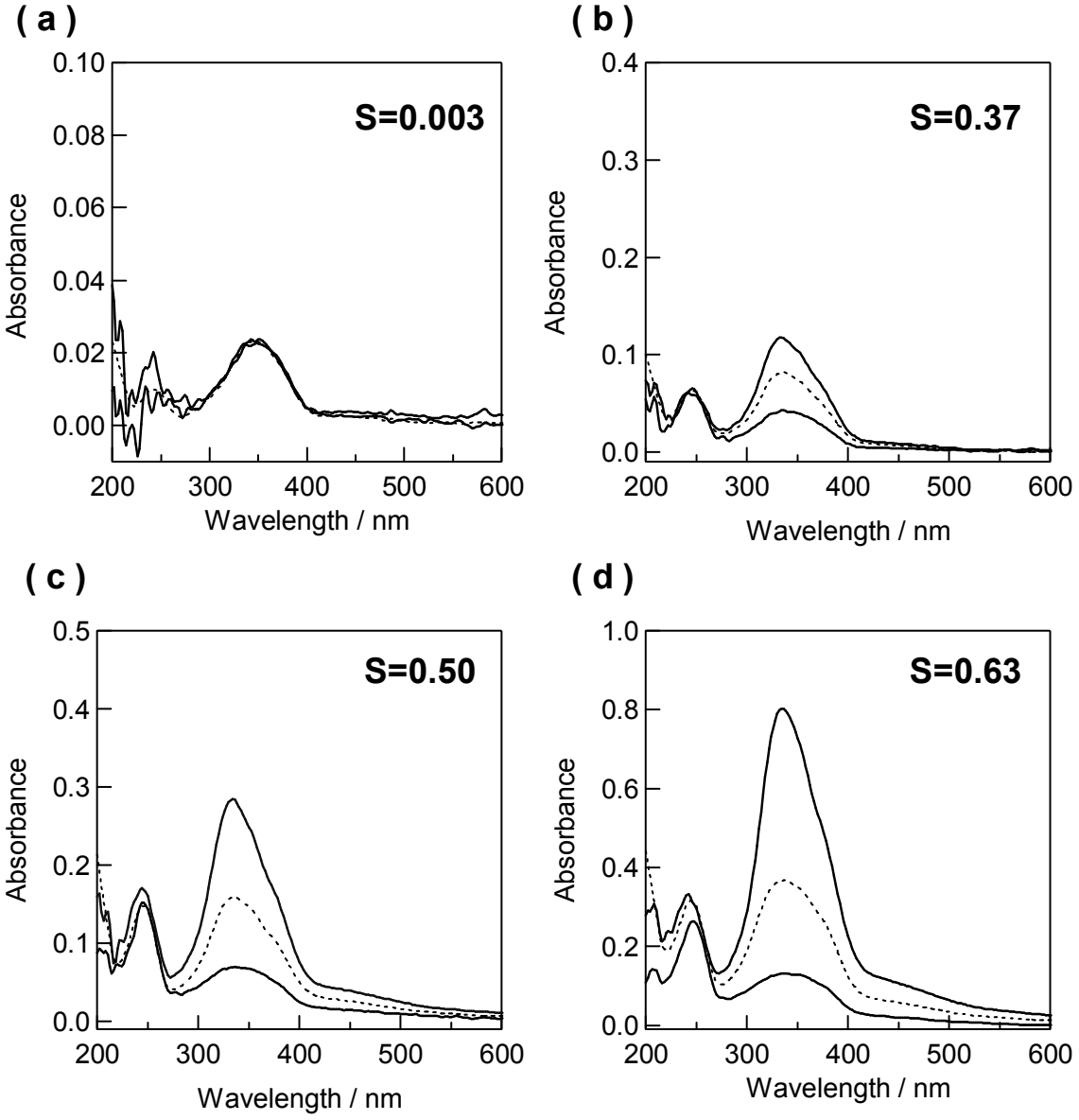

Figure 3-7. Polarized UV–vis spectra of Az-polymer grafted films with irradiation of 436 nm linearly polarized light at 60 oC. The film thicknesses are about 5 nm (a), 9 nm (b), 18 nm (c), and 30 nm (d) by using ellipsometor. Dashed line shows a spectrum taken with non-polarized beam before irradiation of LPL.

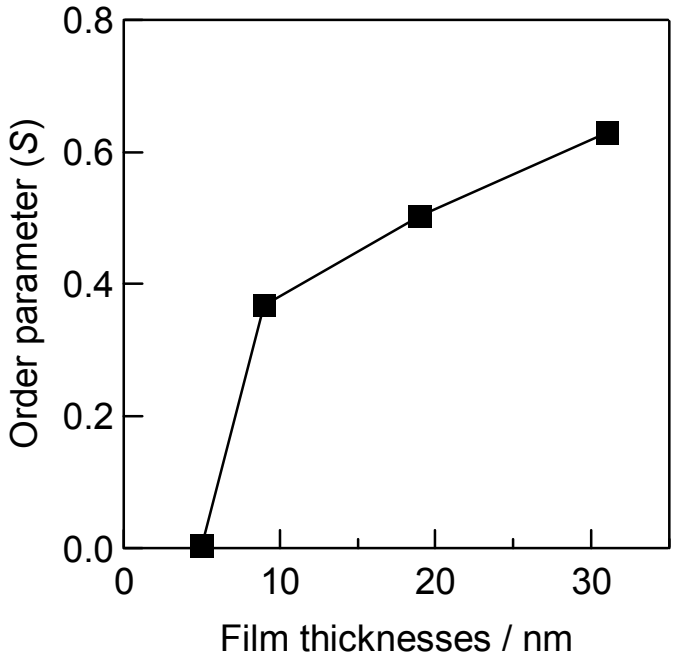

Figure 3-8. Changes in order parameters (S) of the photoinduced alignment as a function of the film thicknesses.

absorbance at λ_{max} increased. Figure 3-7 shows polarized UV-vis spectra of Az grafted substrates at various film thicknesses after exposure to 436 nm LPL. At 5 nm thickness, no dichroism was observed. By increasing film thicknesses or absorbance at λ_{max} before irradiation with 436 nm LPL, the *S* value increased accordingly. The relationship between *S* values and absorbance at λ_{max} before LPL irradiation is shown in Figure 3-8. This result indicates the level of in-plane dichroism obviously depends on the graft length. In case of thinner film thickness, the amount of Az chromophores on the grafted substrate s small. Thus, *S* values measured by polarized UV-vis spectra were almost leveled off. For the grafted film of 9 nm, *S* value was dramatically enhanced to ca. 0.4. From this result, anchored effect of polymer brushes was appeared above 9 nm thickness. When thickness of grafted films became larger, the amount of Az also increased, which will give rise to stronger molecular cooperativity It seems that *S* values became larger according to the thickness increase for this reason.

3.3.3. Controls of Photoalignment of the Smectic LC layer

The direction of smectic LC layers in the Az-polymer grafted substrate after exposure to 436 nm LPL was evaluated by GI-XRD measurements changing the direction of the incident X-ray beam. The configuration of the incident X-ray beam and polarized UV-vis spectra were shown in Figure 3-9. It is expected that a diffraction pattern was observed only when incident direction of X-ray was parallel to the direction of LPL irradiation (direction A).

Figure 3-10a shows 2-dimensional GI-XRD profile of the grafted polymer film recorded on an imaging plate in the incident direction of A. An intense comet-tail-like image running orthogonal to the substrate is an artifact of specular reflection. Diffraction patterns were only observed in the in-plane direction, the periodic structures derived from the smectic LC phase were formed perpendicular to the substrate plane, and LC mesogen being aligned parallel to substrates. This result is in agreement with that of polarized UV-vis absorption spectroscopy. From 1-dimensional XRD pattern monitored in the in-plane direction, a peak was observed at 2θ = 2.43 °, which corresponds to a layer spacing of 3.63 nm (Figure 3-10b). This spacing corresponds to

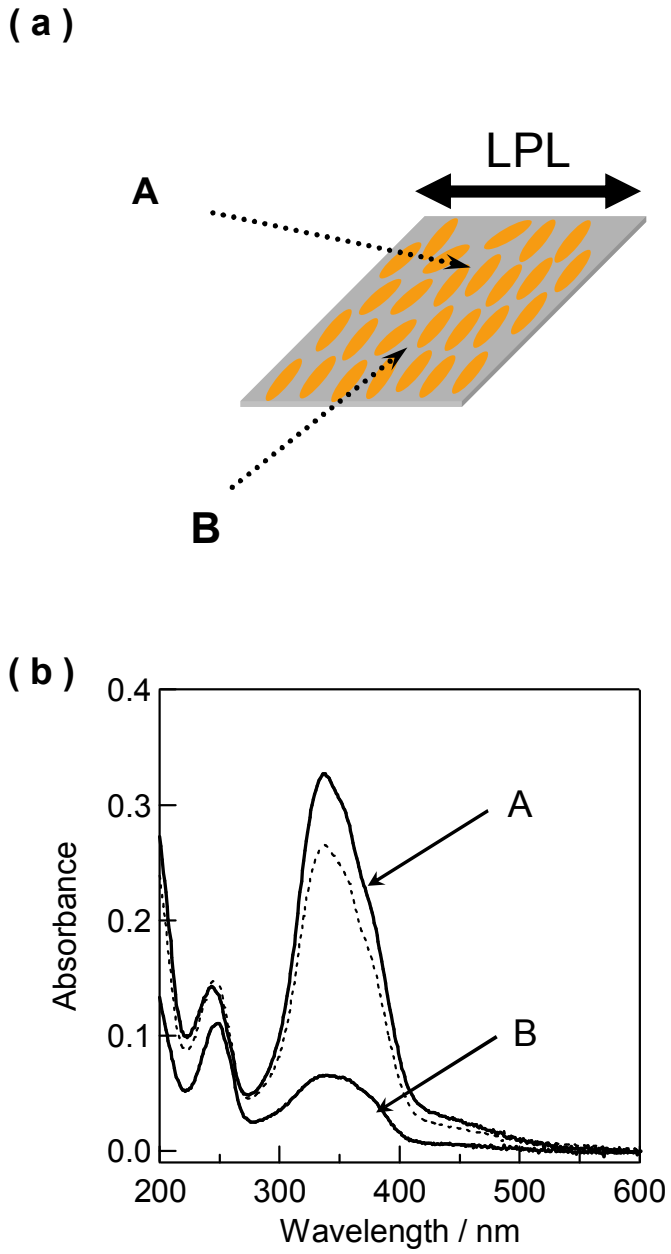

Figure 3-9. Geometry of the GI-XRD measurements of the Az-polymer grafted film (a), and the polarized UV-vis absorption spectra (b). Dashed line shows a spectrum taken with non-polarized beam before irradiation LPL.

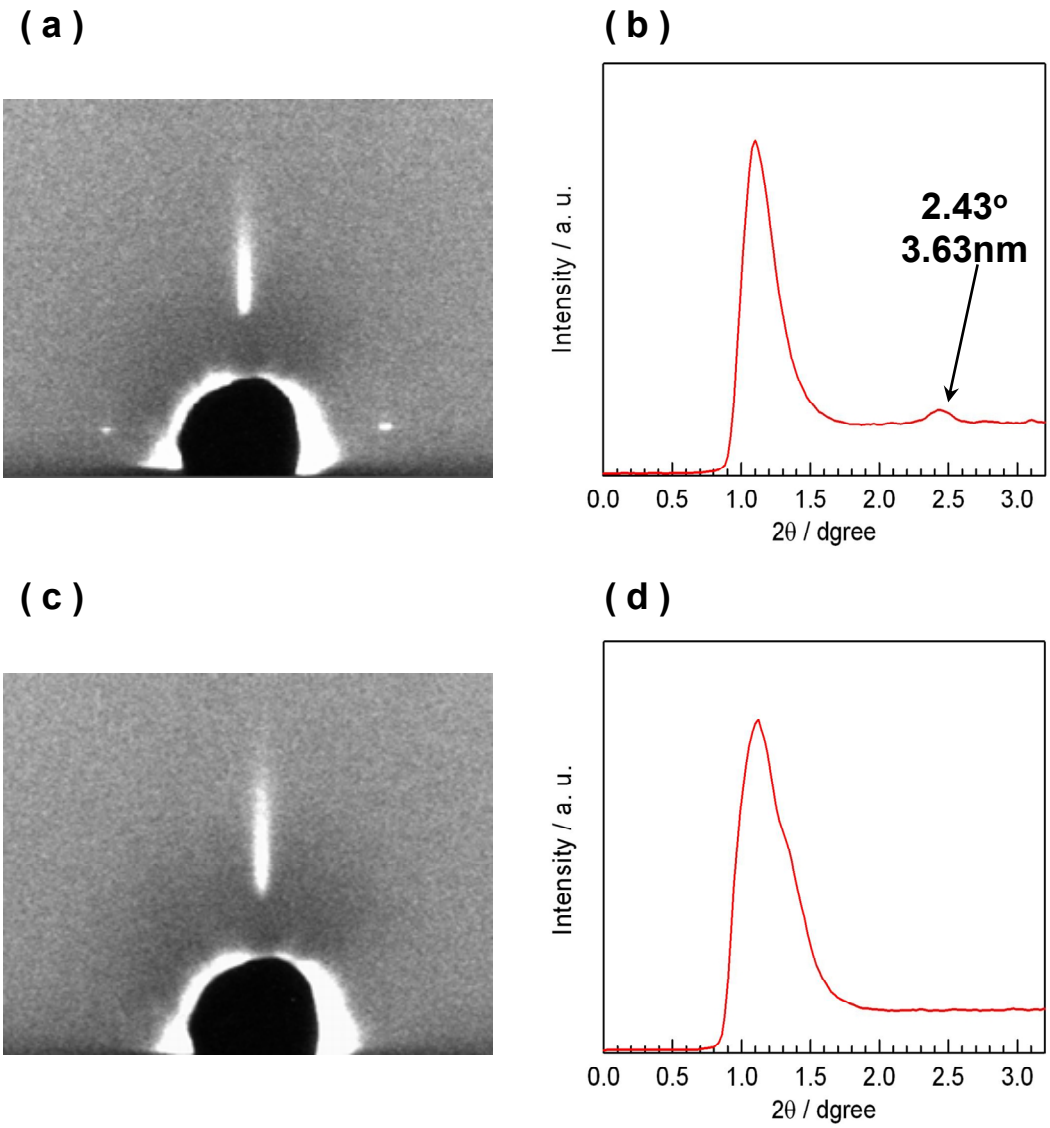

Figure 3-10. 2D GI-XRD pattern of the grafted polymer film recorded on an imaging plate in which the incident direction of X-ray was set as A (a), and B (c). 1D Profile in the in-plane direction extracted from the 2D XRD pattern in which the incident direction of X-ray was set as A (b) and B (d). A strong comet-tail-like line running in the perpendicular direction is a specular reflection.

the result described in Chapter II, suggesting the formation of interdigitated structures of Az side chains. Thus, the direction of smectic LC layers can be tunable by LPL.

In contrast, when the X-ray beam was subjected in the incident direction of B, no diffraction peak was observed in any direction. Thus, obvious regular structures derived of smectic LC layer are not observed in this direction. Above the results, smectic LC layers were aligned by irradiation of LPL and monodomain films were obtained.

3.4. Conclusions

This chapter described the photoalignment behavior of LC mesogens of the Az-polymer grafted substrates. The photoisomerization proceeded in high effectively as in solution. This feature seems to be caused by the parallel orientation of Az chromophores.

Highly ordered in-plane photoalignment of Az mesogens in the grafted substrate was induced by irradiation of linearly polarized visible light, which may also caused by the parallel molecular orientation of the mesogens. The order parameter (*S*) depended on the temperature applied during the LPL photoirradiation. The in-plane dichroism was most effectively generated at 60 °C which corresponds to a slightly higher temperature above T_g of the free polymer. Smectic LC layers were photoaligned and monodomain films were obtained as revealed by GI-XRD measurements.

In the above manners, the particular in-plane orientation of Az groups in the grafted polymer film indicates different photo-responsive nature from that in the conventional spincast film. Further investigation will involve an out-of-plane alignment of Az mesogens, photopatterning through a photomask and so on. it is expected that the grafted polymers with photoresponsive mesogenic groups would provide new types of alignment layers and “command surface” for LC materials.

Reference

[1] Yamamoto, S.; Tsujii, Y.; Fukuda, T. *Macromolecules* **2002**, 35, 6077.

[2] Yamamoto, S.; Ejaz, M.; Tsujii, Y.; Matsumoto, M.; Fukuda, T. *Macromolecules* **2000**, 33, 5602.

[3] Yamamoto, S.; Ejaz, M.; Tsujii, Y.; Fukuda, T. *Macromolecules* **2000**, 33, 5608.

[4] Sakata, H.; Kobayashi, M.; Otsuka, H.; Takahara, A. *Polymer Journal* **2005**, 37, 767.

[5] Lin, J. J.; Silas, A.; Bermudez, H.; Milam, V. T.; Bates, F. S.; Hammer, D. A. *Langmuir* **2004**, 20, 5493.

[6] Granville, A. M.; Brittain, W. J. *Macromol. Rapid Commun.* **2004**, 25, 1298.

[7] Tsujii, Y.; Ohno, K.; Yamamoto, S.; Goto, A.; Fukuda, T. *Adv. Polym. Sci.*, **2006**, 197, 1.

[8] Edmondoson, S.; Osborne, V. L.; Huck, W. T. S. *Chem. Soc. Rev.*, **2004**, 33, 14.

[9] Iwata, R.; Suk-In, P.; Hoven, V. P.; Takahara, A.; Akiyoshi, K.; Iwasaki, Y. *Biomacromolecules*, **2004**, 5, 2308.

[10] Feng, W.; Brash, J.; Zhu, S. *J. Polym. Sci. A Phys. Chem.*, **2004**, 42, 2931.

[11] Balamurugan, S.; Mendez, S.; Balamurugan, S. S. O'Brien, M. J.; López, G. P. *Langmuir* **2003**, 19, 2545.

[12] Jones, D M.; Smith, J. R.; Huck, W. T. S.; Alexander, C. *Adv. Mater.* **2002**, 14, 1130.

[13] Ito, S.; Kuno, J.; Yamashita, K.; Ohoka, M.; Ohkita, H.; Tsujii, Y.; Fukuda, T. *Trans. Mater. Res. Soc. Jpn.*, **2005**, 30, 687.

[14] Piech, M.; Bell, N. S. *Macromolecules* **2006**, 39, 915.

[15] Sakakiyama, T.; Ohkita, H.; Ohoka, M.; Ito, S.; Tsujii, Y.; Fukuda, T. *Chem. Lett.*, **2005**, 34, 1366.

[16] Hamelinck P. J.; Huck, W. T. S. *J. Mater., Chem.*, **2005**, 15, 381.

[17] Xie, S.; Natansohn, A.; Pochon, P. *Chem. Mater.* **1993**, 5, 403.

[18] Fisher. Th.; Läsker, L.; Stumpe, J.; Kostromin, S. G. *J. Photochem. Photobiol. A: Chem.* **1994**, 80, 453.

[19] Geue, T.; Ziegler, A.; Stumpe, J. *Macromolecules* **1997**, 30, 5729.

[20] Fisher, T.; Menzel, H.; Stumpe, J. *Supramol. Sci.* **1997**, 4, 543.

[21] Stumpe, J.; Geue, T.; Fishcer, T.; Menzel, H. *Thin Solid Films* **1996**, 284, 606.

[22] Han, M.; Morino, S.; Ichimura, K. *Macromolecules* **2000**, 33, 6360.

[23] Han, M.; Ichimura, K. *Macromolecules* **2001**, 34, 82.

[24] Han, M.; Ichimura, K. *Macromolecules* **2001**, 34, 90.

[25] Ichimura, K.; Suzuki, Y.; Seki, T.; Hosoki, A.; Aoki, K. *Langmuir* **1988**, 4, 1214.

[26] Kidowaki, M.; Fujiwara, T.; Ichimura, K. *Chem. Lett.* **1999**, 643.

[27] Ruslim, C.; Ichimura, K. *Adv. Mater.* **2001**, 13, 641.

[28] Ichimura, K.; Furumi, S.; Morino, S.; Kidowaki, M.; Nakagawa, M.; Ogawa, M.; Nishiura, Y. *Adv. Mater.* **2000**, 12, 950.

[29] Ichimura, K.; Momose, M.; Fujiwara, T. *Chem. Lett.* **2000**, 1022.

[30] Ichimura, K.; Momose, M. Kudo, K.; Akiyama, H.; Ishizuki, N. *Langmuir* **1992**, 8, 2601.

[31] Seki, T.; Fukuda, K.; Ichimura, K. *Langmuir* **1999**, 15, 5098.

[32] Fukuda, K.; Seki, T.; Ichimura, K. *Macromolecules* **2002**, 35, 1951.

[33] Fukuda, K.; Seki, T.; Ichimura, K. *Macromolecules* **2002**, 35, 2177.

[34] Kawashima, Y.; Nakagawa, M.; Seki, T.; Ichimura, K. *Chem. Mater.* **2002**, 14, 2842.

[35] Kawashima, Y.; Nakagawa, Ichimura, K.; Seki, T. *J. Mater. Chem.* **2004**, 14, 328.

[36] Tian, Y.; Watanabe, K.; Kong, X.; Abe, J.; Iyoda, T. *Macromolecules* **2002**, 35, 3739.

[37] Han, M.; Morino, S.; Ichimura, K. *Chem. Lett.*, **1999**, 645.

[38] Geue, Th.; Ziegler, A.; Stumpe, J. *Macromolecules* **1997**, 30, 5729.

Chapter IV

Fabrication "Low Density" Polymer Brushes Containing Azobenzene Side Chains and Their Molecular Orientations

4.1. Introduction

Chapter II and III described the synthesis, their molecular orientations and photo-alignment of azobenzene (Az) polymer brushes. The Az mesogens are aligned parallel to the substrate and highly anisotropic in-plane photo-alignment by irradiation of linearly polarized light is achieved. In general, the orientation and conformation of polymer in polymer brushes are drastically affected by the graft density.[1] Thus, this chapter focuses on the effect of graft density intentionally attempting to provide low density polymer brushes.

At a low graft density, polymer conformation in the polymer brushes is shrunk and their coil dimension will be similar to that of ungrafted (free) polymer chains. This structure assumes a "mushroom" or "pancake" conformation. With increasing graft density, polymer chains will be obliged to stretch away from the surface, forming the so-called "semi-dilute polymer brush" and "concentrated polymer brush". The concentrated polymer brushes are synthesized by the surface-initiated living radical polymerization.[2]

The high density polymer brushes have characteristic properties quite different and unpredictable from those of the moderately or low dense polymer brushes, such as glass transition temperatures (T_g), wettability, adhesion properties, etc. The T_g of poly(methyl methacrylate) grafted films is varied with the graft density. T_g of high density grafted films ($\sigma \leq 0.7$ chains / nm^2) is higher than that of low density ($\sigma \leq 0.2$ chains / nm^2).[3,4,5] The adsorption behavior of proteins on poly(2-hydroxyethyl methacrylate) brushes as a function of graft density was investigated. The high density brush leads to no protein adsorption and the low density one adsorbed proteins.[6]

Furthermore, gradient surfaces offer powerful avenues enabling systematic

variation of one or more brush properties.[7] Gradient surfaces offer combinatorial platforms for quick and inexpensive investigation of the multivariate phenomenon. Genzer et al. synthesized the grafted polymer gradient synthesized by surface-initiated atom transfer radical polymerization (ATRP) and investigated the formation and application of their structures.[8,9] The initiating dormant species was immobilized with a gradual variation of surface density by the vapor-diffusion method and the graft polymer was assumed to have the same length independent of the initiator density. They also reported the surface morphologies of diblock copolymer brushes,[10] nano-particle dispersion,[11] and cell adhesion[12] by using surface-tethered polymer gradients films.

On the other hand, patterned polymer grafting films were fabricated by using of electron beam (EB) lithography[13] and ultraviolet (UV) light irradiation.[14] Both reports demonstrated same manners. The first step is the fixing of ATRP initiator onto substrates, and the second step is selectively decomposition of the immobilized-initiator on substrates. For patterning of self-assembled monolayers (SAM), vacuum ultraviolet light (VUV) is a powerful tool. The principal advantage of VUV irradiation is that SAMs can be rapidly removed from substrates since the VUV light promotes cleavage. The irradiation of VUV light causes oxygen molecules to transform ozone molecules, followed by the formation of activated oxygen atoms due to the photo-degradation of ozone. The activated oxygen atoms attack hydrocarbons of the SAMs, to generate H_2O and CO_2 species. Sugimura et al. have reported that the SAMs formed from octadecyltrimethoxysilane and others on an outermost silica layer of a silicon wafer are decomposed by exposure to VUV light.[15]

In the above the backgrounds, this chapter describes the synthesis of low density liquid crystalline (LC) Az polymer brushes and their molecular orientation. A density control of ATRP initiator-modified surface is attempted by irradiation with VUV light. It is also anticipated that the orientation of Az in low density grafted films are different from that in high density grafted films.

4.2. Experimental Section

4.2.1. Materials

Starting compounds for syntheses were purchased from Tokyo Kasei Kogyo (TCI Inc.), Kanto Kagaku, and Aldrich Co. Copper Bromide (CuBr) was washed with acetic acid and diethyl ether for several times, and dried in vacuum.[16,17] Toluene as solvents was dehydrated by distillation from sodium with benzophenone. Az containing methacrylate (5Az10MA)[18,19,20] and silane coupling reagent bearing ATRP initiated group (BHE)[21] were synthesized according to previous literature. The details of syntheses were described in Chapter II.

Quartz plates (1 cm ×1.5 cm) were washed with a saturated KOH / EtOH solution, and pure water under ultrasonic wave treatment. Their static contact angle of water was 8 ± 2 ° (hydrophilic plates). Silicon wafer substrates (1 cm × 1.5 cm) were washed with acetone under ultrasonic wave treatment for 5 min. Both substrates were cleaned by exposure to UV ozone for 45 min using ozone cleaner (Nippon Laser & Electronics) before the surface modification reaction. BHE-SAMs were prepared by Chemical vapor adsorption (CVA) method.[22]

The high-density Az grafted substrates (PMA(Az) graft) and spincast films used here were prepared as described in Chapter II.

4.2.2. Preparation of Low Density Polymer Brushes

4.2.2.1. Irradiation by Vacuum Ultraviolet Light

Immobilization of ATRP initiator was prepared by chemical vapor adsorption (CVA) method. Details on the synthesis were described in Chapter II. The typical water contact angles of prepared substrates were about 78 ° (silicon wafer) and 76.1 ° (quartz), respectively. The substrates modified with a BHE monolayer was by irradiation with 172 nm vacuum ultraviolet light emitting from a xenon excimer lamp (UER20-172A, Ushio Inc., λ = 172 nm and 10 mW/cm^2) under a reduced pressure of 5 Pa for several minutes. Finally, the samples were dried under vacuum and stored in nitrogen atmosphere.

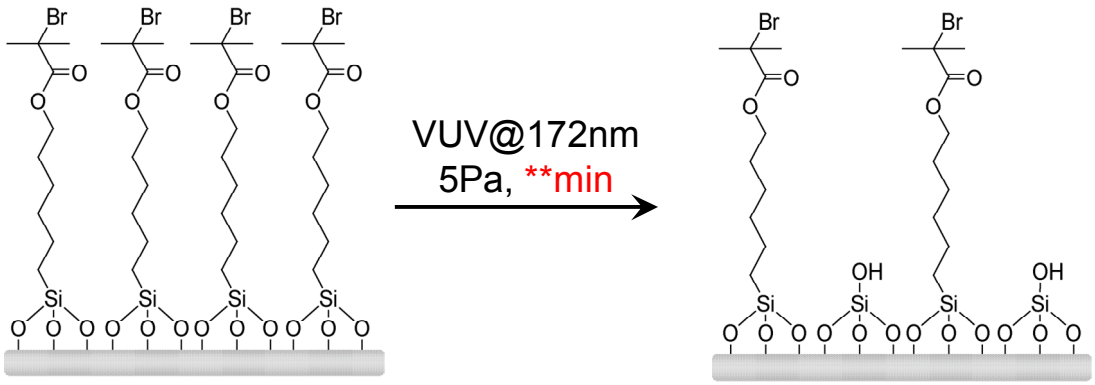

Scheme 4-1. Synthetic route of BHE-SAMs with irradiation of vacuum ultraviolot light.

4.2.2.2. Surface-initiated Atom Transfer Radical Polymerization

The polymerization conditions are the same as described in Chapter II. Polymerization conditions were chosen as $[M]/[I]_{free}$ = 200/1 and $[M]_0$ = 1.0 mol dm^{-3}. 7 mg (0.05 mmol) of Cu(I)Br, 492 mg (1.0 mmol) of the Az containing monomer 5Az10MA, 1 mg (0.005 mmol) of ethyl 2-bromoisobutyrate as a free initiator, and 11.5 mg (0.05 mmol) of 1,1,4,7,10,10- hexamethyltriethylentetraamine as a ligand were dissolved in 1.25 ml of dry toluene and filled with nitrogen. The mixture was degassed by freeze-pomp-thaw cycle for three times. In a glove box, initiator-modified quartz or silicon substrates were added in polymerization solution and sealed. The flask was placed in the preheated 80 °C oil bath for 12 hours. After the polymerization, polymer grafted substrates were washed with tetrahydrofuran (THF) for several times to remove unreacted monomer and free polymer, and dried at room temperature.

4.2.3. Measurements

X-ray photoelectron spectroscopy (XPS) was measured by ESCA-3300 (Shimadzu) and operating to confirm the formation of the initiator monolayer with an MgK_α (1253.6eV). All binding energies were referenced to Si 2p at 99.34 eV.

Contact angle of water was carried out by a FACE CA-XP (Kyowa Interface Science). The contact angle values were obtained by averaging the results of over 5 points of measurements.

UV–vis absorption spectra of the graft substrates and spincast films at room temperature were taken with an Agilent 8453 spectrometer (Agilent Technology). UV-vis spectroscopic study at various temperatures was performed on an MCPD-2000 UV-vis spectrometer (Ohtsuka Electronics) combined with a deuterium-halogen lamp MC-2530 (Ohtsuka Electronics) equipped with a Mettler FP82HT hot stage at a heating or cooling rates of ±1 °C/min.

X-ray diffraction (WAXD) measurements were obtained with a Rigaku ATX-G operating with CuK_α radiation (0.154 nm).

4.3. Results and Discussion

4.3.1. Preparation of Sparse Self-Assembled Monolayer of the ATRP Initiators

The irradiation with 172 nm light was carried out under an air atmosphere and under a reduced pressure of 5 Pa. Contact angle of the BHE-SAMs for water were monitored as a function of irradiation time. Under an air atmosphere, the contact angle of 78° (silicon wafer) decreased to 30° by the exposure for 5 min. This result suggested that some organic substances still remained on the silica surface. In contrast, the hydrophobic surface modified with the BHE-SAM was altered completely to a hydrophilic surface with a contact angle lower than 5° by the exposure for 3 min under a pressure of 5 Pa. The decrease of the water contact angle implies that all organic substances were removed from the silicon wafer surface. According to these results, the photoinduced decomposition of the other films on silica surfaces was performed at 5 Pa for further investigations.

Figure 4-1 indicates an enhancement of wettability of BHE-SAM by irradiation with vacuum ultraviolet light. It was suggested that all of the BHE-SAMs were decomposed by the exposure for at least 3 min. With irradiation at 1 and 2 min, the contact angle remained almost constant at around 30°. This result is similar to that of the previous report of photodegradation behavior of chloromethylphenylsilane-SAMs.[23] It seems that the sample surface is covered with carboxyl groups leading to the constant water contact angles observed. The same behaviors were observed on the silicon wafer and quartz substrates.

Figure 4-2 demonstrates XPS spectra of the BHE monolayer on silicon wafer surface that was irradiated with VUV light. The bromine 3d orbital signal intensity decreased when the BHE-SAM has been VUV irradiated. The plot of difference intensity of Br 3d signals as a function of VUV irradiation time is shown in Figure 4-3. The intensity at 30 s irradiation became comparable to that of a cleaned silicon surface. The contact angles at 30 s in both substrates were around 50 °. In above manners, the bromine atoms were desorbed complicatedly, however, the monolayer surface was covered with the organic layer such as alkyl chains or those containing a carboxyl group.

On the other hand, the water contact after exposure for 10 s more increased than

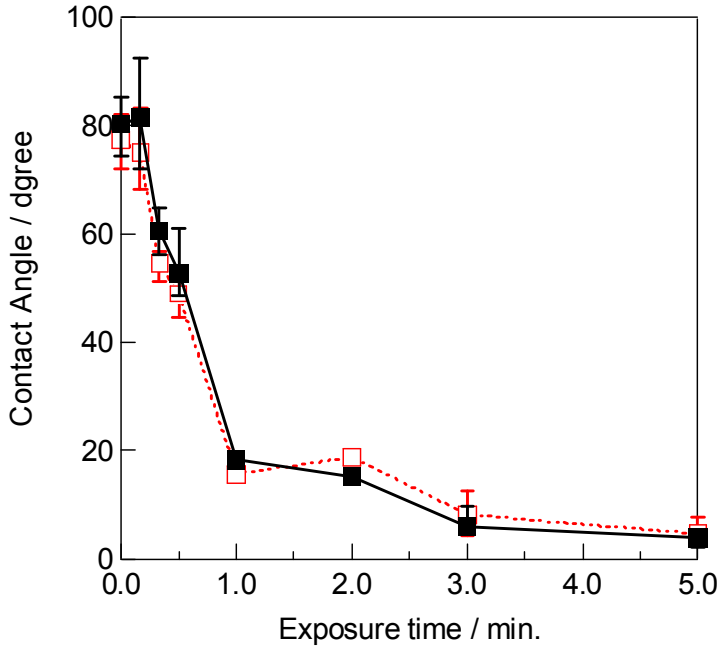

Figure 4-1. Water contact angle changes of BHE monolayers on silicon wafer (■) and quartz (□) after exposure to vacuum UV light under a pressure of 5 Pa.

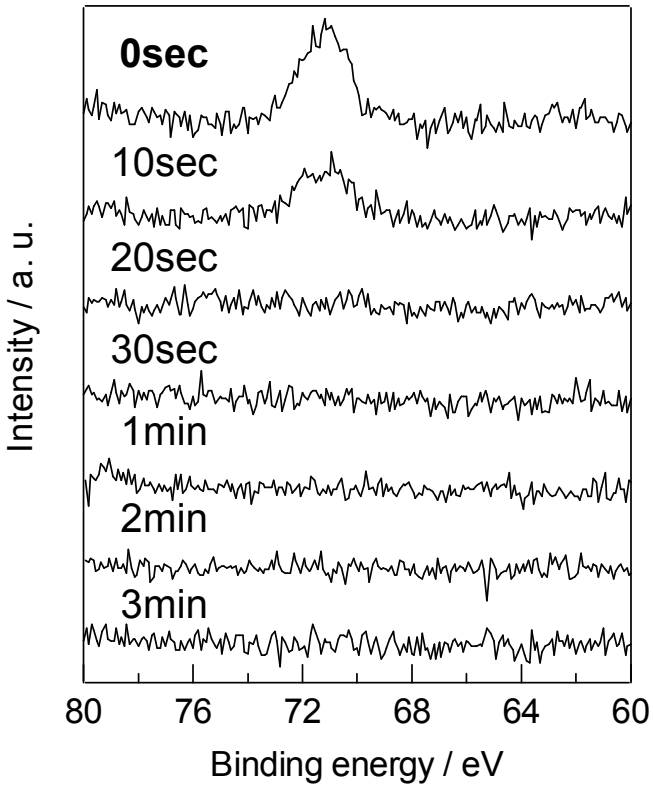

Figure 4-2. XPS spectra of Br 3d after irradiation with VUV light at various irradiation times.

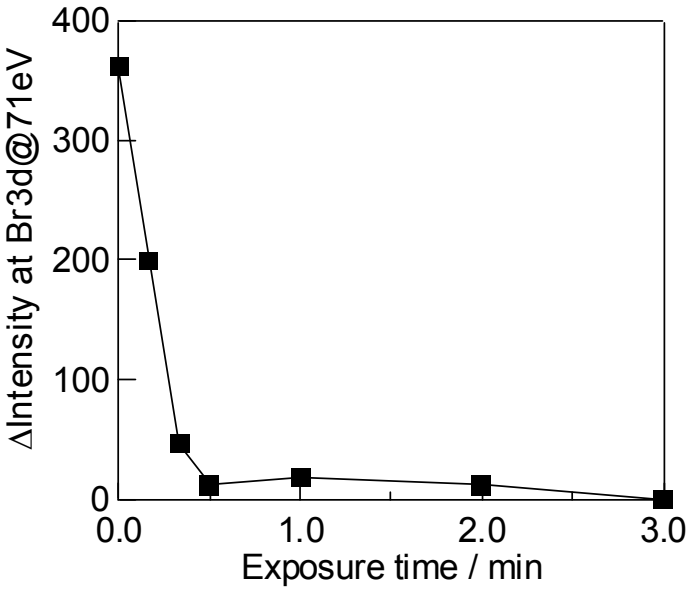

Figure 4-3. Intensity of Br 3d signals on silicon wafer after exposure to vacuum UV light under a pressure of 5 Pa.

that before exposure to VUV light, regardless of the intensity of Br 3d was a half of that. In general, the water contact angles of alkyl silane such as octadecylsilane are around 90 - 100°.[24,25,26] It is suggested that ester groups in BHE molecules including bromine atoms are photodecomposed selectively for irradiation with VUV light, and a chemical conversion from bromine head groups to hydrophobic alkyl groups.

Based on above results, the VUV irradiation conditions are determined as for 10s at 5 Pa. The BHE-SAMs in the sparse state were used in the ATRP polymerization.

4.3.2. Characteristics of Low Density Polymer Grafted Films

4.3.2. 1. UV-vis Spectroscopic Measurements

The thickness of the film synthesized by ATRP is about 5 nm as revealed by ellipsometry. Since the thickness of Az-containing grafted polymer film synthesized from the BHE-SAM without VUV irradiation (in Chapter II) was about 10 nm, the effect of graft density was obvious. Figure 4-4 shows UV-vis spectrum of the grafted films synthesized from the sparse BHE-SAM. The absorbance of the π–π* transition shifted to 326 nm and the stronger H-type aggregation was formed. This spectral shape was unchanged by repeated washing with THF. The molecular orientation of Az units in side chain is roughly estimated by the ratio of absorption intensities at the π–π* to ϕ–ϕ* band, since the π–π* transition is directional dependent while the ϕ–ϕ* transition at 244 nm is insensitive to the chromophore orientation. The $A_{\phi-\phi^*}/A_{\pi-\pi^*}$ ratio was 1.10. Thus, Az mesogen was found to be aligned in a perpendicular state to the substrate.

The molecular orientation in THF solution, spincast films, high and low density grafted films estimated by UV-vis spectra measurements are summarized in Figure 4-5. In THF solution, absorption maximum (λ_{max}) of the π–π* long-axis transition of Az was positioned at 352 nm, indicative formation of no aggregates. The spincast and grafted films showed the λ_{max} around 320 and 338 nm, respectively, indicative of the formation of H-type aggregates of Az units. On the other hand, the spectrum of low density grafted films also formed H-type aggregates, and the shape of spectrum was similar to that of spincast films. However, the extent of blue shift was less than spincast films, and the $A_{\phi-\phi^*}/A_{\pi-\pi^*}$ ratio was also smaller (spincast film: ca. 1.85). This result indicates

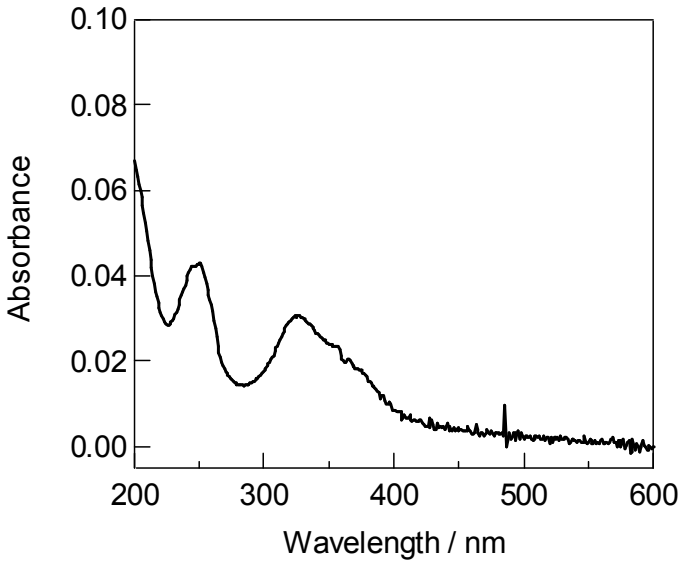

Figure 4-4. UV-vis absorption spectrum of "low density" Az-polymer grafted substrate on quartz substrate at room temperature. The film thickness is about 5 nm.

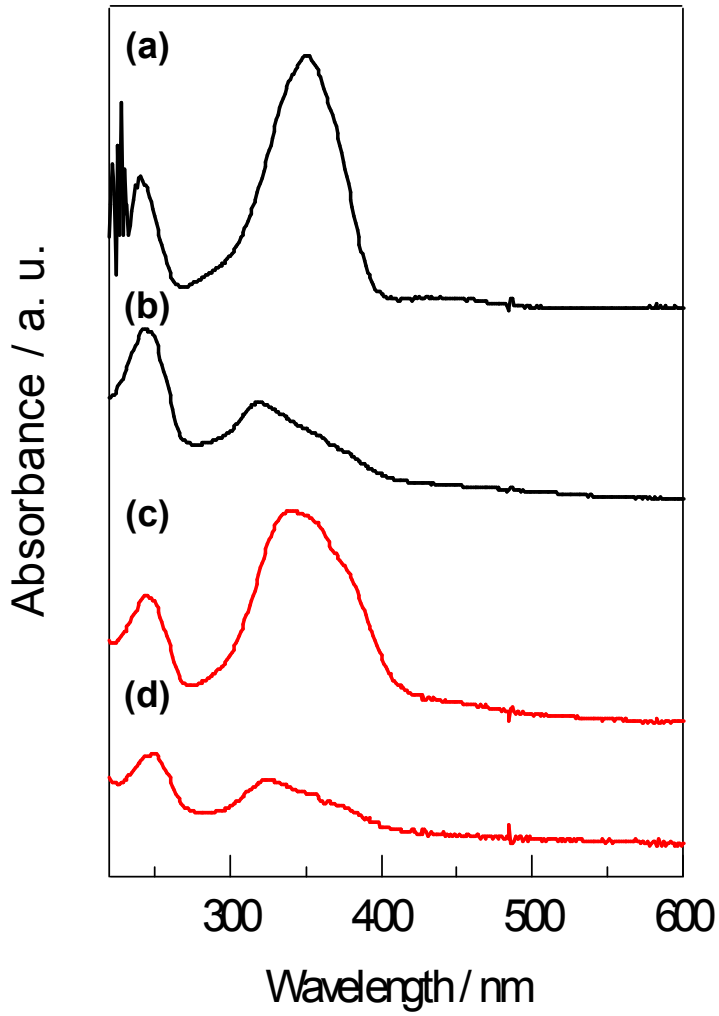

Figure 4-5. UV-vis absorption spectra of PMA(Az) in THF solution (a), spincast films (b), high density Az grafted films (thickness is about 10 nm) (c), and low density Az grafted films (d).

that the mesogenic groups align in normal orientation for the low density grafted films, and this orientation behavior is very similar to that of the spincast film of smectic LC polymer.[27,28] In other word, the LC orientation was critically changed by the parameter of graft density. If their density is low, their LC orientation becomes perpendicular state to the substrate.

The orientation of the Az groups in the grafted polymers on the substrate at various temperatures was further evaluated by UV-vis absorption spectrum measurements. Figure 4-6a displays the UV-vis spectra of a low density Az grafted film at various temperatures on cooling process. The absorbance of the π–π* transition band gradually decreased without no shift in λ_{max}, whereas the spectral features of the ϕ–ϕ* band were unchanged. At later stages, λ_{max} was shifted to 320 nm, and H-aggregate was formed. Such change in absorbance should be ascribed to the change in the molecular orientation from a random to perpendicular state on the substrate. The same tendency was observed in the case of spincast films (Figure 4-6b, the details is described in Chapter II). This spectral change was observed reversibly in the grafted polymer film, however, that in the spincast film was observed only 1st cooling process. This difference should be derived from the anchoring to the substrate.

4.3.2.2. X-ray Diffraction Experiments

Figure 4-7 shows XRD patterns of the low density grafted films and spincast films. In spincast films, two diffraction peaks were observed at 2θ = 2.70 and 5.26° corresponding to (001) and (002) diffractions, respectively, of the smectic layers (d_{001} = 3.26 nm). This layer spacing of d_{001} is equal to that of the result by using GI-XRD measurements (in Chapter II), which corresponds to a long-range ordering of approximately the length of the fully extended Az side chain, suggesting a formation of interdigitated structures of Az side chains.

A diffraction pattern in the low density grafted films was also observed at 2θ = 2.68° corresponding to (001) of the smectic layers (d_{001} = 3.30 nm) (Figure 4-7b). The layer spacing is almost equal to that in the spincast film. These facts indicate that the orientation behavior is similar to that in spincast films.

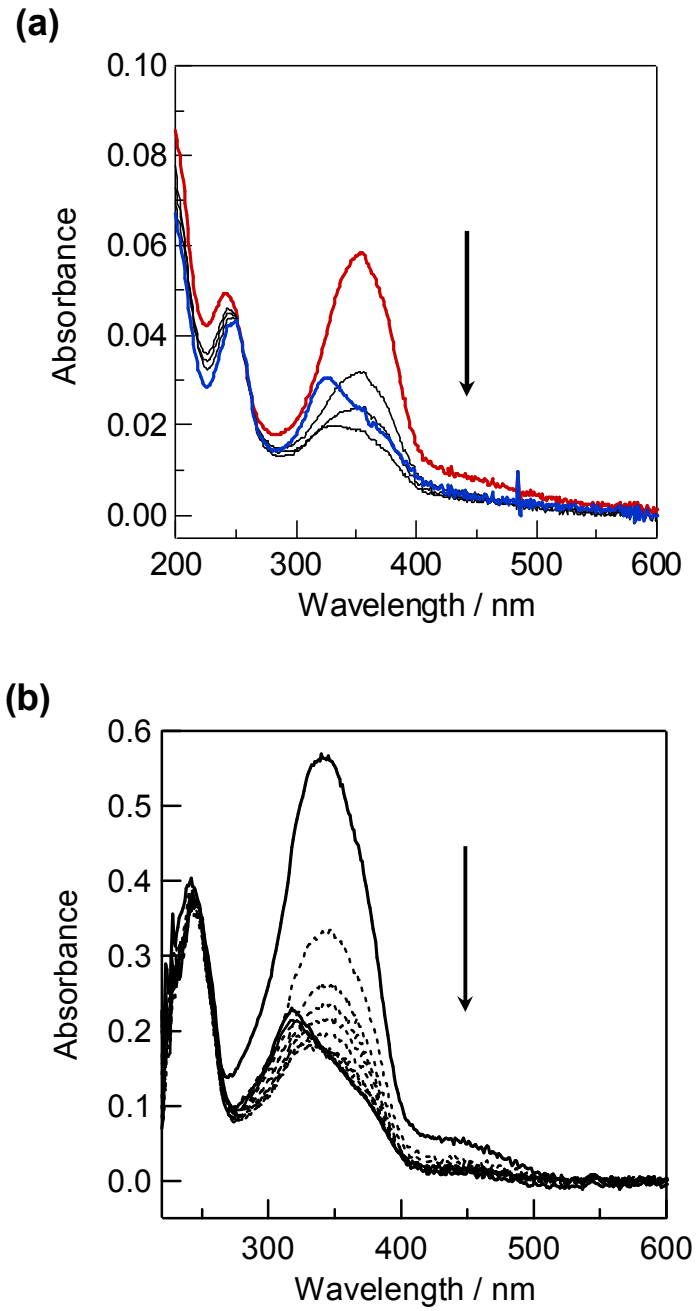

Figure 4-6. UV-vis absorption spectra of low density grafted substrate (a) and spincast films (b) at various temperatures on cooling process.

4.3.3. The Orientation of LC Mesogen in the Low Density Grafted Film

The LC orientations in the Az grafted films and spincast films are illustrated in Figure 4-8. The orientation in the high density Az grafted films and spincast films were described in Chapter II. In the spincast film, the Az mesogens adopt a homeotropic alignment to the substrate plane by annealing. In contrast, parallel alignment of Az units is attained in the high density grafted films.

In contrast, the Az mesogens in low density grafting film also formed a homeotropic alignment to the substrate plane as indicated from UV-vis absorption spectrum and XRD patterns. It is assumed that the polymer conformation is randomized and forms a "mushroom" structure. Since the coil dimension in low density grafted films is similar to that of free polymer chains, the Az orientation in the side chains should be also similar. The result on the reorientation of Az on cooling process also supports this model. If graft density is adequately high, the decrease of absorbance on cooling process is not observed (described in Chapter II). Thus, polymer chains have sufficient flexibility as in the spincast film, although they are tethered onto a substrate. Consequently, by decreasing of graft density, the Az orientation becomes similar to the free polymer.

4.4. Conclusion

This chapter demonstrated the preparation of low density polymer brushes containing Az molecules in the side chain. Evaluations of the molecular orientation of Az mesogen are made, and the relationship between the molecular orientation and graft density was discussed. The Az molecules oriented in a perpendicular state to the substrate as revealed by UV-vis spectra and XRD measurements. Thus the graft density critically affects LC orientation in polymer grafted films.

The next step of this research will be to prepare gradually density changed of LC mesogen on the polymeregrafted substrate or micro-patterned grafted polymer films by irradiation of VUV light through a photomask. Furthermore, tuning the graft density of polymer brushes formed on a dynamic hydrogel surface as the supporting substrate seems to be fascinating. A couple of efforts have been made to introduce polymer

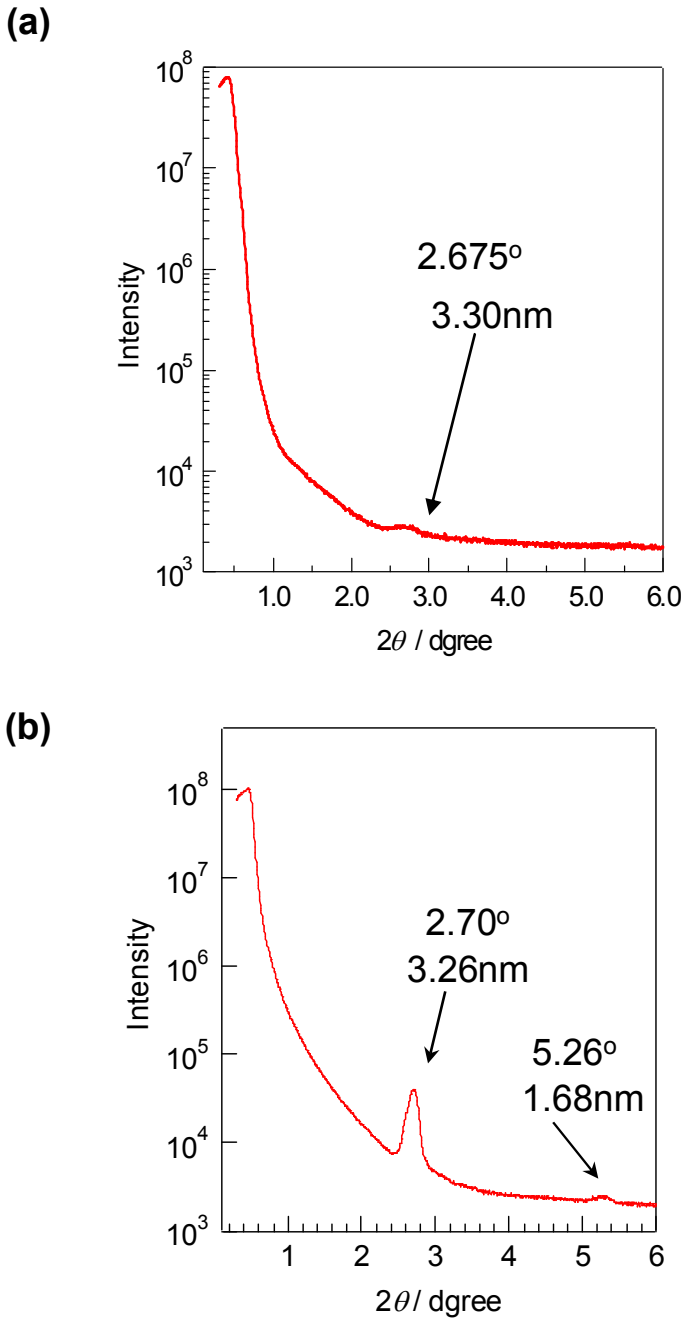

Figure 4-7. XRD profiles for the low density grafted films (a) and spincast films (b)

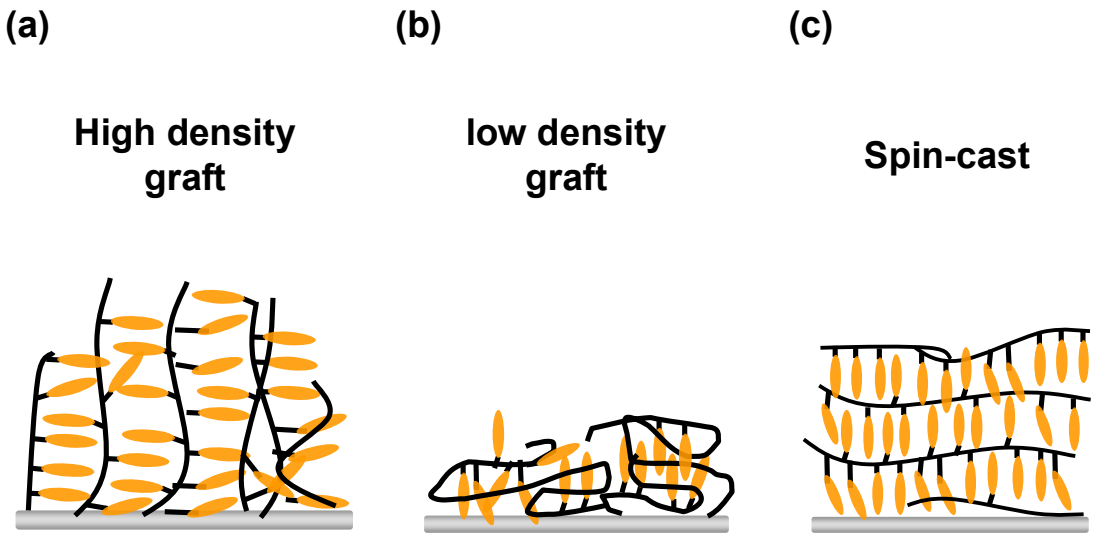

Figure 4-8. Schematic illustration of the orientation of mesogenic Az groups in the high density grafted polymer films (a), low density grafted films (b) and spincast film (c).

brushes on a gel[29] or elastomer,[30] but to my knowledge no work focuses on the reversible density control. Reversible changes of the graft density will be realized in such systems.

Reference

[1] Advincula, R. C.; Brittain, W. J.; Caster, K. C.; Rühe, J. (Ed.) *Polymer Brushes*, WILEY-VCH, **2004**.

[2] Tsujii, Y.; Ohno, K.; Yamamoto, S.; Goto, A.; Fukuda, T. *Adv. Polym. Sci.* **2006**, 197, 1.

[3] Yamamoto, S.; Tsujii, Y.; Fukuda, T. *Macromolecules* **2002**, 35, 6077.

[4] Prucker, O.; Christian, S.; Bock, Harald, Rühe, J.; Frank, C. W.; Knoll, W. *Organic Thin Films Structure and Applications*, Frank, C. W. (Ed.), ACS, **1998** Chapter 17 pp233.

[5] Prucher, O.; Christian, S.; Bock, H.; Rühe, J.; Frank, C. W.; Knoll, W. *Macromol. Chem. Phys.* **1998**, 199, 1435.

[6] Yoshikawa, C.; Goto, A.; Tsujii, Y.; Fukuda, T.; Kimura, T.; Yamamotto, K.; Kishida, A. *Macromolecules* **2006**, 39, 2284.

[7] Bhat, R. R.; Tomlinson, M. R.; Wu, T.; Genzer, J. *Adv. Polym. Sci.* **2006**, 198, 51.

[8] Wu, T.; Efimenko, K.; Genzer, J. *J. Am. Chem. Soc.* **2002**, 124, 9394.

[9] Bhat, R. R.; Tomlinson, M. R.; Genzer, J. *J. Polym. Sci. B; Polym. Phys.* **2005**, 43, 3384.

[10] Tomlinson, M. R.; Genzer, J. *Langmuir* **2005**, 21, 11552.

[11] Bhat, R. R.; Genzer, J. *Appl. Sur. Sci.* **2006**, 252, 2549.

[12] Bhat, R. R.; Chaney, B. N.; Rowley, J.; Lievmann-Vinson, A.; Genzer, J. *Adv. Mater.* **2005**, 17, 2802.

[13] Tsujii, Y.; Ejaz, M.; Yamamoto, S.; Fukuda, T.; Shigeto, K.; Mibu, K.; Shinjo, T. *Polymer* **2002**, 43, 3837.

[14] Iwata, R.; Suk-In, P.; Hoven, V. P.; Takahara, A.; Akiyoshi, K.; Iwasaki, Y. *Biomacromolecules* **2004**, 5, 2308.

[15] Sugimura, H.; Ushiyama, K.; Hozumi, A.; Takai, O. *Langmuir* **2000**, *16*, 885-888.

[16] Börner, H. G.; Beers, K.; Matyjaszewski, K.; Sheiko, S. S.; Möller, M *Macromolecules*

2001, 34, 4375.

[17] Keller, R. N.; Wycoff, W. M. *Inorg. Synth.* **1946**, 2, 1.

[18] Tian, Y.; Watanabe, K.; Kong, X.; Abe, J.; Iyoda, T. *Macromolecules* **2002**, 35, 3739.

[19] Kadota, S.; Aoki, K.; Nagano, S.; Seki, T. *Trans. Mater. Res. Soc. Jpn.* **2005**, 30,659.

[20] Kadota, S.; Aoki, K.; Nagano, S.; Seki, T. *Coll. and Surf. A Phys. Eng. Asp.*, **2006**, 284-285, 535.

[21] Ohno, K.; Morinaga, T.; Koh, K.; Tsujii, Y.; Fukuda, T. *Macromolecules* **2005**, 38, 2137.

[22] Hozumi, A.; Yokogawa, Y.; Kameyama, Y.; Sugimura, H.; Hayashi, K.; Shinohara, H.; Takai, O. *J. Vac. Sci. Techno. A* **2001**, 19, 1812.

[23] Saito, N.; Hayashi, K.; Sugimura, H.; Takai, O. *J. Mater. Chem.* **2002**, 12, 2684.

[24] Sugimura, H.; Hayashi, K.; Amano, Y.; Takai, T.; Hozumi, A. *J. Vac. Sci. Technol. A* **2001,** 19, 1261.

[25] Ye, T.; Wynn, D.; Dudek, R.; Borguet, E. *Langmuir* **2001**, 17, 4497.

[26] Sugimura, H.; Hozumi, A.; Kameyama, T.; Takai, O *Surf. Interface Anal.* **2002**, 34, 550.

[27] Geue, T.; Zieglar, A.; Stumpe, J. *Macromolecules*, **1997**, 30, 5729.

[28] Han, M.; Morino, S.; Ichimura, K. *Chem. Lett.*, **1999**, 645.

[29] Ohsedo Y.; Takashina R.; Gong J. P.; Osada Y. *Langmuir* **2004**, 20, 6549.

[30] Yoshida T.; Doi M.; Kanaoka S.; Aoshima S. *J. Polym. Soc., A; Polm. Chem.* **2005**, 43, 5704.

Chapter V

Sharp Temperature Dependency of 2D Spreading Behavior in Amphiphilic Block Copolymer at the Air-water Interface

5. 1. Introduction

The monolayers of synthetic polymer were first described by Katz and Samwel in 1928.[1] Since then, the numerous numbers of knowledge have been reported to the Langmuir monolayer of polymers and their spreading behavior.[2,3] In general, polymer chains adopt different conformations in solutions and at the air-water interface. In solutions, polymers generally exist as random three-dimensional coils whose bounding dimensions are a few tens of nanometers. In contrast, they are stretched upon spreading on water, and the polymer chains are assumed to be extended with the repeating units being adsorbed on the air-water interface. Thus, the Langmuir-Blodgett technique may provide ultrathin polymer films showing characteristic features derived from the extended conformations.

Many efforts have recently been directed to block copolymers. Block copolymers are useful materials as nanometer-scale ordered microphase separated patterns in bulk films,[4,5,6] thin films, micelles in solution,[7] and at air-water interface.[8,9] In particular, monolayers prepared by the Langmuir-Blodgett (LB) method are attracting research attention because of the feasibility of precise structure control at molecular levels. When block copolymers are spread on water, characteristic two-dimensional morphologies are formed based on microphase separation. Block copolymers containing a polystyrene block form two-dimensional surface micelle aggregates.[10,11,12,13,14] The aggregates formed from hydrophobic block chains are rigid enough on water and do not change their shapes because of the stronger cohesive force among the chains on water and the relatively high glass transition temperature. The resulting aggregate structures are altered by various parameters such as physical and chemical characteristics of blocks (amphiphilic nature, solubility, molecular weight, block size, and so on) and

processing factors such as spreading solvent, concentration of spreading solution, subphase temperature, compression speed.[15,16,17] Baker and co-workers observed the morphologies of a predominantly hydrophobic polystyrene-*block*-poly(ethylene oxide) (PS-PEO) monolayers by using atomic force microscopy, and found the significant effects on the concentration of the spreading solution on the air-water interface.[17] The factors affecting the spreading behavior and resulting morphologies are dissipative, and thus have not been well understood.

With regard to the solvent, interesting observations have been reported. When block copolymers are dissolved in a selective solution, a solvent which is good for only one segment, the insoluble blocks associate and form the core of micelle structures, whereas the soluble blocks form a corona structure.[7] These morphological structures are changed by using various amphiphilic block copolymers, their proportions of segments, and solvent conditions.[18,19] Sohn et al. reported that two-dimensional micelles of polystyrene-*block*-poly(4-vinyl pyridine) (PS-P4VP) switch their nanopatterns through core-corona inversion of micelles by selective solvents.[20]

On the other hand, to tune or modify the nanopatterns by external stimuli such as light or temperature is a challenging attempt. In our laboratory, a novel triblock copolymer correspond to azobenzene containing polymethacrylate and poly(ethylene oxide) (PEO), respectively, and spreading and light-responsive phase separation behavior on water and substrate surfaces.[21,22] For tuning by light, however, photo-responsive unit are required in block copolymer.

The above the knowledge in mind, novel characteristic spreading behaviors of amphiphilic block copolymer at the air-water interface are described in this chapter. A material used here is PS-P4VP, which is a conventional amphiphilic diblock polymer. If the nanopatterns composed by such conventional block copolymers can be changed by some stimuli, new applications in nanotechnologies such as tunable two-dimensional template will be anticipated. It is shown here that the spreading behavior shows an unexpected abrupt change at a very narrow temperature range.

5.2. Experimental Section

5.2.1. Materials

The block copolymer, PS_{158}-$P4VP_{32}$ (Chart 5.1), was synthesized by anionic polymerization. The number average molecular weight of each block was 16400 (158 units) and 3600 (32 units) for PS and P4VP blocks, respectively, with the total polydispersity (M_w / M_n) of 1.10. The PS_{158}-$P4VP_{32}$ was dissolved in various organic solvents; chloroform, cyclohexane, toluene, benzene, cyclohexanone, 1,4-dioxane, ethyl acetate, and methyl cyclohexane. The concentration of the spreading solutions was ca. 1.0×10^{-3} mol dm^{-3} per pyridine unit. The PS homopolymer was purchased by Aldrich co. ltd. The number average molecular weight of each block was 29300 (290 units) with the polydispersity (M_w / M_n) of 1.05. The concentration of the spreading solution was 1.0×10^{-3} mol dm^{-3} per styrene unit.

5.2.2. Spread Behaviors at the Air-water Interface

The spreading behaviors of PS_{158}-$P4VP_{32}$ were evaluated on pure water (Milli-Q grade, 18 MΩ cm, pH = 5.8) using a Lauda FW-1 film balance. The temperatures of a water subphase were controlled by water circulation at various temperatures in the accuracy of ± 0.1 °C using a Yamato-Komatsu CTE-22W. After evaporation of the spreading solvent, the film on water was compressed at a speed of 30 cm^2 min^{-1}. The surface pressure was recorded versus molecular area per styrene unit.

Brewster angle microscopy (BAM) images were taken on a Nippon Laser Electronics NE-LB/EMM633. *p*-Polarized light from a 10 mW He-Ne laser (633nm) was reflected at the air-water interface at the Brewster angle of 53.1°. The reflected beam passed through an analyzer fixed near 0° to the incident polarization was directed with an interference-free CCD camera (Hamamatsu Photonics). The obtained images were captured to the computer with PIX-MPTV/U1W (PIXELA).

5.2.3. Aggregation Properties in Solutions

Dynamic light scattering (DLS) profiles were taken with an Otsuka Electronics ELS-7300K electrophoretic light scattering spectrophotometer equipped with a 10mW

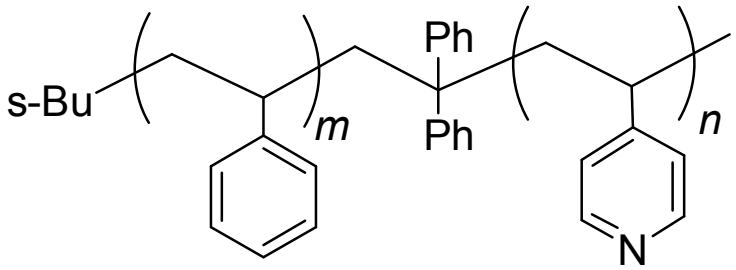

Chart 5-1.

He-Ne laser. The PS_{158}-$P4VP_{32}$ in cyclohexane or chloroform solutions were kept at 10 or 20 °C by water circulation at in the accuracy of ± 0.2 °C using a Lauda RE104 and then subjected to light scattering measurements. The diameters of the polymer or polymer aggregates were estimated by this method.

UV-vis transmittance spectra in solution were taken with an Agilent 8453, and turbidities were measured by monitoring transmittance at 500 nm through 1 cm quartz cell at various temperatures. The solution temperatures were controlled by water circulation at various temperatures in the accuracy of ± 0.2 °C using a Lauda RE104.

5.3. Results and Discussion

5.3.1. Spreading Behavior at the Air-water Interface

The surface pressure-area (π - A) curves which obtained by spreading from various solvents such as benzene, chloroform, cyclohexane, cyclohexanone, methyl cyclohexane, toluene, and 1,4-dioxane at temperatures ranging from 10 °C to 40 °C are shown in Figure 5-1. π- A curves displayed no plateau region derived from the P4VP block[17] and the shapes of these curves were similar to that of polystyrene homopolymer. This feature is ascribed to a large PS contents (83 wt %) of block copolymer. Most of solvents gave similar spreading behaviors at 10 - 40 °C in which almost notemperature dependency was observed. When spread from 1,4-dioxane, the areas was narrower than those from other solvents. The reason is caused by water solubility of 1,4-dioxane. It can be mixed with water, thereby, the amount of polymer deposited for 1,4-dioxane spread at the air-water interface is less than that deposited for other solvents. On the other hand, spreading behaviors from cyclohexane and methyl cyclohexane were observed drastic surface area changes between 10 - 20 °C.

Hereafter, the spread behaviors on water from chloroform and cyclohexane solution were examined in more details for representative examples. When the PS-P4VP was spread from chloroform, the occupying areas per styrene unit were 0.090, 0.086, 0.083, and 0.078 nm^2 at 10, 20, 30, and 40 °C, respectively, indicating that the area change was negligible in this temperature range. Solvents used here except for cyclohexane and methyl cyclohexane gave essentially the same results. In sharp

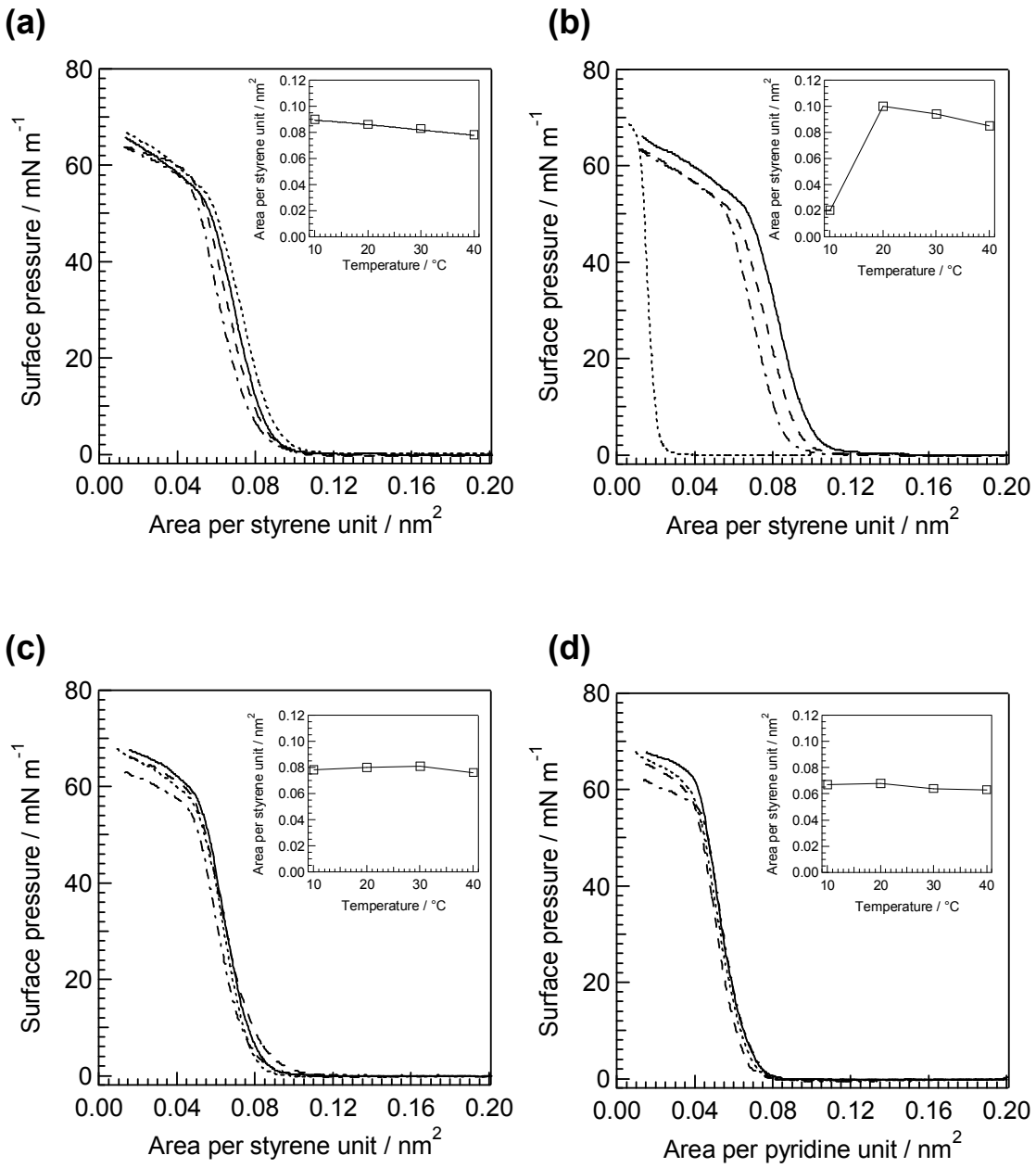

Figure 5-1. Surface pressure-area curves of PS158-P4VP32 at various temperatures spread from chloroform (a), cyclohexane (b), benzene (c), cyclohexanone (d), toluene (e), methyl cyclohexane (f), ethyl acetate (g), and 1,4- dioxane (h). The inset shows relationship between area per styrene unit and subphase temperatures.

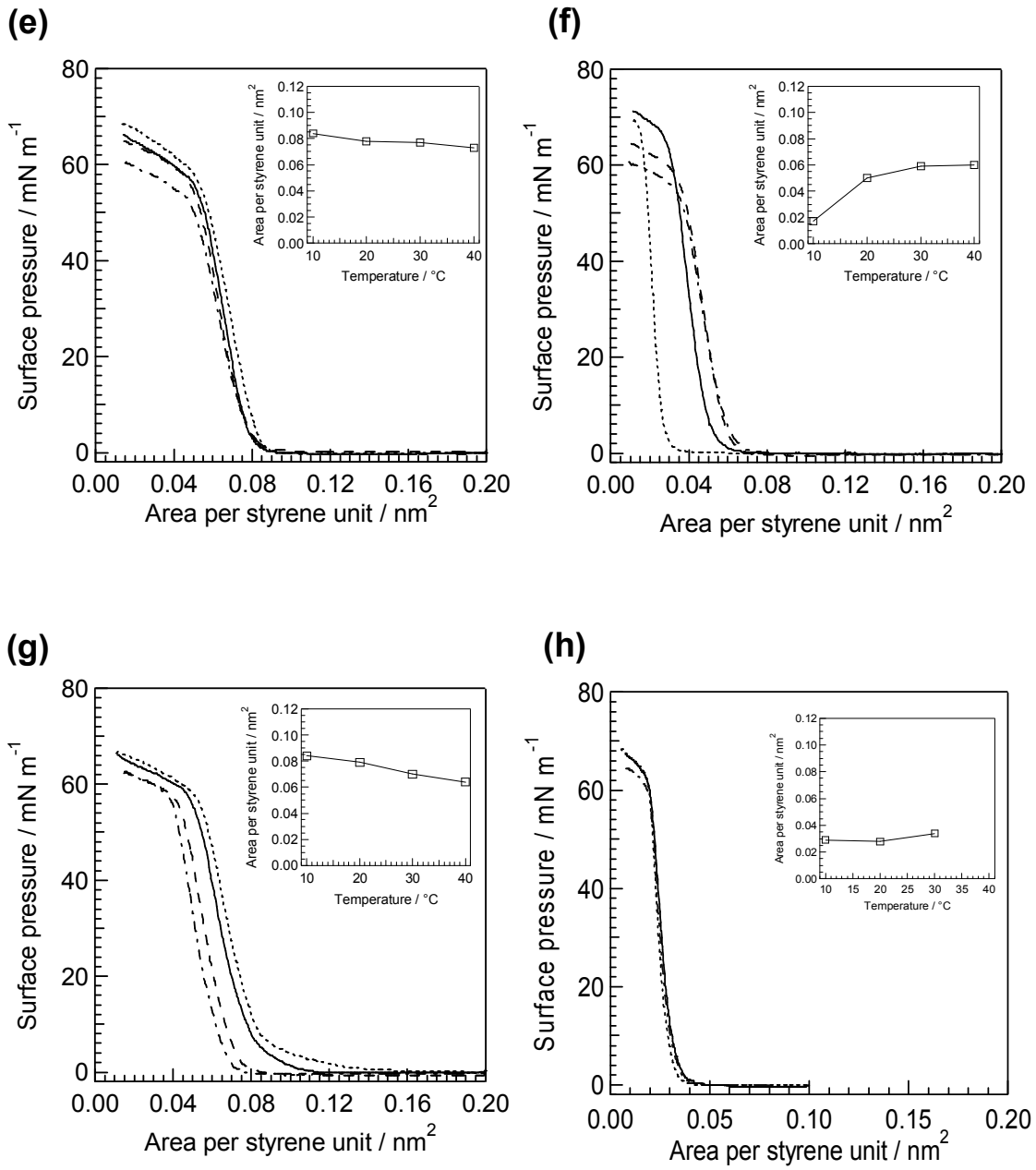

Figure 5-1. Continued.

contrast, when cyclohexane was used as the spreading solvent, drastic temperature dependence was observed (Figure 5-1b). The shape of the π - A curves at 20, 30, and 40 °C are similar to that obtained for chloroform, giving the occupying areas of 0.10, 0.094, and 0.085 nm^2 at 20, 30, and 40 °C, respectively. On the other hand, the limiting areas of the PS-P4VP film showed a drastic decrease, providing 0.021 nm^2 at 10 °C. Thus, a sudden area change occurred at a narrow temperature range between 10 and 20 °C. Spreading from methyl cyclohexane also showed similar significant temperature dependence, but the area change was not as drastic as observed for cyclohexane (Figure 5-1f).

To grasp the area change behavior, π-A curves were measured in more details at narrow temperature region at 10 - 20 °C. Figure 5-2 depicts the π - A curves of PS-P4VP spread from cyclohexane at temperatures between 10 and 20 °C (a), and the occupying area per styrene unit as a function of the subphase temperature (b). At 11 - 13.5 °C, the occupying areas were small and stayed constant at ca. 0.02 nm^2. Above 16 °C, the area was retained again at a constant area of ca. 0.10 nm^2. A sharp increase of the occupying area of PS-P4VP film was observed within only two degrees between 14 and 16 °C. In the above manners, an abrupt area increase by a factor of five was observed at 14-16 °C. The relationship between occupying area per styrene unit and subphase temperatures exhibited a sigmoidal shape (Figure 5-3). Among many solvents employed here, only cyclohexane and methyl cyclohexane gave the sharp area change with temperature change. These two solvents correspond to the theta solvents for PS. As the control, the spreading behavior of a homopolymer of PS from cyclohexane solution exhibited no sudden area change (Figure 5-4). Their occupying areas were gradually and monotonously decreased by increasing subphase temperatures. Thus, P4VP segments of the block copolymers contribute a great deal to this area changing phenomenon. It is thus concluded that use of theta solvent on spreading for the block copolymer is essential for the large temperature dependency.

The influence of spreading from various solvents was summarized in Table 5-1. Common properties of cyclohexane and methyl cyclohexane on PS-P4VP are as follows: i) They are selective solvent which dissolved only PS segment, ii) their diffusion speed

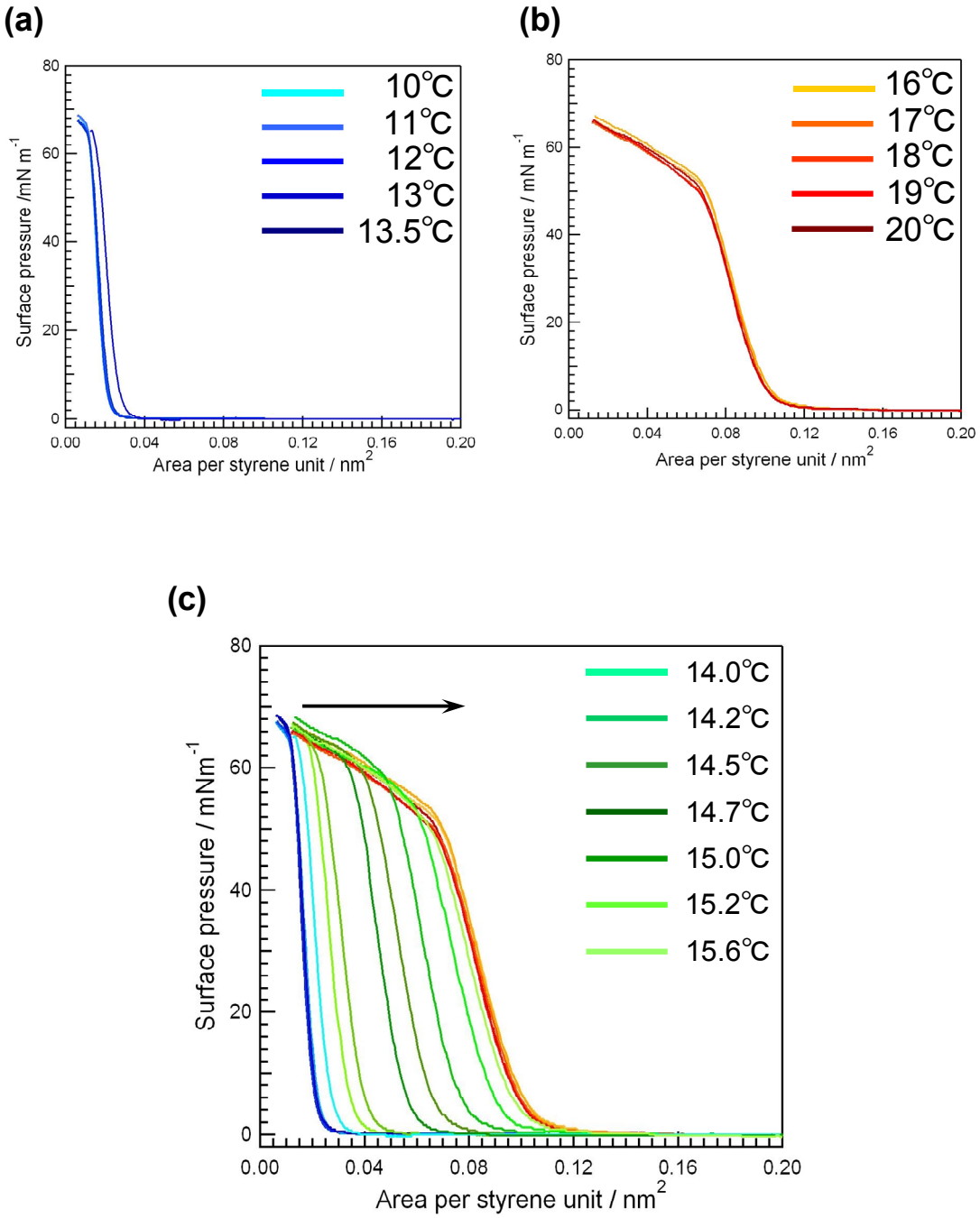

Figure 5-2. Surface pressure-area curves of PS158-P4VP32 spreading from cyclohexane solution at 10-13.5 oC (a), 16-20 oC (b), and 14-16 oC (c).

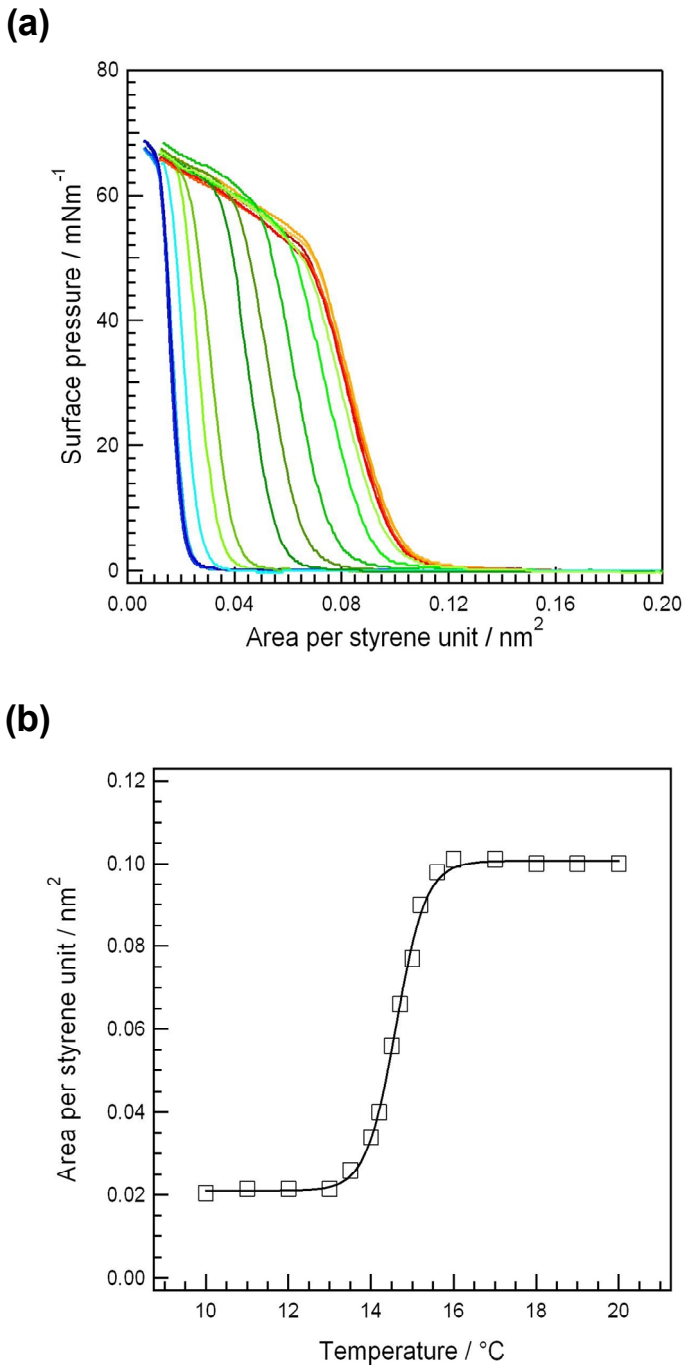

Figure 5-3. Surface pressure-area curves of PS158-P4VP32 spread from cyclohexane at 10-20 oC (a), and the relationship between area per styrene unit and subphase temperatures (b).

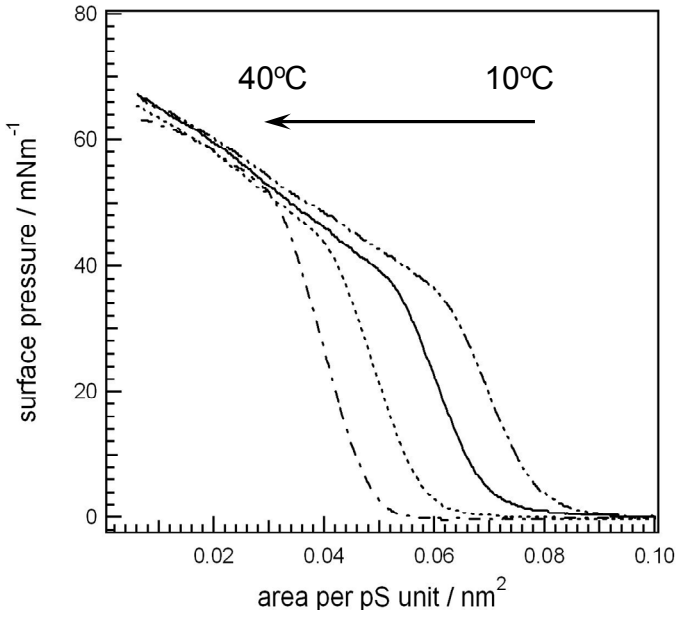

Figure 5-4. Surface pressure-area curves of PS290 (homopolymer) spread from cyclohexane solution at 10 ~ 40 oC.

Table 5-1. Summary of spreading behaviors from various solvents

Solvent	Solubility*		θ-solvent	*Spreading behavior*	*Change area by temp.*
	PS	P4VP			
Cyclohexane	○	×	○	−	○
Methyl Cyclohexane	○	×	○	−	○
Toluene	○	×	×	−	×
Ethyl Acetate	○	×	○	+	×
1,4-Dioxane	○	×	×	soluble	×
Chloroform	○	○	×	+	×
Cyclohexanone	○	×	×	+	×
Benzene	○	○	×	−	×

* : *POLYMER HANDBOOK Third edition*, (Wiley) or solubility test

ascribed to the solvent viscosity is low, and iii) they belong to theta solvents for PS. Spreading solvents used in this experiment were of various solubilities for each block segment.[23] PS segment can be dissolved in all solvent and P4VP segment are dissolved in only chloroform and benzene. These results suggest that the spreading behaviors were not dependent on the solubility for each segment. These results are reinforced by Lennox et al.'s report. They indicated that there were no difference in surface morphologies of PS-PEO block copolymers when spread from toluene and chloroform.[24] On the other hand, cyclohexane solution spread on the water surface remains stable for duration of a few seconds. For chloroform etc. the solvents spreads rapidly and disappears immediately on the water surface. Kajiyama et al. reported that PS ultrathin films are formed owing to moderate spreading ability of the solution on the water. The morphologies of PS thin films depended on the dissipation speed of solvent.[25] The same tendency is observed here.

5.3.2. Brewster Angle Microscopic Observations

In Brewster angle microscopy (BAM) observation, a Langmuir film is visualized as bright parts in the image, and exposed water surface are observed as dark parts.[26,27] Figure 5-5 displays BAM images of the PS-P4VP films spread from cyclohexane solution at 10 °C (a), and 20 °C (b). The PS-P4VP film at 10 °C on water exhibited large irregular bright domains with strong light reflectance even before the pressure was applied. These bright parts correspond to 3D aggregates of PS-P4VP. The size of the domains ranged a few hundred micrometers. Probably, these aggregates were formed immediately after spreading onto water. Upon compression, these aggregates were gathered and observed at whole areas at 50 mN m^{-1}. In contrast, the PS-P4VP film on water at 20 °C was characterized by smaller flat domains with low contrast (Figure 5-5b). As the surface pressure was increased, the domains were fused to form a highly homogeneous monodomain.

BAM images of the spread film from a chloroform solution at 10 °C and 20 °C are displayed in Figure 5-6. The domain structures of the film with low contrast were observed similar to those observed for spreading from cyclohexane at 20 °C. Such

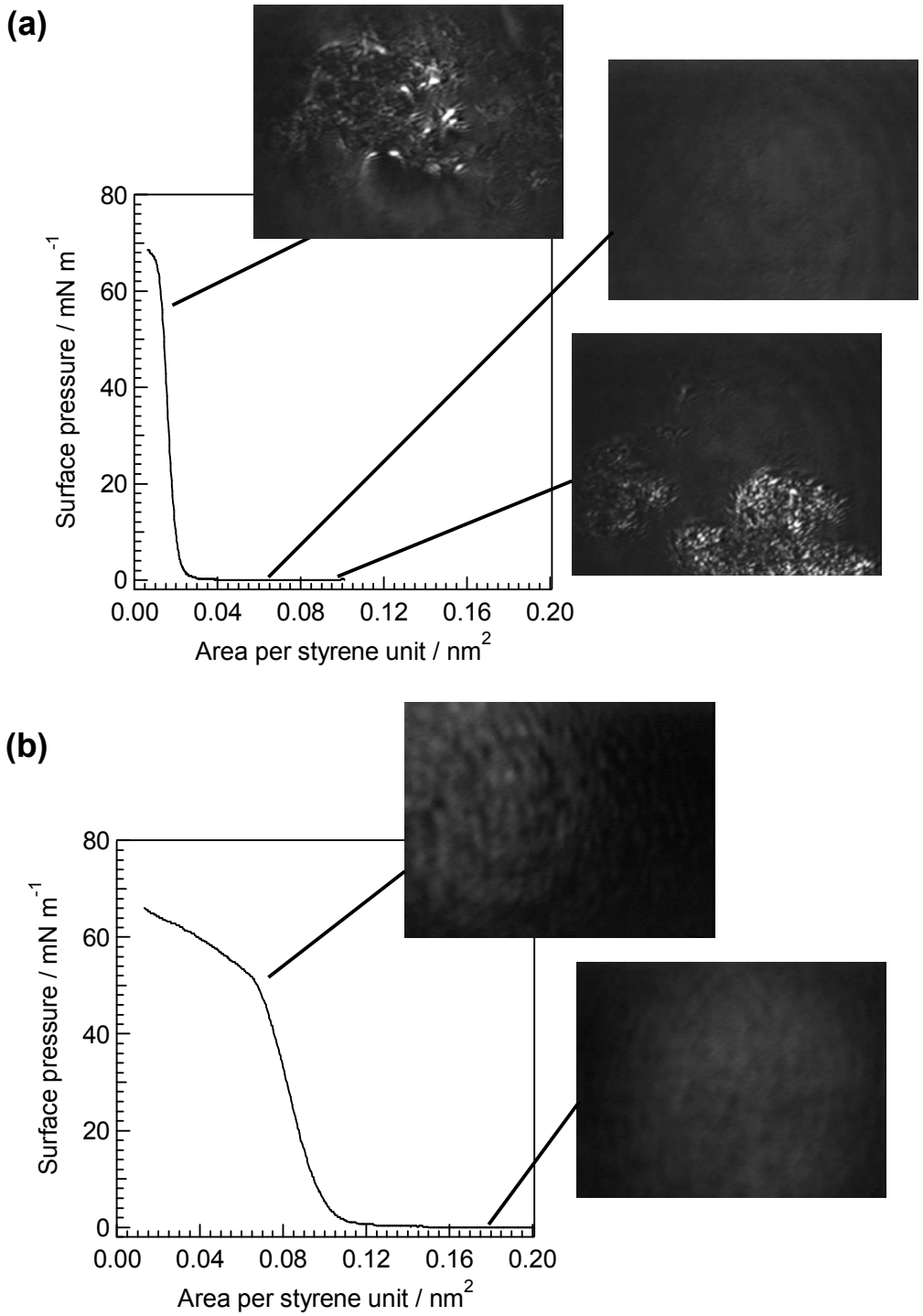

Figure 5-5. BAM images of PS_{158}-$P4VP_{32}$ films on the water surface spread from cyclohexane at 10 ºC (a), and 20 ºC (b).

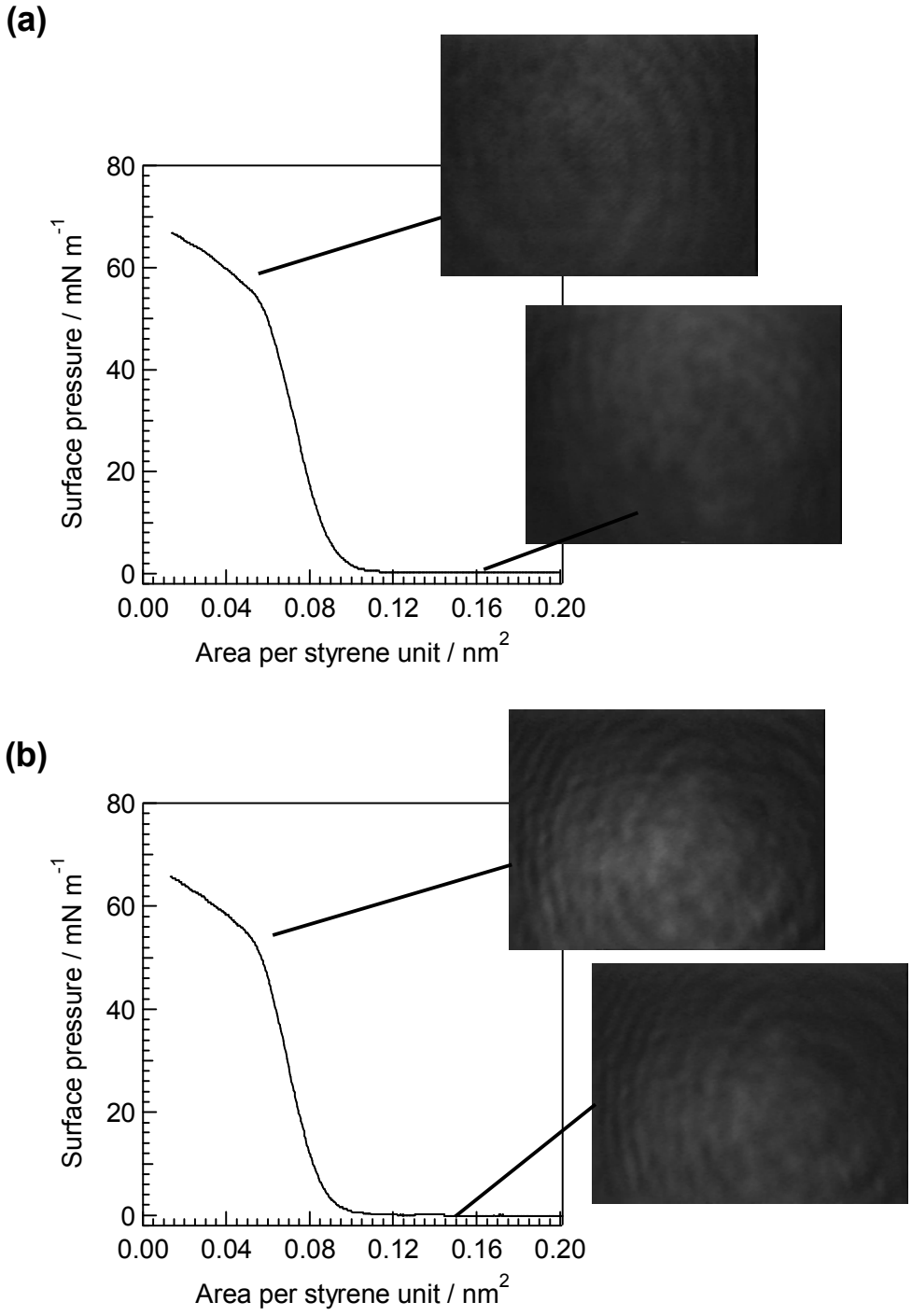

Figure 5-6. BAM images of PS158-P4VP32 films on the water surface spread from chloroform at 10 oC (a), and 20 oC (b).

homogeneous layers (homogeneous at the level of BAM resolutions) observed on spreading from chloroform and from cyclohexane at higher temperatures, should not be composed of an ideally extended monolayer judging from the smaller areas than the supposed cross section of a styrene unit.

Thus, from BAM images, irregular aggregates of PS-P4VP when spread from cyclohexane at 10 °C occurred, probably derived from the interaction between polymer and cyclohexane solvent. Such structure seems to be immediately formed after solvent evaporation.

5. 3. 3. Thermally Induced Area Changes

Figure 5-7 shows the area change at a constant surface pressure (1 mN m^{-1}) when the temperature of subphase was changed. On the cooling process starting from 16 °C to 10°C, the area of polymer film was unchanged. On heating process starting from 10 °C to 16°C no area change was not observed, either. Thus, the area of polymer film did not show reversible changes after the spreading solvent was vaporized. In other words, it is suggested that the sharp area changes occurred not only by the interaction between the polymer and temperature-controlled subphase but also the polymer chains and spreading solvent. Next, the effect of temperature of spreading solvents was evaluated.

Figure 5-8 displays the π - A curves of PS_{158}-$P4VP_{32}$ spread from chloroform (a) and cyclohexane (b). If this sharp area change is only affected by subphase temperature and is not affected by solution temperature, two spreading behavior should show the same behavior without dependence on solution temperature. Red lines in Figure 5-8 obtained when the solutions was cooled before spreading, and black lines obtained when maintained at room temperature. In fact, spread behavior was not altered. Combined with BAM images, it is concluded that the sharp area changes were caused by interaction between the polymer chain and selective solvent such as cyclohexane.

5. 3. 4. Aggregation Behavior in Solutions

Figure 5-9 illustrates photographs of PS_{158}-$P4VP_{32}$ in cyclohexane solution at

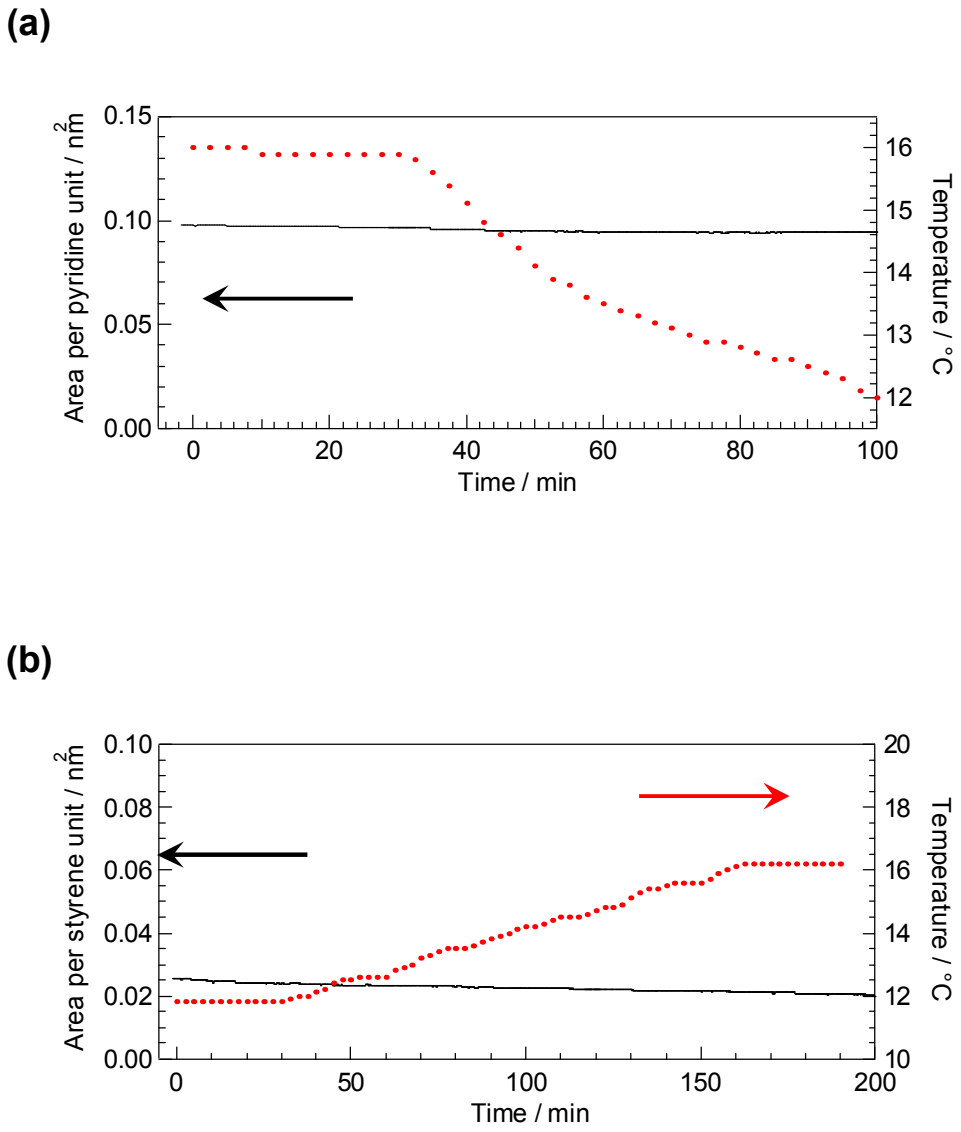

Figure 5-7. Time courses the area change of the PS158-P4VP32 on the water surface on subphase temperature changes monitored at a constant pressure of 1 mN m-1.

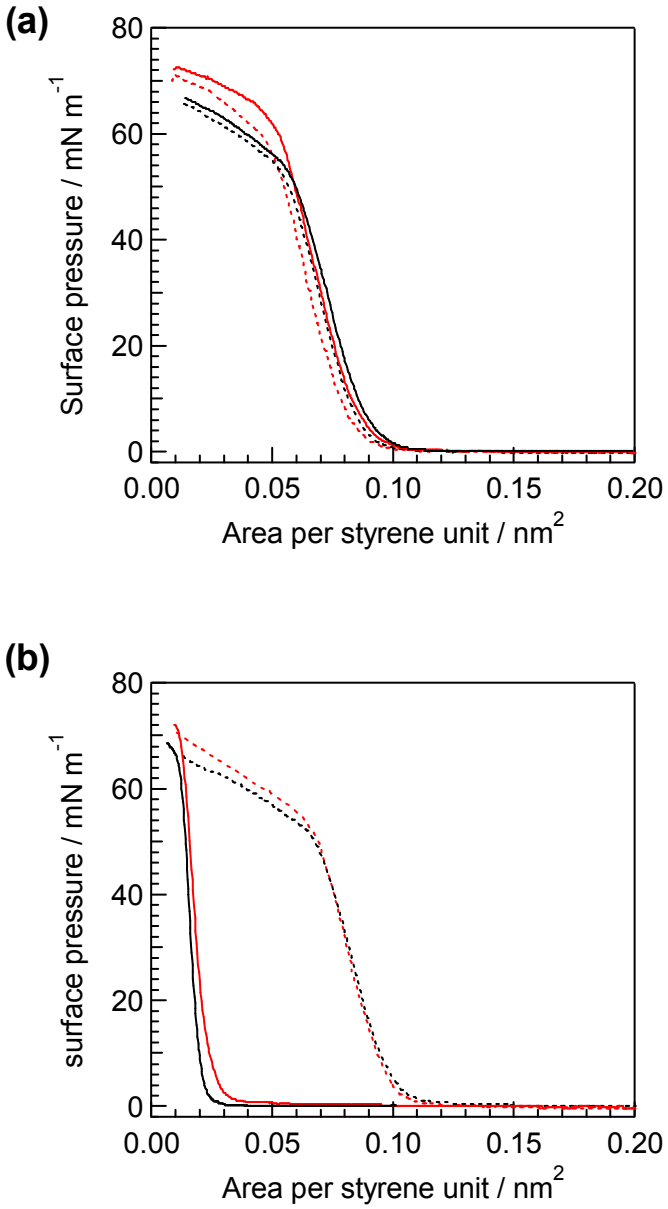

Figure 5-8. Surface pressure-area curves of PS158-P4VP32 spread from chloroform (a) and cyclohexane (b) at 10 oC (solid line) and 20 oC (dashed line). Red lines indicate data obtained when the solution was cooled before spreading

10–20 °C. When PS_{158}-$P4VP_{32}$ was dissolved in cyclohexane, the solution was transparent at 20 °C, but became clouded at 10 °C. The turbidity of the solvent was also altered by temperature change. It is therefore suggested that the aggregation state of the polymer is changed in cyclohexane. The turbidity change sharply occurred at 14–16 °C, exactly the identical temperature range where the area change occurred on water. Figure 5-10 exhibits transmittance at 500 nm of PS_{158}-$P4VP_{32}$ dissolved in cyclohexane and chloroform solutions at various temperatures. The cyclohexane solution was transparent and their transmittance exceeded 95 % between 17 and 20 °C. From 10 to 15.5 °C, in contrast, the solution became highly turbid. A sudden increase of the transmittance was observed in a narrow range between 15.5 and 17 °C. This behavior is closely correlated with the area change at the air-water interface. In chloroform, in contrast, the solution remained transparent at all temperatures examined, and the turbidity change and thus transmittance change were not observed (Figure 5-10 closed circle).

Dynamic light scattering (DLS) measurements were performed for the estimation of aggregate size in the two solvents. Distribution histograms of aggregate diameter obtained in this method are shown in Figure 5-11. In cyclohexane, their grain diameters ranged 1.6 ± 0.15 μm at 10 °C and 30 ± 8 nm at 20 °C. Thus, the aggregate size was altered by more than 50 times in diameter. This change was observed reversibly. At higher temperatures, PS_{158}-$P4VP_{32}$ should form micelles-like structure where P4VP and PS blocks forms an inside core and outside corona, respectively. These sizes were comparable with those of other reported amphiphilic block copolymers containing polystyrene.[10] At lower temperatures, the structures should agglutinate to constitute larger sized aggregates. In chloroform solution, their grain diameters ranged 54.7 ± 15 nm at 10 °C and 52.4 ± 10 nm at 20 °C (Figure 5-11c, d). PS_{158}-$P4VP_{32}$ should also form micelles-like structure, however, changes in the aggregate size were not observed in chloroform as expected from the absence of turbidity change.

5.3.5. The Aggregation Behavior in Solution and on Water Surface

The aggregation state of PS_{158}-$P4VP_{32}$ in solution affects the sharp area change

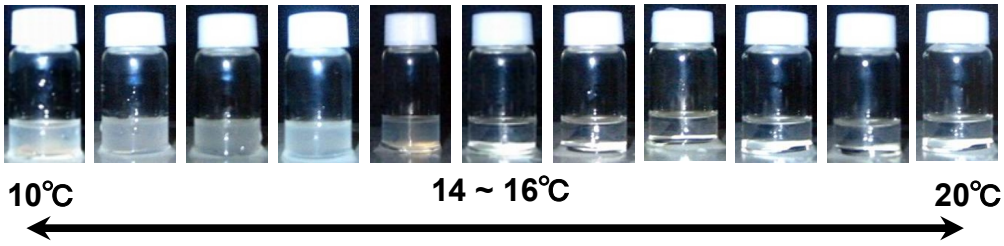

Figure 5-9. Photographs of PS158-P4VP32 in cyclohexane solution at 10-20 oC.

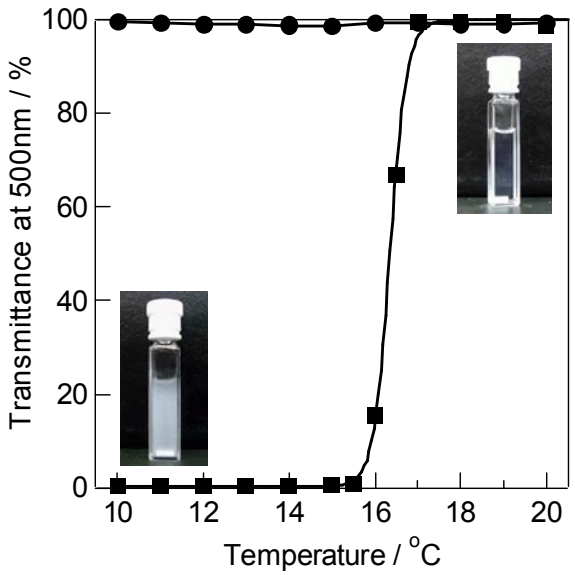

Figure 5-10. Transmittance of PS_{158}-$P4VP_{32}$ solutions of chloroform (circle) and cyclohexane (square) at 500 nm at various temperatures from 10 °C to 20 °C.

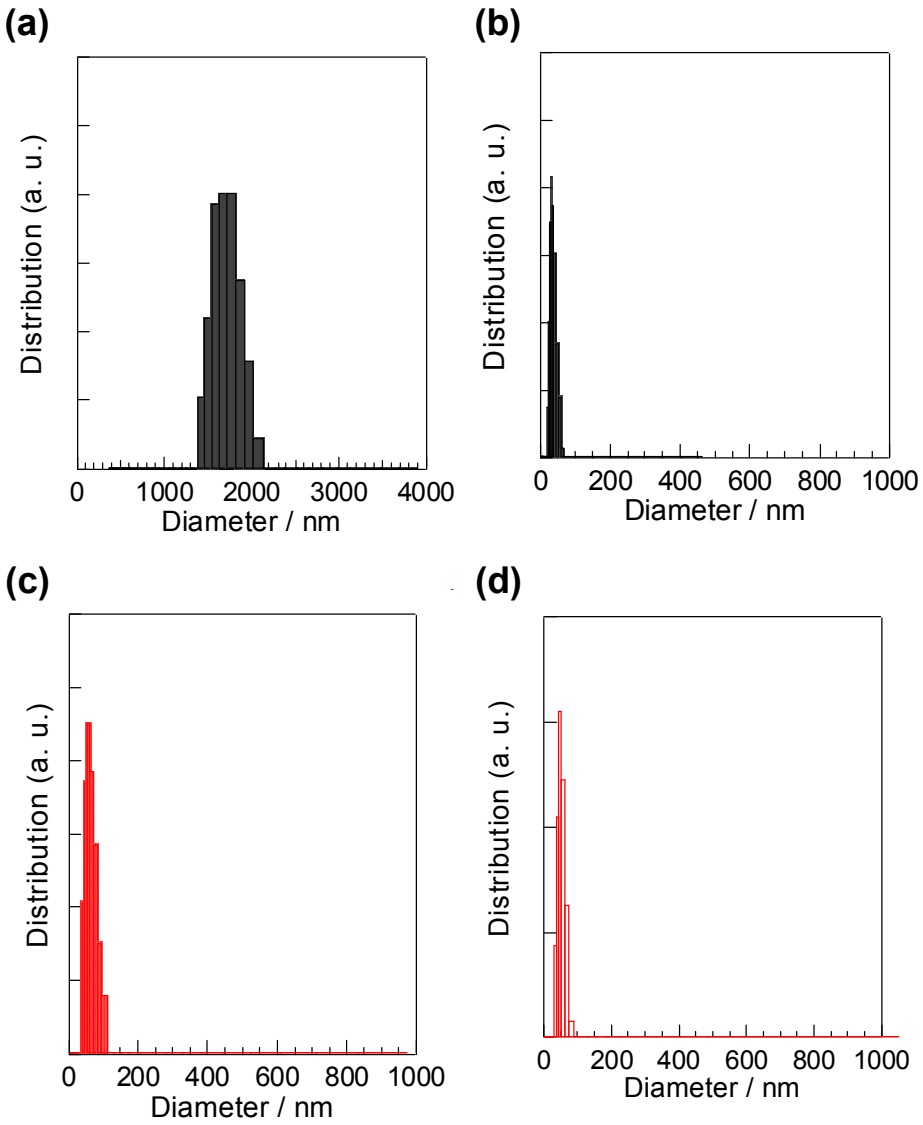

Figure 5-11. DLS histograms of PS-P4VP in cyclohexane solution at 10 oC (a), at 20 oC (b), in chloroform solution at 10 oC (c), and at 20 oC (d).

at the air-water interface as revealed by transmittance and DLS measurements. Now, the temperature induced diameter change of aggregate in cyclohexane mentioned above can be understood in terms of chain extension of polymer chains of PS block. In general, the conformations of single polymer chains in solution have an extended coil at higher temperatures and in good solvents, while have a collapsed globule state at lower temperatures and in poor solvents. The coil-globule transition between the extended and collapsed state occurs under particular conditions of temperatures[28] and solvent compositions (Figure 5-12).[29]

The abrupt temperature dependency observed here implies that such coil-globule transition should be involved in this system. Most probably, such temperature induced transition of PS occurs around 14–16 °C in cyclohexane. A previous static light scattering study revealed that the radius of gyration of PS (homopolymer, $M_n = 2.7 \times 10^7$) in cyclohexane abruptly changes around 32 °C, the theta temperature of this system.[30] The transition temperature around 15 °C in the present system is significantly lower than this. However, the transition temperature largely depends on the molecular weight of PS,[31] and a shift to lower temperature for the considerably shorter chain of PS used in this study ($M_n = 1.6 \times 10^4$) seems reasonable.

A schematic model of aggregation change in cyclohexane is shown in Figure 5-13. At 20 °C, PS chains adopt an extended coil state forming micelles in cyclohexane. When solution temperature is cooled below 14 °C, PS chains transfer from a coil to a compact globular state and become dissoluble in cyclohexane. Then, these micelles agglutinate and form larger aggregates. Consequently, the aggregate size of PS-P4VP in cyclohexane is largely altered by temperature change.

Since the temperature range of the abrupt area change shown in Figure 5-3b exactly agrees with that of the aggregation change dissolved in the identical solvent, essentially the same process should be involved at the air-water interface (Figure 5-13b). In spreading onto the air-water interface, the solution at the ambient temperature (ca. 20 °C) is rapidly changed to the subphase temperature before the solvent evaporates. If the subphase temperature is lower than the theta temperature (~14 °C), PS-P4VP forms large aggregates. After evaporation of the solvent, the aggregates are frozen to form

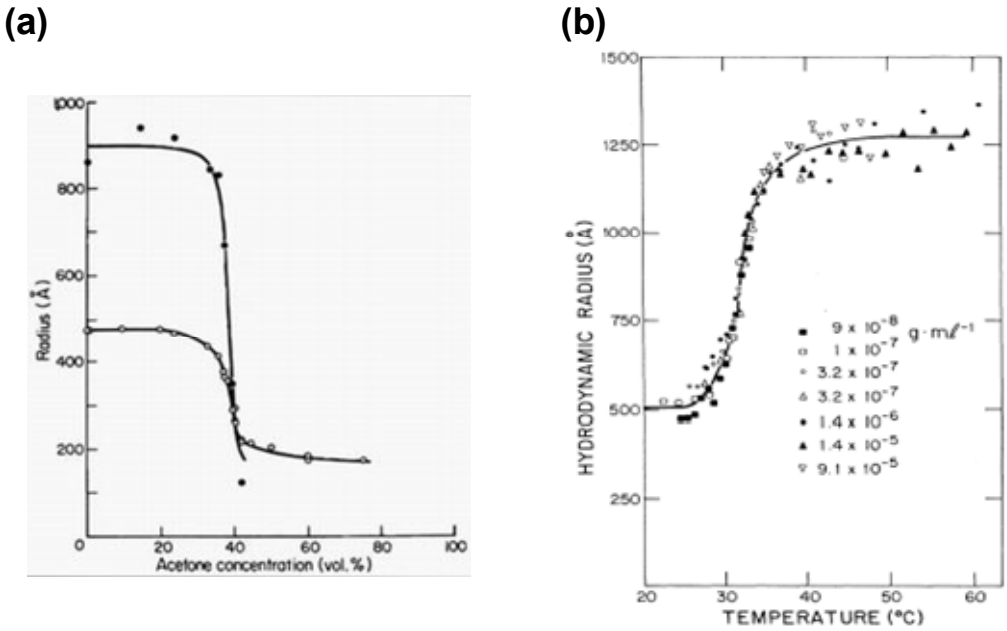

Figure 5-12. Examples for the coil-globule transition (taken from reference 28, 29). The solvent composition dependence (a) and the temperature dependence (b).

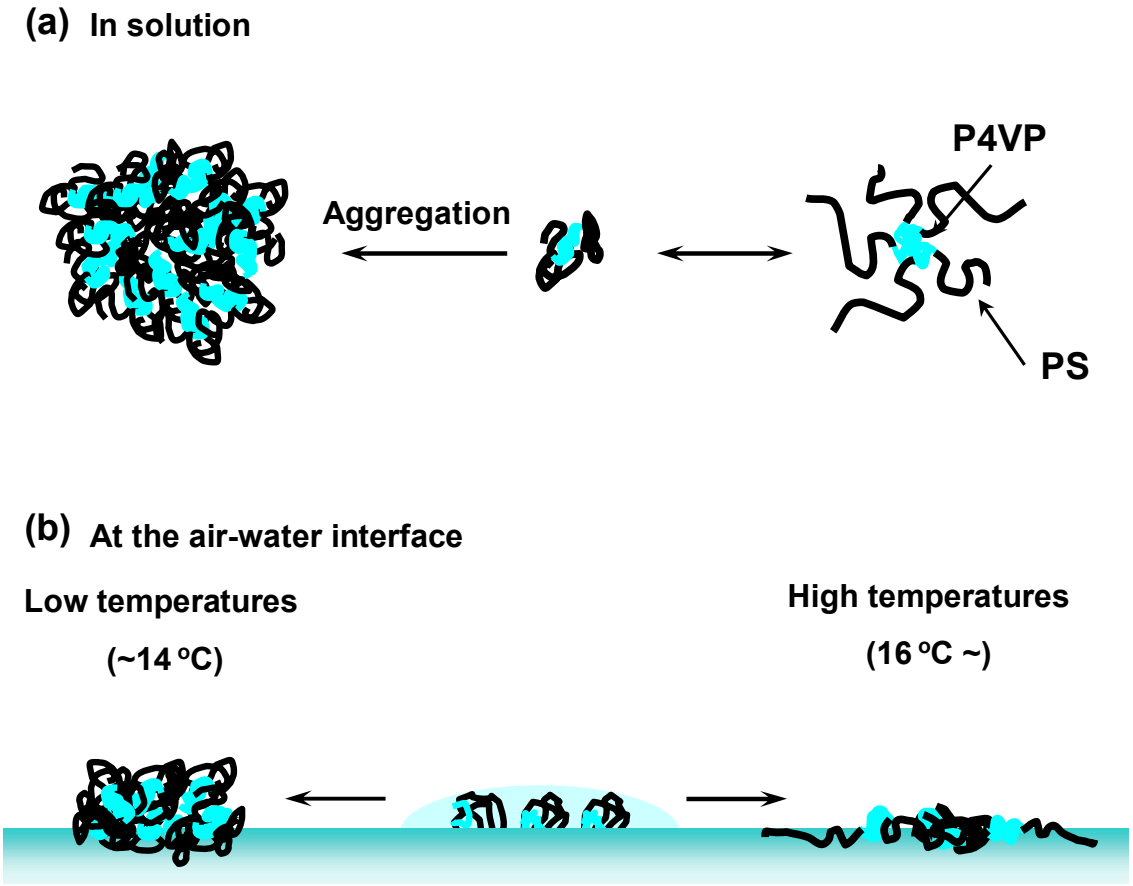

Figure 5-13. Schematic illustration of the conformation of PS-P4VP in cyclohexane solution (a), and their spread behaviors at the air-water interface (b).

irregular 3D structures aggregates. If the subphase temperature is higher than 16 °C, PS-P4VP is spread as a single micelle state to form a homogeneous thin film.

Thus, in the present system, the aggregation state in solution is directly reflected in the two-dimensional spreading behavior at the air-water interface even after the spreading solvent was evaporated. To our knowledge, such clear relationship between the solution state and the two-dimensional spread one has not been reported so far. In other words, the conformational state and thus the aggregation states in this block copolymer system are frozen and memorized on the water surface.

5.4. Conclusion

In this chapter, a new finding regarding the obvious relationship between the aggregate diameter in solution and the 2D area spreading behavior at the air-water interface for a block copolymer. This phenomenon should be strongly coupled with the degree of chain extension characterized by a theta solvent for one of the blocks used for spreading. An unexpectedly large (5-folds) area change on water is observed at very narrow temperature range by around 2 °C. These results are only observed when spread from cyclohexane and methyl cyclohexane, and the PS homopolymer dose not bring about this effect.

In theta solvent, PS-P4VP amphiphilic block copolymer formed micelle-like structures. Most probably, such behavior is attributed to the thermally induced coil-globule transition taking place in the theta solvent for PS. Around these conditions, the aggregation state in solution is robustly memorized during the spreading process on water.

The characteristic surface area change is observed by using conventional block copolymers. It is anticipated that this phenomenon will also occur in the the combinations of polymer and theta solvent. Other combinations (such as poly(*N*-isopropyl acrylamide) in water and poly(methyl methacrylate) in water/*tert*-butyl alcohol mixed solution etc.) would be applicable.

Reference

[1] Katz, J. R.; Samwell, P. J. P. *Naturewissenschaften* **1928**, 16, 592.

[2] Gaines, G. L. *Langmuir* **1991**, 7, 834.

[3] Ulman, A. *An Introduction to Ultrathin Organic Films from Langmuir-Blodgett to Self-Assembly* Academic press, **1991**.

[4] Park, C.; Yoon, J.; Thomas, E. L. *Polymer* **2003**, *44*, 6725.

[5] Hadjichristidis, N.; Pispas, S.; Floudas, G. *Block Copolymers: Synthetic Strategies, Physical Properties, and Applications*, Wiley-interscience, **2003**.

[6] Hamley, I. W. *Developments in Block Copolymer Science and Technology*, Wiley, **2004**.

[7] Hamley, I. W. *Block Copolymers in Solution: Fundamentals and Applications*, Wiley, **2005**.

[8] Cox, J. K.; Eisenberg, A.; Lennox, R. B. *Curr. Opin. Colloid Interface Sci.***1999**, *4*, 52.

[9] Hamley, I. W. *Developments in Block Copolymer Science and Technology*, Wiley, **2004**.

[10] Zhu, J.; Eisenberg, A.; Lennox, B. R. *J. Am. Chem. Soc.* **1991**, 113, 5583.

[11] Zhu, J.; Eisenberg, A.; Lennox, R. B. *Langmuir* **1991**, *7*, 1579.

[12] Zhu, J.; Eisenberg, A.; Lennox, R. B. *Macromolecules* **1992**, *25*, 6547.

[13] Meli, M.-V.; Badia, A.; Gru¨tter, P.; Lennox, R. B. *Nano Lett.* **2002**, *2*, 131.

[14] Baker, S. M.; Leach, K. A.; Devereaux, C. A.; Gragson, D. E. *Macromolecules* **2000**, 33, 5432.

[15] Lu, Q.; Bazuin, C. G. *Nano Lett.* **2005**, *5*, 1309.

[16] Seo, Y.; Paeng, K.; Park, S. *Macromolecules* **2001**, 34, 8735.

[17] Devereaux, C. A.; Baker, S. M. *Macromolecules* **2002**, 35, 1921.

[18] Soo, P. L.; Eisenberg, A. *J. Polym. Sci.Part B: Polym. Phys.* **2004**, 42, 923.

[19] Zhang, L.; Shen, H.; Eisenberg, A. *Macromolecules* **1997**, 30, 1001.

[20] Sohn, B.-H.; Yoo, S.-I.; Seo, B.-W.; Yun, S.-H.; Park, S.-M. *J. Am. Chem. Soc.* **2001**, 123, 12734.

[21] Kadota, S.; Aoki, K.; Nagano, S.; Seki, T. *J. Am. Chem. Soc.* **2005**, 127, 8266.

[22] Kadota, S.; Aoki, K.; Nagano, S.; Seki, T. *Coll. and Surf. A Phys. Eng. Asp.*, **2006**, 284-285, 535.

[23] Brandrup, J.; Immergut, E. H. (Ed.) *POLYMER HANDBOOK Third Edition*, Wiley

interscience, **1989**.

[24] Cox, J. K.; Yu, K.; Constantine, B.; Eisenberg, A.; Lennox, R. B. *Langmuir* **1999**, 15, 7714.

[25] Shuto, K.; Oishi, Y.; Kajiyama, T.; Han, C. C. *Polymer Journal* **1993**, 25, 291.

[26] Honig, D.; Mobius, D. *J. Phys. Chem.* **1991**, 95, 4590.

[27] Henon, S.; Meunier, J. *J. Rev. Sci. Instrum.* **1991**, 62, 936.

[28] Swislow, G.; Sun, S.-T.; Nishio, I.; Tanaka, T. *Phys. Rev. Lett.* **1980**, 44, 796.

[29] Nishio, I.; Sun, S.-T.; Swislow, G.; Tanaka, T. *Nature* **1979**, 281, 208.

[30] Slagowski, E.; Tsai, B.; McIntyre, D. *Macromolecules* **1976**, 9, 687.

[31] Chu, B.; Wang, Z. *Macromolecules* **1988**, 21, 2283.

Chapter VI

Temperature Dependent Aggregation Behaviors of Polystyrene-Based Block Copolymers at the Air-water Interface

6.1. Introduction

Polymer chains in general adopt different conformations in solution and at the air-water interface. The conformations of single polymer chains have a random three-dimensional extended coil at high temperatures and in good solvents, while they have a collapsed globule state or dissolved as an aggregate at low temperatures and in poor solvents.[1] The phase transition between the extended and collapsed state, namely, the coil-globule transition, occurs under the particular temperature[2] or solvent composition.[3] This principle has applied to volume phase transition of cross-linked polymer networks (*i. e.* gels).[4] When block copolymers are dissolved in a solvent which is good only for one segment, the insoluble blocks associate and form the core of micelle structures, whereas the soluble blocks form a corona.[5] These colloidal aggregates are switched reversibly by solution temperature[6] or solution compositions.[7,8]

In contrast, polymer chains are stretched upon spreading on water with the repeating units being adsorbed on the air-water interface.[9] The chain conformation of hydrophobic polymers on water is affected by the spreading solvent used. The conformation of polystyrene (PS) spread onto water surface is different by spreading solvents. Kajiyama et al. investigated the conformation and packing of PS chains in two-dimensional ultrathin film of which the thickness is less than the molecular dimension.[10,11] Kumaki reported that the formation monomolecular particle of PS with a diameter of ca. 50 nm is performed by spreading benzene solution onto a water surface.[12,13] On the other hand, surface morphorogies of surface micelle structures such as polystyrene-*block*-poly(ethylene oxide) (PS-PEO) were not dependent on the solubility for each segment; toluene and chloroform.[14] For thin films, morphologies of block copolymers are also altered by solvent conditions.[15] Sohn et al. reported that 2D

micelles of polystyrene-*block*-poly(4-vinyl pyridine) (PS-P4VP) switch their nanostructures through core-corona inversion of micelles by selecting solvents of each blocks.[16]

In Chapter V, the characteristic spreading behavior of amphiphilic block copolymer, PS-P4VP at the air-water interface was described. An abrupt temperature dependent change in aggregate size of polymer micelles has been observed when cyclohexane is used as the solvent. The size of the polymer micelle in solution is directly reflected to the two-dimensional spreading behavior at the air-water interface.

This chapter describes some extended investigations in this subject, focusing on the influence of PS segments and PS compositions in amphiphilic block copolymers. To evaluate the influence of PS segments, solution properties were observed in other types of amphiphilic diblock copolymers, polystyrene-*block*-poly(ethylene oxide) (PS-PEO) and polystyrene-*block*-poly(2-vinyl pyridine) (PS-P2VP). PEO or P2VP segment does not dissolved in cyclohexane. If the same behaviors as PS-P4VP in cyclohexane are observed for other types of PS-based block copolymers, the interpretation based on the theta solvent for PS will be justified. Furthermore, the influence of the length of PS block was explored for the series of PS-P4VP.

6.2. Experimental Section

6.2.1. Materials

All polymers used in this chapter are shown in Chart 6-1. The amphiphilic block copolymers, PS_m-$P4VP_n$, were synthesized by living anionic polymerization. Molecular characteristics of block copolymers are listed in Table 6.1. The PS content of the block copolymers were 76, 83, 88 and 94 wt%, and dubbed as PS_{88}-$P4VP_{28}$, PS_{158}-$P4VP_{32}$, PS_{256}-$P4VP_{34}$, and PS_{555}-$P4VP_{35}$, respectively. The concentration of the spreading solutions was ca. 1.0×10^{-3} mol dm^{-3} per pyridine unit.

The amphiphilic block copolymer, PS_{101}-PEO_{40} was synthesized by atom transfer radical polymerization[17,18] starting from a PEO macroinitiator.[19,20] The number average molecular weight of each block was 10100 (101 units) and 2000 (40 units) for PS and PEO segments, respectively, with the total polydispersity (M_w / M_n) of 1.14.

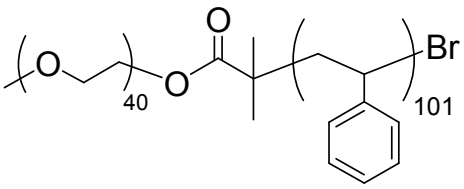

PS-PEO

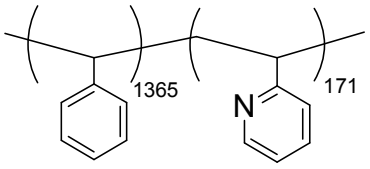

PS-P2VP

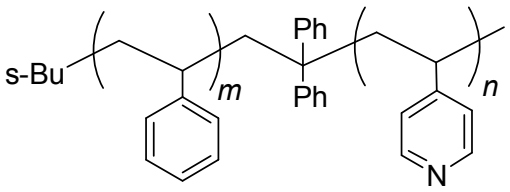

PS-P4VP

Chart 6-1.

Table 6-1. Characterizations of PS_m-$P4VP_n$ used in this study

Polymer	m	n	M_w/M_n	PS composition
PS_{88}-$P4VP_{28}$	88	28	1.14	76 wt %
PS_{158}-$P4VP_{32}$	158	32	1.10	83
PS_{256}-$P4VP_{34}$	256	34	1.09	88
PS_{555}-$P4VP_{35}$	555	35	1.09	94

The concentration of the spreading solutions was ca. 1.0×10^{-3} mol dm^{-3} per ethylene oxide unit.

The amphiphilic block copolymer, PS-P2VP was provided from Prof. Y. Matsushita.[21] The number average molecular weight of each block was 142000 (1365 units) and 18000 (171 units) for PS and P2VP segments, respectively, with the total polydispersity (M_w / M_n) of 1.05. The concentration of the spreading solutions was ca. 1.0×10^{-3} mol dm^{-3} per pyridine unit.

6.2.2. Spreading Behaviors at the Air-water Interface

The spreading behaviors of PS_m-$P4VP_n$ were evaluated on pure water (Milli-Q grade, 18 MΩ cm, pH = 5.8) using a Lauda FW-1 film balance. The temperatures of a water subphase were controlled by water circulation at various temperatures in the accuracy of ± 0.1 °C using a Yamato-Komatsu CTE-22W. After evaporation of the spreading solvent, the film on water was compressed at a speed of 30 cm^2 min^{-1}. The surface pressure was recorded versus molecular area per styrene unit.

6.2.3. Aggregation Properties in Solutions

UV-vis transmittance spectra in solution were taken with an Agilent 8453, and turbidities were measured by monitoring transmittance at 500 nm through 1 cm quartz cell at various temperatures. The solution temperature was controlled by water circulation at various temperatures in the accuracy of ± 0.2 °C using a Lauda RE104. The concentrations were ca. 1.0×10^{-3} mol (4VP unit) dm^{-3}.

6.3. Results and Discussion

6.3.1. Aggregation behavior in Solution for Other Block Copolymers

Figure 6-1 displays the transmittance of PS-PEO and PS-P2VP in chloroform (good solvent for PS) and cyclohexane (theta solvent for PS) at 500 nm at various temperatures. Only in cyclohexane solution, a sudden increase of the transmittance was observed in a narrow range between 20 and 23 °C. The same tendency was observed for PS-P2VP. The turbidity change occurred in a narrow temperature region between 28

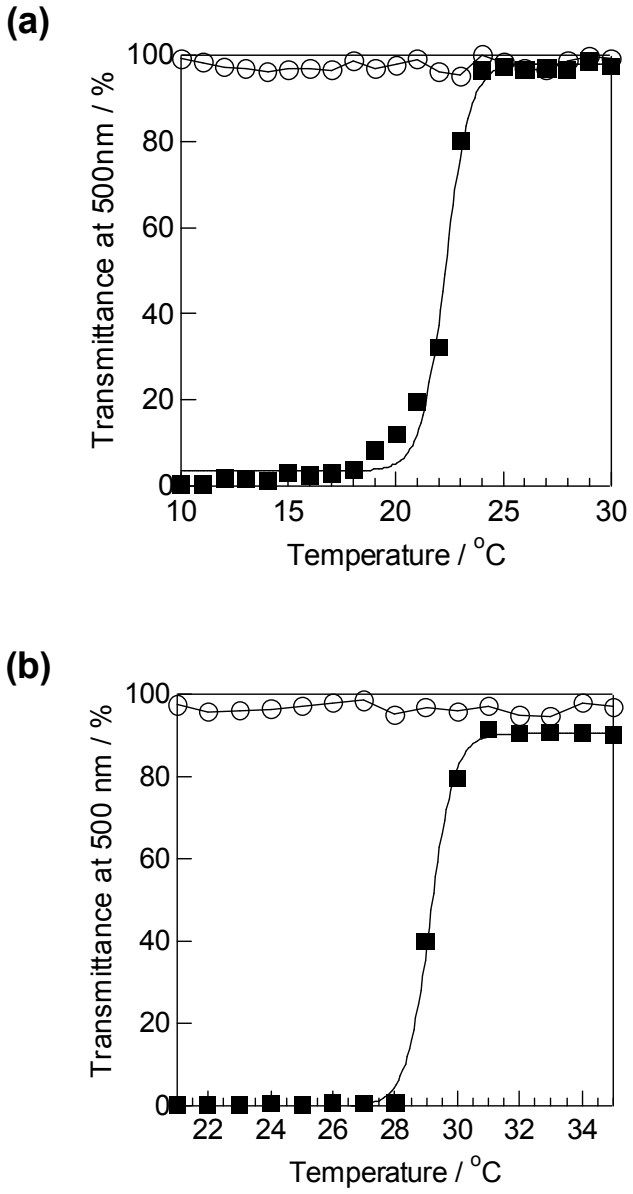

Figure 6-1. Transmittance change at 500 nm for of PS101-PEO40 (a) and PS1365-P2VP171 (b) in chloroform (circle) and cyclohexane (square) at various temperatures.

and 31 °C. This result indicates the turbidity change hardly influenced by the type of hydrophilic block such as P4VP, PEO and P2VP.

As mentioned in Chapter V, the turbidity change should be brought about by aggregation changes of block copolymer due to the coil-globule transition. On the other hand, the turbidity change of PS homopolymer in cyclohexane solution was not observed. From the previous work, the hydrodynamic radius change of polymer chains ranged from 50 nm to 150 nm when a large molecular weight polymer (M_w = 2.6 × 10^7) is used.[2,22] Therefore, the conformational change of the PS chains itself does not cause the turbidity change. In other word, by using block copolymers, the coil-globule transition was clearly visualized as the macroscopic event observable in the turbidity change. Consequently, small changes about several ten nanometers trigger aggregation changes in the micrometer-scales.

6.3.2. Effect of the PS Compositions of the PS-P4VP in Solutions

The changes of transmittance in solution examined for the series of PS_m-$P4VP_n$ are shown in Figure 6-2. In all polymers, the tendency of the temperature-dependent turbidity change was similar, however, the increase in the PS content from 76 to 94 wt%, led to systematic elevations of the transition temperatures. The temperature ranges of the transition were from 9 to 14, 15.5 to 17, 19.5 to 20.5 and 23 to 25.5 °C for PS_{88}-$P4PV_{28}$, PS_{158}-$P4VP_{32}$, PS_{256}-$P4VP_{34}$ and PS_{555}-$P4VP_{35}$, respectively. It is thus indicated that the coil-globule transition temperature of PS_m-$P4VP_n$ is clearly affected by the length of PS block. A previous static light scattering study by Tanaka et al. revealed that the radius of gyration of PS in cyclohexane abruptly changes around 32 °C.[2,3] In the present case, the temperature range was decreased by 10 to 20 °C. The lowered transition temperature should be ascribed to the effect of connected other segment and the difference in the molecular weight. Cyclohexane is non-dissolvable solvent for the P4VP segment. Thus, P4VP segment interrupts the resolving property of PS. Regarding the difference in the molecular weight, Chu and Wang et al. showed that the transition temperature significantly shifts to a lower range when the molecular weight becomes lower.[23] For example, the transition temperature shifts from 39.5 to 12.6 °C as

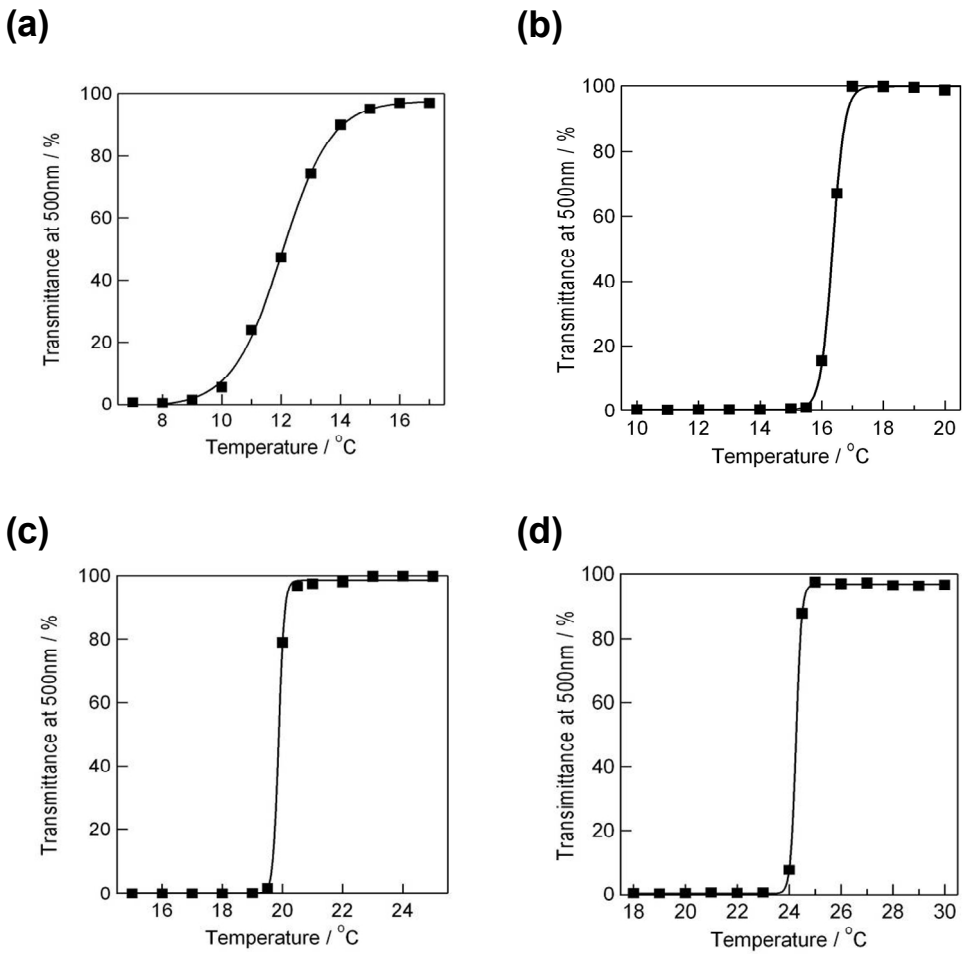

Figure 6-2. Transmittance change at 500 nm for PS_{88}-$P4VP_{28}$ (a), PS_{158}-$P4VP_{32}$ (b), PS_{256}-$P4VP_{34}$ (c), and PS_{555}-$P4VP_{35}$ in cyclohexane solutions at various temperatures.

M_w becomes from 4.6×10^4 to 1.0×10^4 in methyl cyclohexane, also a theta solvent for PS. Tanaka et al. adopted PS with $M_w = 2.7 \times 10^7$, and that of the PS block of the copolymer employed in this study ranges 9.1×10^3 to 5.8×10^4. Thus, the reduction in the transition temperature seems reasonable.

6.3.3. Effect of the PS Compositions of the PS-P4VP at the Air-water Interface

The temperature range of the transition evaluated by the area change at the air-water interface also indicated systematic changes similar to that in cyclohexane solutions. Figures 6-3 and Figure 6-4 show the spreading behaviors of PS_m-$P4VP_n$ spread from cyclohexane at various subphase temperatures (Figure 6-3) and the relationship between occupying areas and subphase temperatures (Figure 6-4). All PS_m-$P4VP_n$ indicated temperature dependency by subphase temperatures. Their temperature ranges of the area change were from 9 to 12 °C, 14 to 16 °C, 17 to 20 °C and 15 to 25 °C, for PS_{88}-$P4PV_{28}$, PS_{158}-$P4VP_{32}$, PS_{256}-$P4VP_{34}$ and PS_{555}-$P4VP_{35}$, respectively. However, the apparent transition range of PS_{555}-$P4VP_{35}$ obviously became broader. The broadening of the transition temperature range observed for PS_{555}-$P4VP_{35}$ is related to the large chain length of PS component. Upon spreading on water, the solvent evaporates rapidly and therefore the conformation and aggregate state is quickly frozen. When the longer chains are quickly frozen, various states of micelle size will be produced due to possible chain entanglements. In other words, the transition broadening should occur for the kinetic reason. In contrast, the chain conformation and aggregate states in solution are always in an equilibrium state, indicating the sharp transition independent of the chain length.

The coil-globule phase transition temperatures estimated in solution and at the air-water interface for PS_{88}-$P4PV_{28}$, PS_{158}-$P4VP_{32}$, PS_{256}-$P4VP_{34}$ and PS_{555}-$P4VP_{35}$ are summarized in Figure 6-5. The transition temperature ascended with the increase in PS segments of PS_m-$P4VP_n$ and they came close the value of PS homopolymer. The relationship also strongly suggests that the polymer micelle-like structure is commonly formed in these four polymers. In the process of spreading onto the water surface from the cyclohexane solution, the state of micelle-like aggregate is memorized and retained

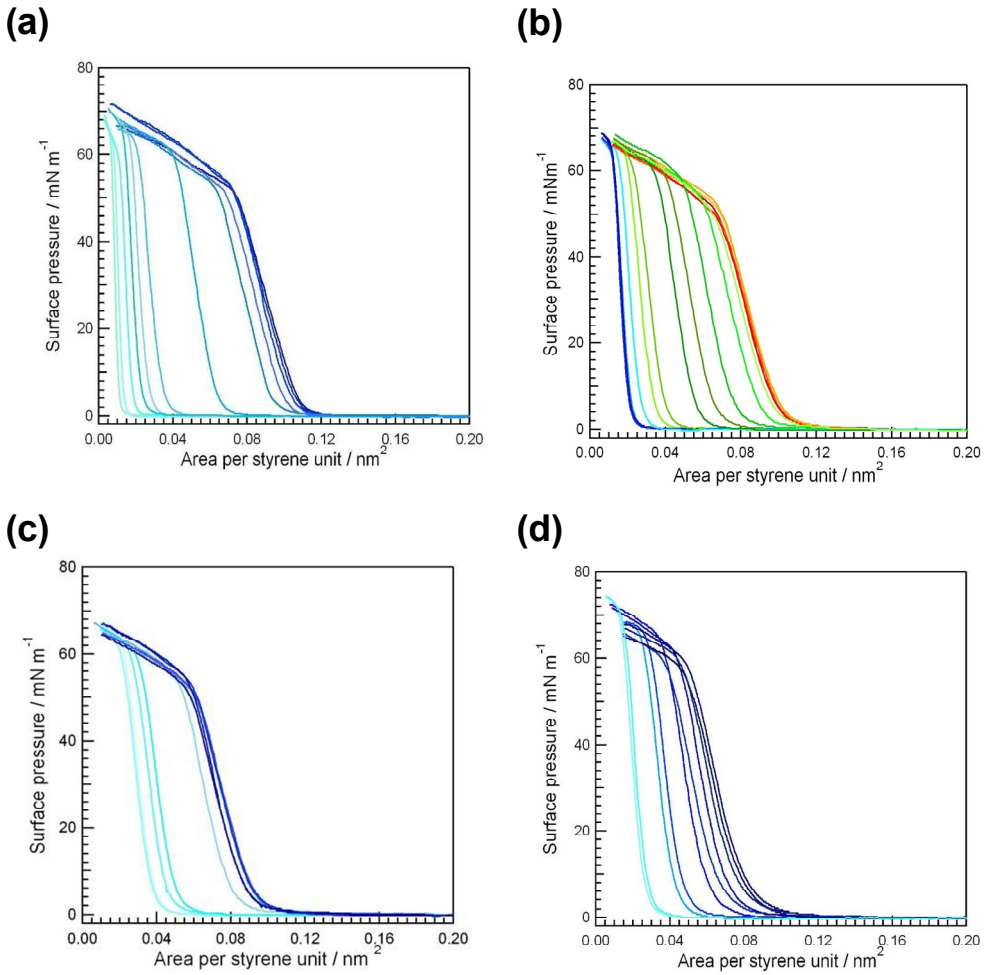

Figure 6-3. Surface pressure-area curves of PS_{88}-$P4VP_{28}$ (a), PS_{158}-$P4VP_{32}$ (b), PS_{256}-$P4VP_{34}$ (c), and PS_{555}-$P4VP_{35}$ at various subphase temperatures.

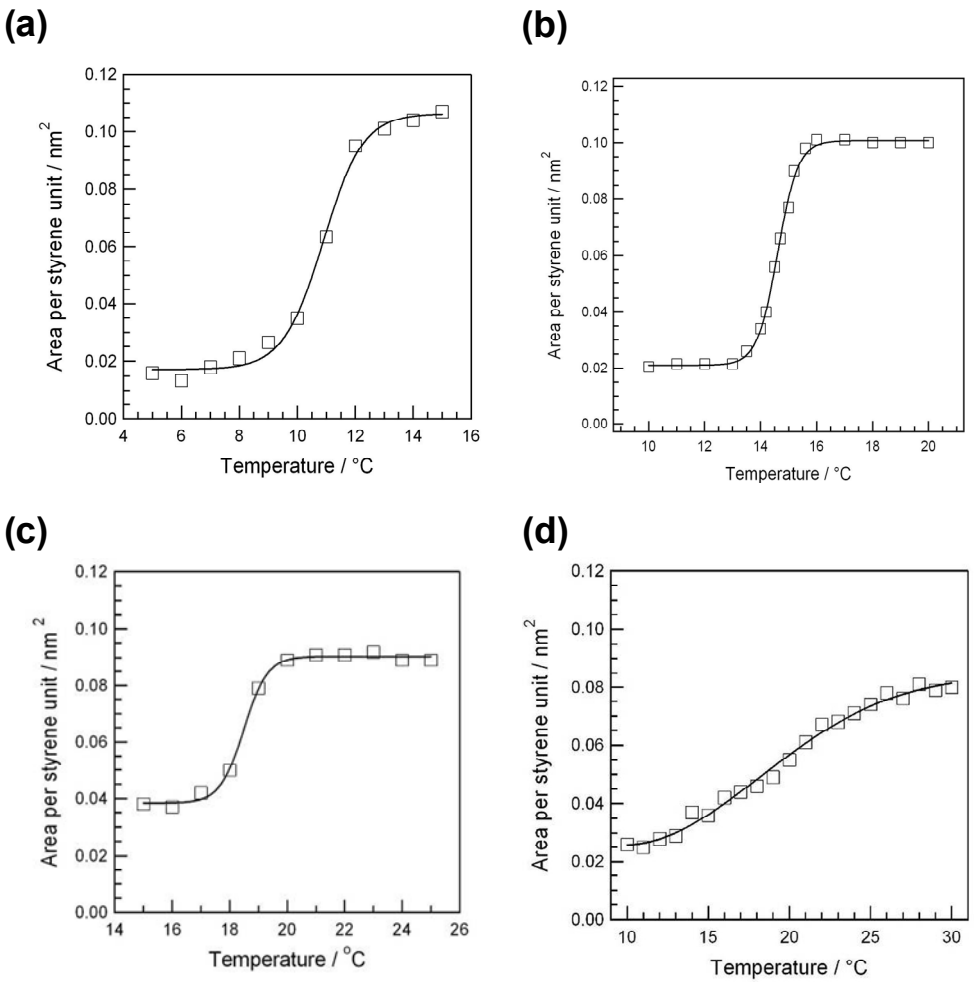

Figure 6-4. The relationship between area per styrene unit and subphase temperatures for PS_{88}-$P4VP_{28}$ (a), PS_{158}-$P4VP_{32}$ (b), PS_{256}-$P4VP_{34}$ (c), and PS_{555}-$P4VP_{35}$ (d).

during the rapid evaporation of the solvent. The close correlation between the aggregation state in the solvent and the film area on water can be explained by such assumption.

6.4. Conclusions

This chapter focused on the obvious relationship between the aggregates in theta solution and the spreading behavior at the air-water interface when a theta solvent for PS segments: cyclohexane is used for spreading. In the theta solution, same turbidity changes were observed for three types of PS-based amphiphilic block copolymers including PS-PEO, PS-P2VP, and PS-P4VP. Thus, such behavior is most probably triggered by the thermally induced coil-globule transition of PS. On the other hand, with the increase in the molecular weight of PS led to elevation of the transition temperature. From both sets of data, aggregation changes induced by temperatures change can be visualized both in solutions and at the air-water interface. Consequently, the new aspects obtained in this study should be of help in fundamental understandings in polymer chain conformations and in polymer thin film technology.

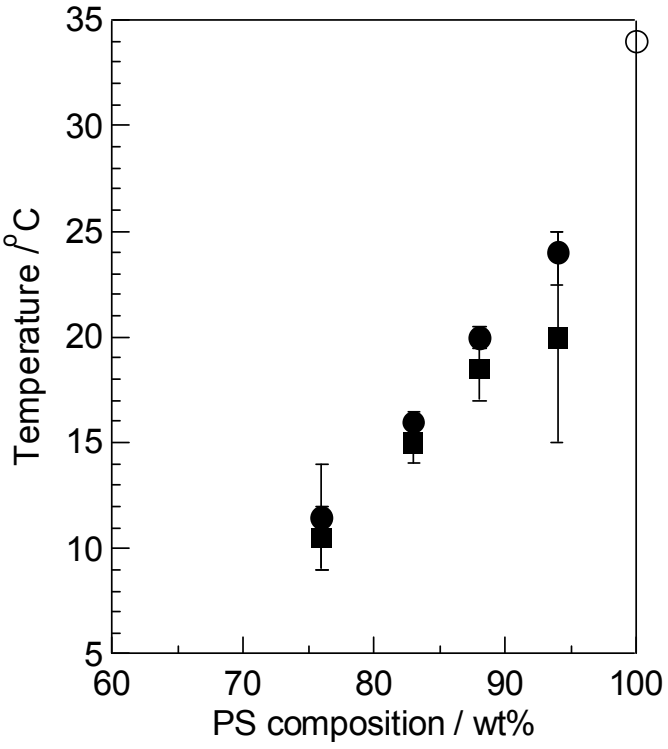

Figure 6-5. The transition temperature estimated by the turbidity change in cyclohexane solution (●) and change at the air-water interface when spread from cyclohexane (■) as a function of PS composition. The open circle (○) indicates that theta temperature of PS (*M*w = 2.7 × 107) in cyclohexane solution (taken from reference 2).

Reference

[1] Strobl, G. R. *The Physics of Polymers*, Springer-Verlag, **1997**.

[2] Swislow, G.; Sun, S.-T.; Nishio, I.; Tanaka, T. *Phys. Rev. Lett.* **1980,** 44, 796.

[3] Nishio, I.; Sun, S.-T.; Swislow, G.; Tanaka, T. *Nature* **1979**, 281, 208.

[4] Tanaka, T.; Fillmore, D. J. *J. Chem. Phys.* **1979**, 70, 1214.

[5] Hamley, I. W. *Block Copolymers in Solution: Fundamentals and Applications*, Wiley, **2005**.

[6] Arotçarena, M.; Heise, B.; Ishaya, S.; Laschewsky, A. *J. Am. Chem. Soc.* **2002**, 124, 3787.

[7] Soo, P. L.; Eisenberg, A. *J. Polym. Sci.Part B: Polym. Phys.* **2004**, 42, 923.

[8] Discher, D. E.; Eisenberg, A. *Science* **2002**, 297, 967.

[9] Gaines, G. L. *Langmuir* **1991**, 7, 834.

[10] Shuto, K.; Oishi, Y.; Kajiyama, T.; Han, C. C. *Polymer Journal* **1993**, 25, 291.

[11] Shuto, K.; Oishi, Y.; Kajiyama, T.; Han, C. C. *Macromolecules* **1993**, 26, 2589.

[12] Kumaki, J. *Macromolecules* **1986**, 19, 2258.

[13] Kumaki, J. *Macromolecules* **1988**, 21, 749.

[14] Cox, J. K.; Yu, K.; Constantine, B.; Eisenberg, A.; Lennox, R. B. *Langmuir* **1999**, 15, 7714.

[15] Albecht, K.; Mourran, A.; Moeller, M. *Adv. Polym. Sci.* **2006**, 200, 57.

[16] Sohn, B.-H.; Yoo, S.-I.; Seo, B.-W.; Yun, S.-H.; Park, S.-M. *J. Am. Chem. Soc.* **2001**, 123, 12734.

[17] Jankova, K.; Chen, X.; Kops, J.; Batsberg, W. *Macromolecules* **1998**, 31, 538.

[18] Wang, J.-S.; Matyjaszewski, K. *J. Am. Chem. Soc.* **1995**, 117, 5614.

[19] Tian, Y.; Watanabe, K.; Kong, X.; Abe, J.; Iyoda, T. *Macromolecules* **2002**, 35, 3739.

[20] Ashford, E. J.; O'Dell, N. R.; Billingham, N. C.; Armes, S. P. *Chem. Commun.* **1999**, 1285.

[21] Matsushita, Y.; Noro, A.; Iinuma, M.; Suzuki, J.; Ohtani, H.; Takano, A. *Macromolecules* **2003**, 36, 8074.

[22] Sun, S.-T.; Nishio, I.; Swislow, G.; Tanaka, T. *J. Chem. Phys.* **1980**, 73, 5971.

[23] Chu, B.; Wang, Z. *Macromolecules* **1988**, 21, 2283.

Chapter VII

Summary and Outlook

This doctoral thesis deals with two characteristic stimuli-responsive polymer thin films fabricated by utilizing surface-initiated polymerization and Langmuir-Blodgett (LB) technique. Both films are strongly coupled with the effect of interfaces. The former part deals with the molecular alignment of liquid crystalline polymer brushes containing azobenzene (Az) molecules by synthesized of surface-initiated living radical polymerization. Their molecular orientations of mesogenic molecules by thermal annealing and photo irradiation were evaluated by UV-vis spectra, grazing-incidence X-ray diffraction measurements.

In chapter II, novel liquid crystalline Az-polymer grafted films were synthesized by surface-initiated atom transfer radical polymerization and the molecular orientations of Az mesogenic groups were investigated in detail. Az-polymer grafted films were successfully synthesized and the chain lengths were controlled by polymerization time and initial monomer concentrations. The orientation of Az units in grafted films was found to adopt parallel alignment. This orientation behavior was a fully different from those of spincast films. Therefore, the orientation of polymer chains and mesogens can be altered without losing their characteristics by tethering one chain end on the substrate surface.

Chapter III focused on photochemical properties of Az-polymer grafted films. The efficient photoisomerization behavior and highly ordered in-plane photoalignment induced with irradiation of linearly polarized visible light were found, which should be caused by the parallel orientation of Az molecules. As a result, monodomain films were obtained by LPL photoirradiation. Furthermore, this alignment could be erased by thermal annealing and rewritten by LPL photoirradiation. Thus, it has a potential of novel photoalignment films that would be an alternative of mechanically rubbed ones.

Chapter IV focuses on the graft density intentionally attempting to provide low

density polymer brushes and demonstrated that the graft density critically affects the molecular orientation of Az unit. A sparse initiator monolayer was prepared by exposure to vacuum UV light, and low density Az-polymer grafted substrates were obtained. In this case, the Az orientation was perpendicular to the substrate plane as shown by UV-vis absorption and XRD measurements. It is anticipated that patterned or gradient polymer brushes and reversible tuning of the graft density by some means will lead to new polymer surface technological aspects in photonic device systems or biomaterials.

This work is still at a basic stage of research, however, many implications and outlooks can be drawn from the data. The valuable knowledge is that the mesogen can align freely on-demand by light irradiation. Furthermore, the orientations of liquid crystalline mesogen are dependent by graft densities. Main chain conformations in polymer brushes are in general affected by graft densities, however, the direct observation of polymer states is difficult. Thus, it is highly important that information on the mesogen orientation in the side chains reflects the conformation of main chains. One may expects that the application is not limited to solid surfaces demonstrated in this work but can be extended to various surfaces, such as organic and inorganic particles, polymer surface, resins, and soft matters; *i. e.* hydrogels and elastomers.

In the latter part of this thesis attentions are paid to amphiphilic block copolymers and LB technique. Here the very sharp temperature dependency of 2D area of amphiphilic block copolymer ultrathin film was observed at the air-water interface.

In Chapter V, the obvious relationship between the aggregate diameter in solution and the spreading behavior at the air-water interface for a block copolymer, PS-P4VP, was revealed. An unexpectedly large surface area change on water was observed at very narrow temperature range. These results were only observed when spread from theta solvents for PS segment. In a theta solvent, PS-P4VP formed thermal dependent micelle-like structures attributed to the coil-globule transition. Therefore, the aggregate state in solution is robustly memorized during the spread process on water.

The similar temperature dependency was observed by using other amphiphilic block copolymers bearing PS segment such as PS-PEO, PS-P2VP (Chapter VII). In

theta solution, same turbidity changes were observed as in the case of PS-P4VP. The molecular weight of PS was systematically changed, and the increase in molecular weight led to elevation of the transition temperature of the coil-globule transition both in solution and at the air-water interface.

This work has a special significance in an aspect that conventional PS-based block copolymers without particular thermo-responsive segment are used. Because PS is widely used, their characteristic features have been well known. Such phenomena would be found in general (frequently used) polymer systems. It can be expected to novel applications in nanotechnologies such as tunable two-dimensional templates would be feasible. The combinations of polymer and theta solvent have been extensively reported. One of the most alluring polymer chains is probably poly(*N*-isopropyl acrylamide) in water. Therefore, it is anticipated that this surface area changes will lead to provide fundamental research in polymer materials and expand to applications for multiple thermo-responsive polymer materials.

As described above, unique characteristics of polymer thin films are found by "minor" preparation methods. Their characteristics are drastically changed by exploiting the influence from interface. Unique organized structures fabricated in this thesis would expand the novel functionalized polymer materials. The aspects proposed in this work are expected to contribute a great deal for new designs and progresses in the fabrication of functional polymer thin films.

Publications

1) Takayuki Uekusa, Shusaku Nagano, and Takahiro Seki, “Sharp Temperature Dependency of 2D Spreading Behavior in Amphiphilic Block Copolymer at the Air-water Interface”, *Colloids and Surface A: Physicochemical and Engineering Aspects*, **2006**, 284-285, 207-211.
2) Takayuki Uekusa, Satoshi Shimma, Shusaku Nagano, and Takahiro Seki, “Temperature Dependent Aggregation Behavior of Polystyene-Based Amphiphilic Block Copolymers at the Air-water Interface”, *Transactions of the Materials Research Society of Japan*, **2006**, 31, 265-268.
3) Takayuki Uekusa, Shusaku Nagano, and Takahiro Seki, “Unique Molecular Orientation in a Smectic Liquid Crystalline Polymer Film Attained by Surface-Initiated Graft Polymerization”, *Langmuir*, **2007**, in press
4) Takayuki Uekusa, Shusaku Nagano, and Takahiro Seki, “Fabrications and Photoalignment of Liquid Crystalline Azobenzene Polymer Brushes”, *Macromolecules* in preparation

Other Related Publication

1) Sadayuki Asaoka, Takayuki Uekusa, Takeshi Yamada, Hirohisa Yoshida, and Tomokazu Iyoda, “Syntheses and Nanostructure of Amphiphilic Liquid Crystalline Block Copolymers with Varios Mesogene Units” *Transaction of the Materials Research Society of Japan*, **2006**, 31, 536-540.

Presentations

1) Takayuki Uekusa, Shusaku Nagano, Takahiro Seki, “Sharp Temperature Dependent Spreading Behavior of Amphiphilic Block Copolymers on Water” *The 54th Spring Meeting of the Society of Polymer Science, Japan* (Yokohama, May 2005).

2) Takayuki Uekusa, Shusaku Nagano, Takahiro Seki, “The Temperature Dependent Changes in Aggregates of Amphiphilic Block Copolymers at Air/water Interface” *The 11th International Conference on Organized Molecular Films (LB11)* (Sapporo, Jun 2005)
3) Takayuki Uekusa, Shusaku Nagano, Takahiro Seki, “Sharp Temperature Dependency of Spreading Behavior in Amphiphilic Block Copolymers at the Air-water Interface” *The 54th Polymer Symposium of the Society of Polymer Science* (Yamagata, September 2005).
4) Takayuki Uekusa, Shusaku Nagano, Takahiro Seki, “Aggregate Behaviors and Temperature Dependence of Amphiphilic Block Copolymers Bearing Polystyrene blocks at the Air-water Interface” *The 16th Symposium of the Material Research Society of Japan* (Tokyo, December 2005).
5) Takayuki Uekusa, Shusaku Nagano, Takahiro Seki “Preparation of the Photo-functional Polymer Brush Structure by Langmuir Blodgett Method” *The 16th Symposium of the Material Research Society of Japan* (Tokyo, December 2005).
6) Takayuki Uekusa, Shusaku Nagano, Takahiro Seki “Synthesis of Hydrogel Surface Coated with Photo Functional Polymer Brushes by Surface-Initiated ATRP” *The 86th Spring Meeting of the Chemical Society of Japan* (Funabashi, March 2006).
7) Takayuki Uekusa, Shusaku Nagano, Takahiro Seki “Surface modification of hydrogels with polymer brush bearing azobenzene moieties” *The 55th Spring Meeting of the Society of Polymer Science, Japan* (Nagoya, May 2006).
8) Takayuki Uekusa, Shusaku Nagano, Takahiro Seki, “Surface Modified Hydrogels with Photo-functional Polymer Brushes”, *The 14th International Conference on Composites or Nano Engineering (ICCE-14)* (Boulder in USA, July 2006)
9) Takayuki Uekusa, Shusaku Nagano, Takahiro Seki, “Graft Polymerization of Photo-functional liquid crystalline polymer onto hydrogel surface”, *The 10th Symposium of Japanese Liquid Crystal Society* (Tokyo, July 2006)
10) Takayuki Uekusa, Shusaku Nagano, Takahiro Seki “Fabrication and their alignment behaviors of photo-functional liquid crystalline polymer brushes” *The 55th Polymer Symposium of the Society of Polymer Science* (Toyama, September 2006).

11) Takayuki Uekusa, Shusaku Nagano, Takahiro Seki “Molecular Orientation and Photoalignment of Azobenzene liquid crystalline polymer brushes” *The 87th Spring Meeting of the Chemical Society of Japan* (Osaka, March 2007).

12) Takayuki Uekusa, Shusaku Nagano, Takahiro Seki “Unique molecular orientation behaviors of liquid crystalline polymer grafted onto substrates” *The 56th Spring Meeting of the Society of Polymer Science, Japan* (Kyoto, May 2007).

Acknowledgements

This thesis is submitted to Department of Molecular Design and Engineering, Graduate School of Engineering, Nagoya University for the degree of Doctor of Engineering.

I would like to express my sincere gratitude to Professor Takahiro Seki for his helpful discussions and his continuous guidance throughout the course of this work.

I would like to thank Associate Professor Yukikazu Takeoka for his valuable discussions and advice as well as his constant encouragement.

I would like to thank Assistant Professor Shusaku Nagano for their useful help, discussions and advices as well as his constant encouragement.

I would like to Mr. Tatsuo Hikage at High Intensity X-ray Diffraction Laboratory for his kindly supporting of XRD, GI-XRD measurements and advice.

I would like to Associate Professor Nagahiro Saito and Ms. Junko Hieda at Takai Laboratory for his kindly supporting of ellipsometoric spectroscopy measurement.

I would like to Dr. Tsuyoshi Nakanishi at Koumoto Laboratory and Dr. Yoshitake Masuda at Advanced Industrial Science and Technology for DLS measurements.

I would like to Professor Yushu Matsushita at Nagoya University for providing the polymer materials and Mr. Satoshi Shimma at Mitsubishi Heavy Industries, LTD. for syntheses of polymers.

I wish to express my special thank to Dr. Norihiro Mizoshita (Toyota Central R&D LABS. INC.) and all members in Seki Laboratory for their generous supports, kind cooperation, and friendship. I thank to Mr. Mitsuo Hara for GI-XRD measurement and Mr. Jun Isayama for DSC measurement and POM observation. I thank to Ms. Yuriko Takagi and Ms. Yuko Ohiwa for her administrative assistants.

Finally, I sincerely thank to my parents, my sister and all of my friends for encouragement, understanding, warm supports and love.

March, 2007

Takayuki Uekusa